A STUDY OF CHARGE MOTION AND ELECTRONIC STRUCTURE OF DEFECTS IN MgO, CaO AND YAG ($Y_3Al_5O_{12}$)

By

KISHALAYA CHAKRABARTI

Bachelor of Science
University of Calcutta
Calcutta, India
1975

Master of Science
University of Calcutta
Calcutta, India
1978

Submitted to the Faculty of the Graduate College
of the Oklahoma State University
in partial fulfillment of the requirements
for the Degree of
DOCTOR OF PHILOSOPHY
July, 1984

A STUDY OF CHARGE MOTION AND ELECTRONIC STRUCTURE OF DEFECTS IN MgO, CaO AND YAG ($Y_3Al_5O_{12}$)

Thesis Approved:

Thesis Adviser

Dean of the Graduate College

ACKNOWLEDGEMENTS

I would like to express my gratitude to my advisor, Dr. G. P. Summers for his advice and encouragement during the course of my studies at Oklahoma State University. It has been a privilege to work with him.

I wish to express my appreciation to other committee members for their critical reading of this manuscript and discussions, with a special mention of Dr. T. M. Wilson for his advice and enlightening discussions concerning the theoretical aspects of this study.

A note of thanks is given to Dr. A. Sen with whom I had the pleasure of working on a theoretical model reported in this dissertation.

Thanks are given to Bryce Jeffries and Pradip Bandyopadhyay for their friendship and help.

I extend my thanks to my wife Rina for her help in drawing several of the diagrams for this dissertation.

Appreciation is also extended to Mr. Heinz Hall and other staffs of Machine Shop and Mr. M. Wayne Adkins of Glass Shop for their immense help during this research project.

Finally, I would like to acknowledge Mrs. Michele Plunkett for her excellent typing of this thesis.

TO

MY GRANDFATHER

AND

MY PARENTS

TABLE OF CONTENTS

LIST OF TABLES

LIST OF FIGURES

CHAPTER I

INTRODUCTION

In this dissertation studies on point defects in MgO and CaO are reported. Studies made on charge motion in $Y_3Al_5O_{12}$ (YAG) are included in an Appendix. Point defects in MgO and CaO, which the dissertation deals with are F type defects. In this chapter, therefore, F type defects will be discussed first and then a survey of the previous studies made on this kind of defects will be given. The actual problems which were investigated for the purpose of this dissertation will be defined next. Table 1 lists some of the physical properties of MgO and CaO and Figure 1 shows their crystal structure.

A. F Type Defects in MgO and CaO

F type defects in MgO and CaO consist of oxygen ion (anion) vacancies containing one or more electrons. These defects are usually produced in MgO and CaO using two main procedures;

1. by irradiation with particles such as electrons, protons or neutrons; (unlike in alkali halides, in alkaline earth oxides, ionizing radiation cannot produce ionic displacement to create any permanent F type defects); or
2. by heating the material at high temperature near the melting point in an atmosphere of the metallic vapor, (thermochemical reduction).

The samples used here were thermochemically reduced by the latter

TABLE I

PHYSICAL PROPERTIES OF MgO AND CaO

Material	Band Gap (eV)	Dielectric Constant (ε_o)	Lattice Constant a_o(Å)	Melting Point (°C)
MgO	7.8, 8.7	9.65	4.211	2800
CaO	7.0, 7.7	11.8	4.81	2600

Source - Feldott, J. M., (56) and the references given in (56).

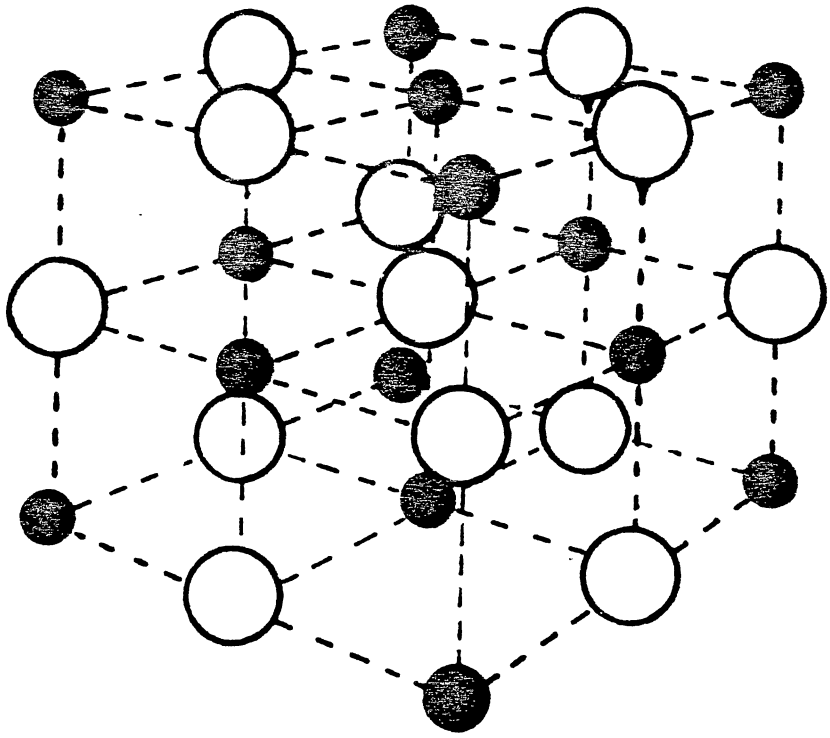

Figure 1. Crystal Structure for the Alkaline Earth Oxides

procedure. This process which is sometimes called subtractive coloration produces anion vacancies in the sample. F centers in an oxide contain two electrons trapped at the oxygen vacancy sites and F^+ centers contain one electron trapped at the anion vacancy sites. However, because the starting materials are often damp, hydrogen is also often introduced into these samples during the growth and the coloration processes.[1,2,3,4]

Hydrogen appears to enter the lattice as H^- ions [or $[H]^+$ ions, in the nomenclature used by Sonder and Sibley[5] for point defects], that is protons each of which have trapped two electrons. Such an entity is positively charged with respect to the divalent oxide lattice and thus can act as an electron trap. These traps largely control the optical and electrical properties of the sample. This is the main subject of investigation in this dissertation. The $[H]^+$ impurity center and F-type defects in alkaline earth oxides have O_h point group symmetry as shown in Figure 2, so long as no distortion or nearby charge compensating impurity is present.

In MgO and CaO the F center is a neutral defect and the F^+ center, which is a singly ionized F-center, is positively charged relative to the lattice. The F center in alkaline earth oxides, is therefore, analogous to the helium atom and the ground and first excited states can be correspondingly referred to as ^1S, ^3S, ^1P, ^3P, etc. Similarly, the F^+ center is analogous to the He^+ ion with a ground state and excited states referred to as, ^2S ^2P, etc. Optical absorption arises when these trapped electrons are excited by incident photons. Figure 3, for example, shows the F and F^+ optical bands in CaO. For MgO, the F^+ and F absorption bands occur at approximately the same energy (5.0 eV).

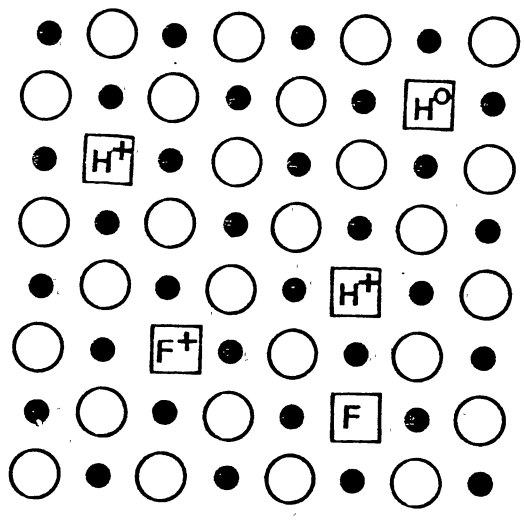

H⁺ Substitutional H^- ion

H⁰ Substitutional $H^=$ ion

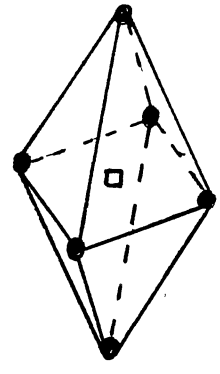

Figure 2. Schematic Diagram for F Type Defects and O_h Symmetry of Defect Site

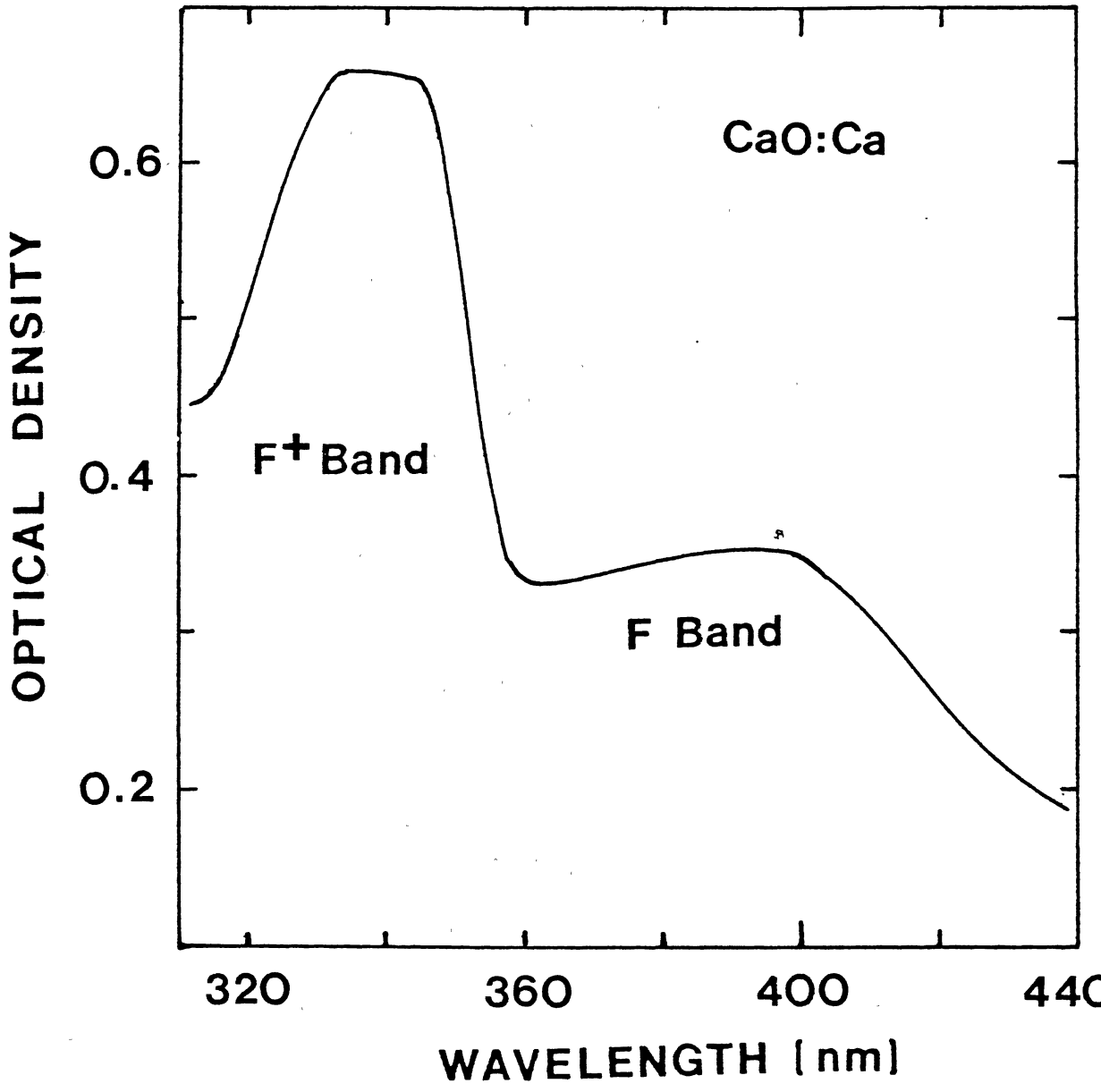

Figure 3. Optical Absorption from F and F^+ Centers in CaO

B. Survey of Experimental Results

Studies have been made on F and F^+ centers in alkaline earth oxides for more than a decade. Henderson and King[6] showed that an optical band near ~ 5 eV is correlated with the intensity of the F^+ center EPR signal in neutron irradiated MgO. Chen et al.[7], however, did not observe this correlation in additively colored and electron irradiated MgO, although they found an optical absorption band at the same energy ~5 eV. Since Wertz et al.[8], showed that F^+ centers can be regenerated in additively colored MgO by ionizing radiation, the conclusion was finally made that F center also absorbs near ~ 5 eV. Therefore, F and F^+ optical absorption bands in MgO are found to coincide at ~ 5 eV.

In CaO, however, the F and F^+ optical absorption bands lie at different energies, at 3.1 eV and at 3.7 eV respectively. Ward and Henseley[9] observed the F center absorption in additively colored crystal and later Henderson et al.[10] also observed the F center absorption at the same energy in CaO crystals colored accidentally during growth.

Henderson et al.[10] also studied the emission resulting from 3.1 eV F center absorption in CaO. They concluded that the emission is associated with two bands, one at 2.0 eV and the other at 2.5 eV. From the lifetime studies they also concluded that the 2.0 eV band corresponds to the $^3T_{1u} \rightarrow {}^1A_{1g}$ transition and 2.5 eV corresponds to $^1T_{1u} \rightarrow {}^1A_{1g}$ transition. Bates and Wood[12] however could not find the 2.5 eV band in different samples and they suggested that it might have originated from transition metal impurities in Henderson's sample. Their studies also revealed that above 300 K, the 2.01 eV band has a high energy shoulder at 2.05 eV, and the lifetime of the luminescence decreased rapidly with temperature, indicating that the emission at 2.05

eV was associated with the allowed $^1T_{1u} \rightarrow {}^1A_{1g}$ transition. This view was later supported by Wood and Wilson[14] by theoretical calculations. The F^+ center absorption at 3.65 eV has been assigned to $^2A_{1g} \rightarrow {}^2T_{1u}$ transition, with a resulting emission at 3.35 eV.

The nature of 2.3 eV emission from F centers in MgO has long been a subject of debate[13-15]. Recently calculations by Wilson[16] have suggested that the 2.3 eV emission in MgO results mainly from a $^1T_{1u} \rightarrow {}^1A_{1g}$ transition above ~ 70K.

In thermochemically reduced MgO and CaO, the $^1T_{1u} \rightarrow {}^1A_{1g}$ F center emissions, which is 2.3 eV (green) for MgO and 2.1 eV (orange) for CaO, have long lived phosphorescence near room temperature. Jeffries et al.[17] attributed this long lived phosphorescence near room temperature to H^- ions which act as metastable electron traps. Gourley and Vance[2] and Vance and Mallard[3] observed sharp infrared absorption lines near 900 cm^{-1} in arc-melted CaO crystals, which they suggested were due to H^- ion vibrations. Gonzales et al.[4] made extensive studies in the infrared region of absorption in thermochemically reduced MgO, CaO and SrO. They also observed sharp lines in the infrared regions in all three materials. They assigned these sharp lines to local mode oscillations of substitutional H^- ions. After this Jeffries et al.[17] suggested that an H^- ion acts as an electron trap and becomes $H^=$ ion capturing an electron. Above a temperature of about 260K, the $H^=$ ion becomes thermally unstable and the third electron can be released into the conduction band. Jeffries et al.[17] suggested that the metastable retrapping of the electron as it moves through the lattice in returning to an F^+ center, where it is eventually captured, is the cause of long life-time of the F center luminescence near room temperature. They also

showed that the lifetime of the luminescence changes dramatically with the concentration of H^- ions in the sample. If the lifetime of the luminescence is defined as the time over which the intensity drops to one tenth of the initial value, then it is seen as is shown in Figure 4, that the lifetime changes from 300 sec to 3 sec with the variance of hydrogen ion concentration in the sample.

C. Statement of the Problem

Previous studies show that hydrogen enters into the alkaline earth oxides during growth and the coloration process and controls the lifetime of luminescence from the F center near room temperature. Tohver[18] has recently detected an ESR signal in these samples, which he has assigned to paramagnetic $H^=$ ions. The H^- ion in MgO and CaO becomes paramagnetic after it has captured an electron which has been optically excited from an F center. The $H^=$ ion is stable only at low temperature, where the thermal release of the third electron from $H^=$ ions can not take place. It is therefore necessary to bleach the sample at low temperature to generate thermally stable $H^=$ ions, prior to ESR study. The objective of this study was to investigate these electron traps, to determine the activation energy of the traps, to study the details of the trapping mechanism, and to find out how the concentration of traps affected the motion of electrons in the sample, thereby changing the decay kinetics of the F center luminescence.

Thermoluminescence (TL) experiments show at what temperature the thermal release of electrons from these traps take place. TL results show that there are two temperature ranges in both MgO and CaO with TL peaks at 260K and 40K for MgO and 320 and 80K for CaO, where electrons

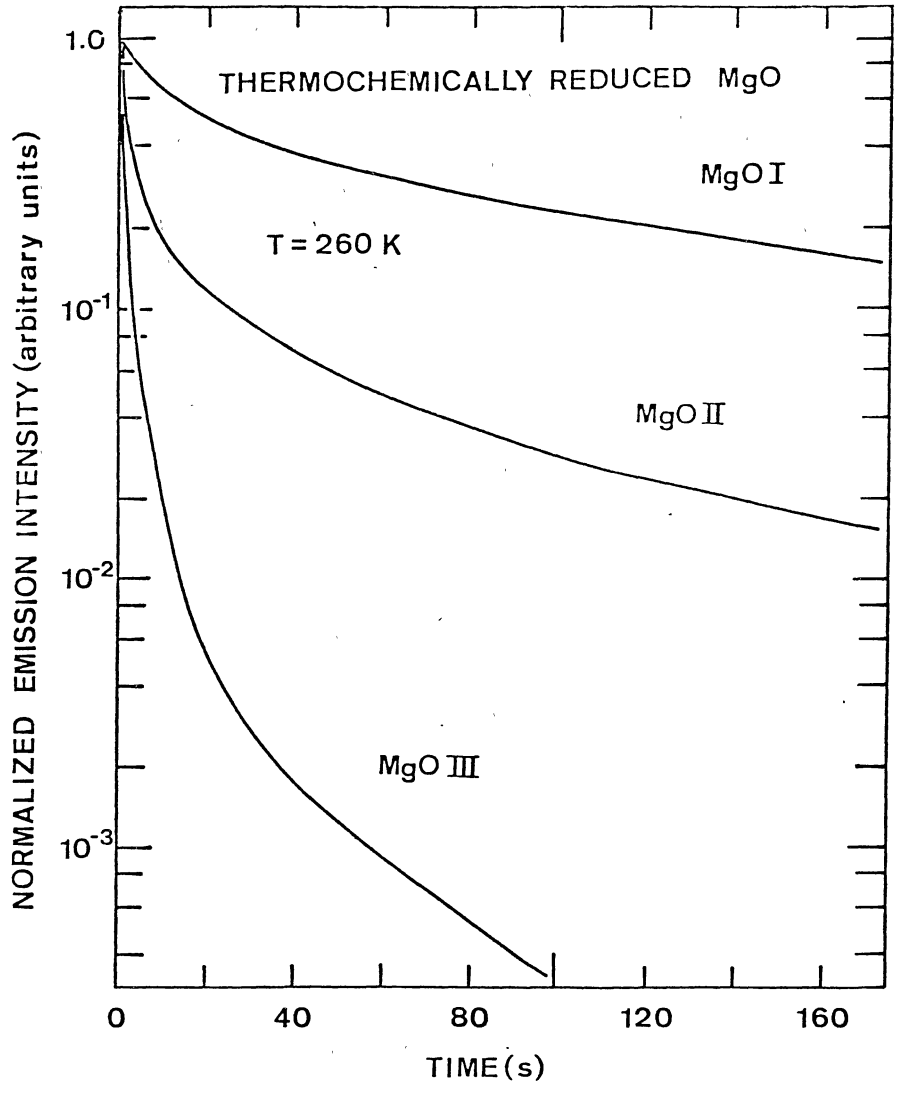

Figure 4. Lifetime of the F Center Luminescence in Various MgO Samples

Source: Jeffries et al.[17]

are released from the traps. TL near room temperature in both materials arises due to the thermal release of electrons from $H^{=}$ ions. However, the exact origin of the electron trap which generates TL at low temperature in these samples, is not yet known. It has been suggested that H^{-} ions may also be a cause of these shallow traps which are associated with low temperature TL.

A detailed study of the F center luminescence decay kinetics at temperatures near both the high temperature and low temperature peaks in several samples will be reported. A theoretical model will be presented that involves the electronic structure of the defects including these two types of effective traps, present in both MgO and CaO, and this model will be employed to explain the decay kinetics in these materials.

Other experiments such as infrared stimulated emission, dark and photoconductivity will be discussed with experimental results to explain how they are used to monitor charge motion and the trapping mechanism involving hydrogen in these samples.

Experimental procedures and the apparatus used are discussed in Chapter III. Experimental results analysis and discussions are given in Chapter IV. In Chapter V, a summary of the results and the scope of further researchers are discussed. Results of the experimental studies made on YAG are included in an Appendix.

CHAPTER II

ELECTRONIC STRUCTURE OF DEFECTS - THEORETICAL BACKGROUND

A. Introduction

F center luminescence in MgO and CaO occurs at 2.3 eV and 2 eV respectively. In this chapter a theoretical calculation made by Wood and Wilson[11] of the electronic structure of the F center in CaO and also a recent calculation by Wilson et al.[16] for the F center in MgO will be outlined. The results of these calculations will be compared with experimentally obtained values for the energies at which F center luminescence occur in the materials. A theoretical calculation made by Wilson[19] to estimate the transition energy of H^- ions will also be discussed.

B. Outline of the Theoretical Model

The theoretical model used by Wood and Wilson[11] to describe the F center in CaO, emphasizes the importance of 1) the electronic structure on the ions neighboring the defect, 2) the electronic and ionic polarization of the surrounding lattice and, 3) the lattice distortion and its effect on the energy levels and wavefunctions of the defect.

In the calculations they divided the crystal into two regions. Near the defect the electronic structure of the neighboring ions was treated in detail in a Hartree-Fock-type approximation, while in the

outer region a simple effective-mass approximation was used. In the two electron center, the effective two-electron Hamiltonian including the effects of dielectric polarization, but neglecting lattice relaxation was expressed in the form

$$H(1,2) = \sum_{i=1}^{2} h_1(\underline{r}_1) + g_{12} \rightarrow \quad (1)$$

where, $h_1(\underline{r}) = -\frac{1}{2}\nabla^2 - \sum_{\nu\neq 0}\{(Z_\nu - N_\nu)|\underline{r} - \underline{R}_\nu|^{-1}$

$+ U_\nu(\underline{r})\} + U_p(\underline{r}),\ r < R_o; \rightarrow \quad (2a)$

$$h_1(\underline{r}) = -\frac{1}{2m^*}\nabla^2 + \varepsilon_{HF} - \frac{2}{r} + U_p(\underline{r}),\ r > R_o \rightarrow \quad (2b)$$

and for all values of $\underline{r}_1$ and $\underline{r}_2$,

$$g_{12}(\underline{r}_1, \underline{r}_2) = r_{12}^{-1} + U_p^{12}(R_o) \rightarrow \quad (3)$$

Z_ν is the atomic number of the ion at $\underline{R}_\nu$, and N_ν is the number of electrons on that ion. ε_{HF} represents the bottom of the conduction band in a Hartree-Fock calculation and m* is the effective mass.

When either one of the F-center electrons moves out of the vacancy, local polarization of the crystal occurs. This dielectric polarization effect must be included in defect calculations in order to obtain satisfactory agreement with experiment. The polarization potential of each electron and its corresponding hole can be broken into two parts, i.e.,

$$U_p(\underline{r}) = U_e(\underline{r}) + U_{ion}(\underline{r}) \rightarrow \quad (4)$$

U_{el} gives the contribution due to the distortion of the electronic orbitals on the neighboring ions (electronic polaron), and U_{ion} gives that due to small displacements of the ions (ionic polaron). The Coulomb and exchange interactions of the F center electrons with the electrons on the ions within the inner region ($r < R_o$) are contained in the effective potential U_ν . The two electron interaction potential g_{12} in Equation (3) includes the Coulomb interaction term of the F-center electrons plus a polarization potential $U_p^{12}(R_o)$ not found in one-electron centers, which accounts for the change in the polarization of the crystal when both electrons move out of the vacancy.

The two-electron wavefunction for this system was approximated by the expansion

$$\psi^{\pm}(1,2) = \sum_{k=1}^{n} C_k \psi_k^{\pm}(\underline{r}_1, \underline{r}_2)\, \chi_{\mp}(\xi_1, \xi_2) \rightarrow \quad (5)$$

in which (+) implies a singlet state of the F-center and (-) implies a triplet. The spin function $\chi_{\mp}(\xi_1,\xi_2)$ has the usual form, and the two-electron basis function $\psi_k^{\pm}$ was expressed in terms of one-electron orbitals by

$$\psi_k^{\pm}(\underline{r}_1, \underline{r}_2) = N_k[f_{k1}(\underline{r}_1)f_{k2}(\underline{r}_2) \pm f_{k2}(\underline{r}_1)f_{k1}(\underline{r}_2)] \rightarrow \quad (6)$$

where, N_k is a normalization factor. This notation emphasizes the need to specify two orbitals, i.e., k_1 and k_2, in order to determine the k_{th} two-electron function. The one-electron orbitals f_{ki} were taken to be

of the form

$$f_{ki} = \bar{N}_{ki} \left(f^{o}_{ki}(\underline{r}) - \sum_{\nu j} \phi_{\nu j}(\underline{r}) \langle \phi_{\nu j} | f^{o}_{ki} \rangle\right) \rightarrow \tag{7}$$

where $\bar{N}_{ki}$ is an orbital renormalization factor. The index ν runs over all the ions in the inner region and $\phi_{\nu j}(\underline{r})$ denotes the jth one-electron orbital on the νth ion. The functions f^{o}_{ki} are of the form

$$f^{o}(\underline{r}) = [(2\beta)^{2n+1}/(2n)!]^{1/2} \; r^{n-1} e^{-\beta r} \kappa_{\Gamma p}(\theta,\phi) \rightarrow \tag{8}$$

$\kappa_{\Gamma p}$ is the cubic harmonic associated with the pth component of the irreducible representation Γ of the O_h point group.

1. Lattice Relaxation

Major portions of the calculations, which will not be shown here, are discussed in the papers by Mostoller and Wood[20] and Boswarra and Lidiard[21], in which the Mott-Littleton model was refined and applied to Frenkel defect calculations.

The total change in energy of the crystal, because of the lattice relaxation was expressed as

$$\Delta E_{cr}(\delta) = \Delta E_{c}(\delta) + \Delta E_{r}(\delta) + \Delta E_{p}(\delta) \rightarrow \tag{9}$$

in which the subscripts c, r, and p stand for Coulomb, repulsive, and polarization, respectively. The relaxation or distortion parameter δ gives the displacement of the lnn ions as a percentage of the nearest-neighbor distance in the perfect crystal.

2. Results of the Calculations

Six configurations of the type given by Equation (6) for each state of the F-center, are used in the calculation. The nonlinear parameters appearing in Equation (8) are optimized for each symmetrized displacement of the first-nearest neighbor (lnn) ions. The total energy change of the crystal is determined by adding to the electronic energy a contribution due to ion-ion interactions. Configuration coordinate curves for A_{1g}, E_g and T_{2g} displacements are constructed by performing the calculations with the neighboring ions fixed in appropriate displaced positions.

ε_{HF} is chosen to give agreement between the calculated and measured peak of the absorption band.

The results of the calculations for the lowest lying states of the F center in CaO are shown in Figure 5. The $^1A_{1g} \rightarrow {}^1T_{1u}$ absorption occurs at 3.05 eV which is in good agreement with experimental result of 3.1 eV. A_{1g} configuration coordinate curves for F center emission of CaO, are shown in Figure 6.

For some time the belief was that the $^1T_{1u} \rightarrow {}^1A_{1g}$ emission occured at 2.5 eV, with the $^3T_{1u} \rightarrow {}^1A_{1g}$ occurring at 2.0 eV. However, Wood and Wilson[10] claims that all their attempt to adjust the parameters in their model to yield these emission lines, while keeping the absorption at 3.1 eV, failed. Their model predicted that $^3T_{1u} \rightarrow {}^1A_{1g}$ and $^1T_{1u} \rightarrow {}^1A_{1g}$ transition should lie within about 0.1 eV of one another and they argued that at temperatures below 300K the $^3T_{1u} \rightarrow {}^1A_g$ band is dominant but above 300K the $^1T_{1u} \rightarrow {}^1A_{1g}$ transition contributes increasingly to the luminescence.

There is a greater difference in the relative sizes and

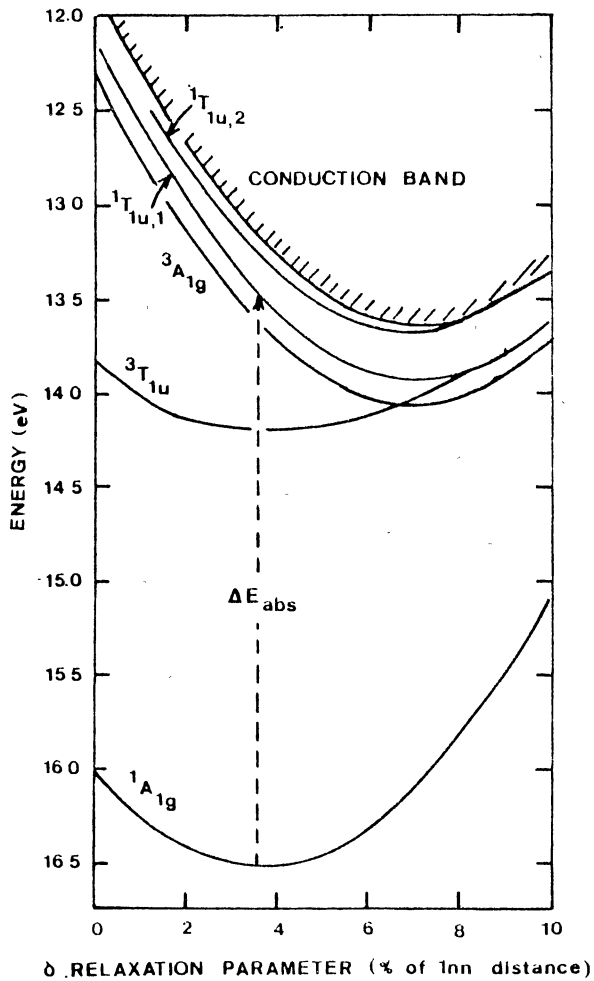

Source: Wood and Wilson

Figure 5. Configuration Co-ordinate Diagram for F Center Absorption in CaO

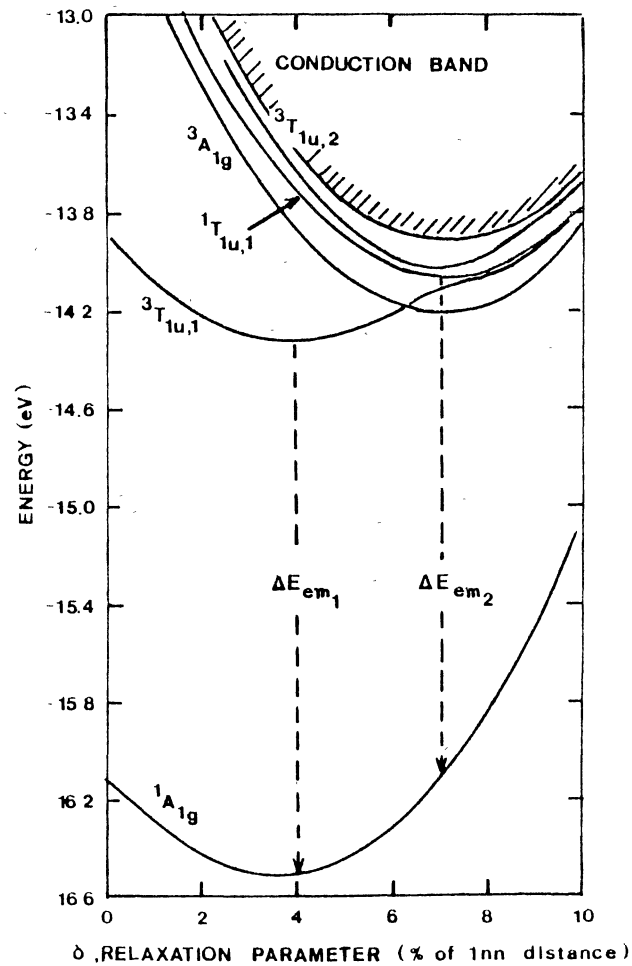

Source: Wood and Wilson

Figure 6. Configuration Co-ordinate Diagram for F Center Absorption in CaO

polarization of the Mg^{2+} and O^{2-} ions in MgO compared to those of the Ca^{2+} and O^{2-} ions in CaO. These differences enhance the difficulty in treating the polarizability of the O^{2-} ion in the Wood/Wilson model in the case of MgO. In earlier calculations made by Wilson and Wood[22], it was necessary to adjust some of the emission parameters in order to obtain reasonable agreement with the observed larger Stoke shift in MgO. However, in the most recent calculation made by Wilson[16], the electronic polarization was treated more precisely and it was not necessary to adjust these parameters. In this calculation he also included the first order correction to the Toyozawa-Hanken-Schottky (THS) expressions[23,24] for the interaction between the electron and the hole via the electronic polarization field. A_{1g} configuration coordinate curves for F center emission in MgO as developed by Wilson is shown in Figure 7. The calculated $^1T_{1u} \rightarrow {}^1A_{1g}$ emission of 2.2 eV is close to the experimentally obtained value of 2.3 eV.

3. Electronic Transition From H^- Ions

U centers in alkali halides consist of hydrogen atoms trapped in anion vacancies. Electronic absorption has been found from these U centers. Wood and Opik[25] have also calculated the electronic structure of U centers in alkali halides and their theoretically calculated values for electronic transitions of U centers are in good agreement with the experimental results.

No experimental results for electronic transitions of H^- ions in thermochemically reduced alkaline earth oxides have been reported so far. However, Wilson[19] has, as yet unpublished, calculations of the expected electronic transition energy for H^- ions in MgO. These

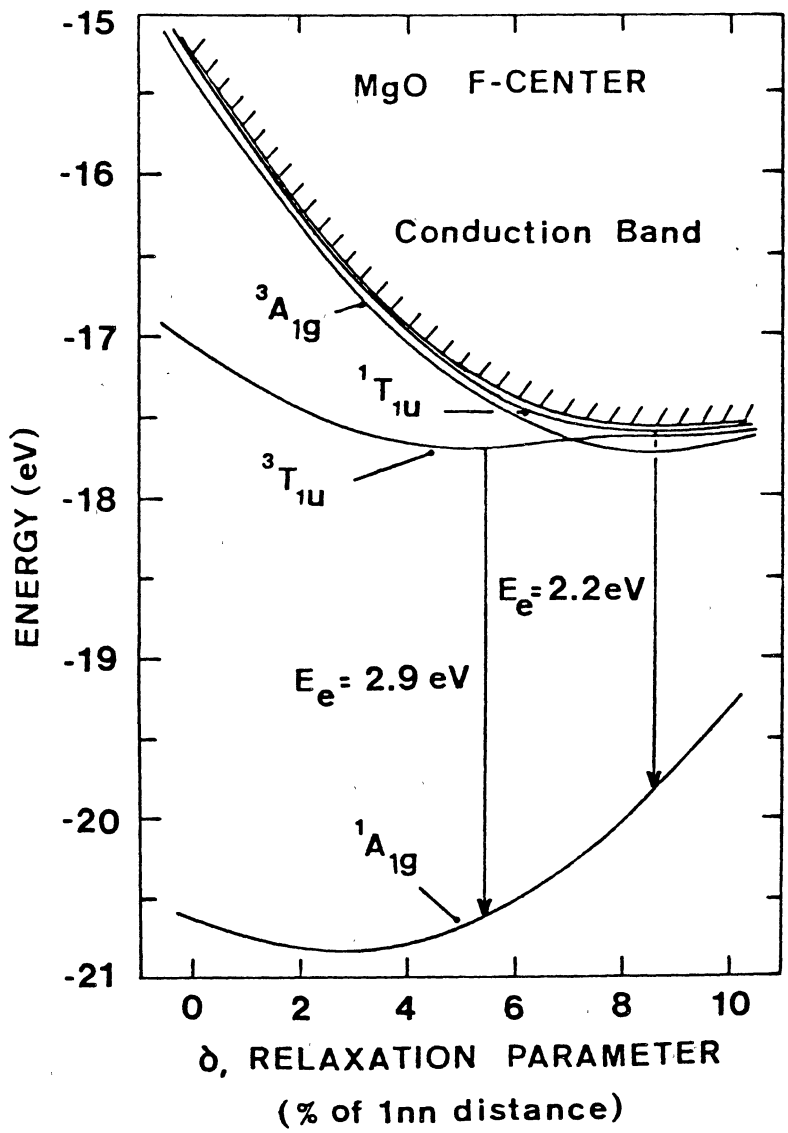

Figure 7. Configuration Co-ordinate Diagram for F Center Emission in MgO

Source: Summers et al.[16]

calculations are similar to those made for F centers, except that in the case of H^- ions extra terms must be introduced to account for the presence of protons in the oxygen vacancy sites. Equation 2(a) and 2(b) for the F center calculations are modified in case of H^- ions in the following way.

$$h_1(\underline{r}) = -\frac{1}{2}\nabla^2 - \frac{1}{r_1} - \sum_{\nu\neq 0}\{(Z_\nu - N_\nu)|\underline{r} - R_\nu|^{-1} + U_\nu(\underline{r})\} + U_p(r),\ r < R_o$$

$$h_1(\underline{r}) = -\frac{1}{2m^*}\nabla^2 + \varepsilon_{HF} - \frac{3}{r} + U_p(\underline{r});\ r > R_o$$

The value obtained for the absorption energy for the $^1A_{1g} - {}^1T_{1u}$ transition in H^- ion in MgO is 7.8 eV, Figure 8. Since a value of 7.8 eV lies near the band edge of the crystal it is expected to be difficult to confirm this result experimentally. But this theoretical result helps us to explain why no electronic absorption from H^- ions has been observed experimentally in the range of 6 eV to 2 eV even in crystals known to contain large concentrations of H^- ions. The theoretical results obtained by Wilson would not appear unreasonable when compared with the results for alkali halides. In the case of alkali halides the optical absorptions of U centers lie a few electron volts higher than those for the corresponding F centers. The results for a few alkali halides are indicated in table (2), which show that there is about 3 eV energy shift towards a higher energy for a U center transition compared to an F center transition in the same alkali halide. In case of MgO the F center absorption lies at 5 eV. Therefore, the calculated value of 7.8 eV for the electronic absorption of H^- ions is quite a reasonable

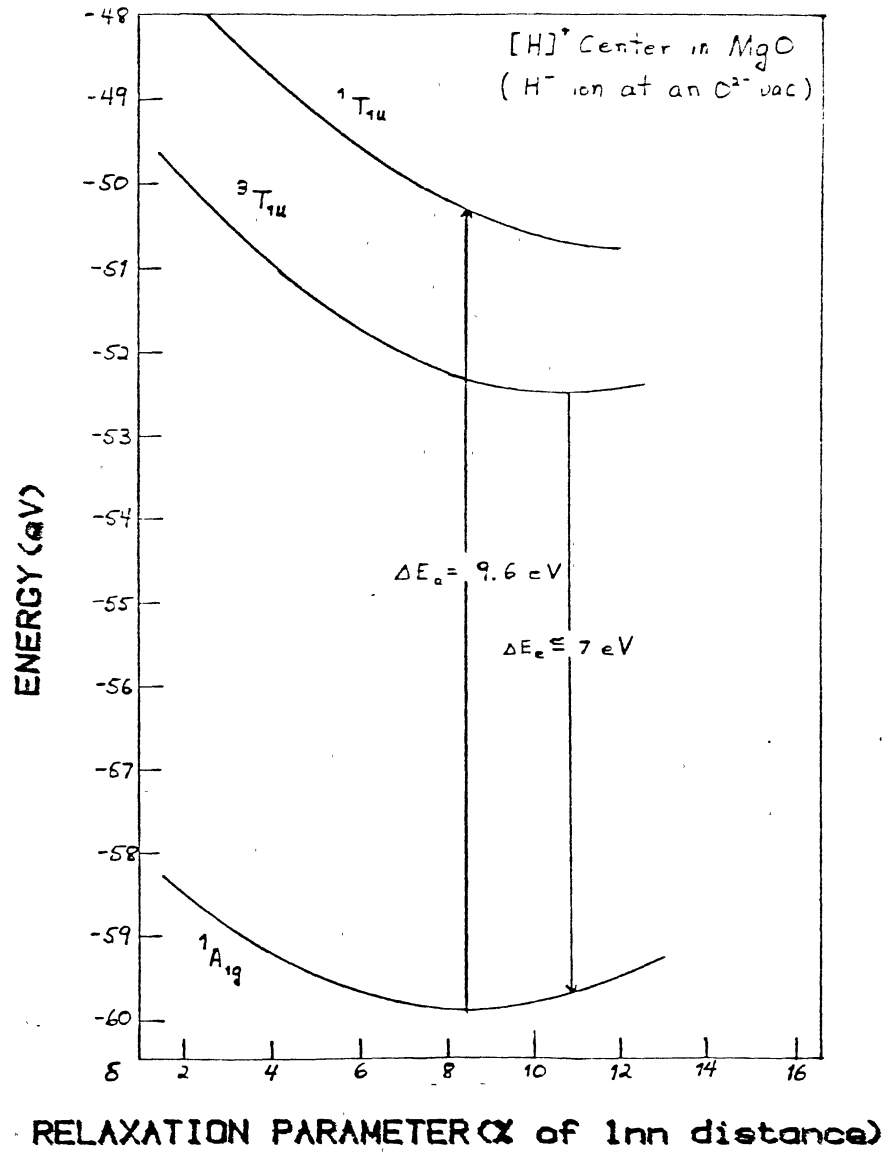

Figure 8. Configuration Co-ordinate Diagram for Absorption from H^- Ion in MgO

Source: T. M. Wilson[19]

TABLE II

ABSORPTION ENERGY OF F CENTER AND U CENTER
IN DIFFERENT ALKALI HALIDE CRYSTALS

Material	E_F(eV)[a]	E_U(eV)[b]	E_U-E_F(eV)
KCl	2.27	5.79	3.52
KBr	2.03	5.44	3.41
KI	1.88	5.08	3.20

(a) Ref. (67).
(b) Ref. (25).

CHAPTER III

SAMPLE PREPARATION, EXPERIMENTAL APPARATUS AND PROCEDURE

A. Introduction

In Chapter I a review of previous studies on F centers in MgO and CaO has been given. H^- ions in these material and their influence on F center emission in the light of recent studies have been discussed. In Chapter II theoretical calculations of the electronic structure of F centers have been described and since this dissertation mainly deals with the nature of the emission from F centers in these crystals, a special emphasis has been given to the calculations of F center emission given by Wood and Wilson for CaO[11] and Wilson[16] for MgO. The result of Wilson's calculation[19] on the electronic absorption from H^- ions has been given. Why the experimental confirmation of this result is difficult has also been explained in the previous chapter.

In this chapter we will first discuss the crystal growth process and how H^- ions are introduced into MgO. The experimental apparatus and procedure will be described next.

B. Sample Preparation: MgO and CaO

The MgO and CaO crystals used in this study were grown by the arc fusion method by Y. Chen at Oak Ridge National Laboratory. The starting materials were respectively high-purity grade MgO powder from Kanto

Chemical Company, Tokyo, Japan and reagent grade $CaCo_3$ powder from Mallinckrod Chemical Company. Crystals of MgO and CaO are normally cloudy when grown. The cloudiness is usually more pronounced in CaO than MgO. Briggs[1] has shown that the cloudiness or opacity of MgO is due to the presence of high pressure hydrogen gas contained in small cavities. The source of hydrogen is moisture absorbed in the MgO starting powder prior to crystal growth. CaO crystals usually contain more hydrogen as an impurity in the starting materials because of the their hygroscopic nature. In both MgO and CaO the opacity arises from a reaction involving hydroxyl ion. Briggs has found[1] that this type of cloudiness can be generated in some previously clear MgO samples by annealing them at high temperature in hydrogen.

Kirklin et al.[26] made an experiment which was a combination of infrared absorption and electron nuclear double resonance which detected a sharp infrared absorption peak at 3296 cm^{-1} which was attributed to an OH^- stretching mode. They also noticed a sharp peak at 3700 cm^{-1} in some MgO crystals which they thought was magnesium peroxides precipitates, which was later supported by experimental results of Glass and Seerle[27], and by Sibley et al.[28].

A short description of Brigg's experiment by which he came to the conclusion that the gas in the cavities in cloudy MgO crystals is in fact hydrogen is discussed below. In the experiment he used two sealed glass tubes, one containing a cloudy crystal and 1 ml of orthphosphoric acid and the other containing the same amount of acid only, which he used as a control. The tubes were then evacuated and the acid frozen by immersion in liquid nitrogen. He then heated the acid in both tubes to 100°C, so that the specimen was dissolved in the acid.

Both the tubes were then attached to the vacuum system of the mass spectrometer. They were evacuated to a pressure of 10^{-6}Torr. The acid was frozen again and the seals were broken. The mass spectrometer showed an increase in mass 2 to ~ 50% above background level for the specimen whereas only 10% for the control. He then performed a similar experiment with a clear crystal and observed a rise in mass the same as the control. Briggs' conclusion was that the cavities in cloudy MgO crystal contain hydrogen gas.

Briggs also suggested that the removal of oxygen ion from the surface of a crystal creates an oxygen vacancy and two electrons. He represented this reaction by the chemical equation

$$H_2 + M_g0 \rightarrow H_20 + Mg + \boxed{0} + 2e$$

where $\boxed{0}$ denotes an oxygen vacancy.

Oxygen vacancies are produced by the thermochemical reduction process in the samples we have studied. In this process, which could also be called "subtractive coloration", the crystals were thermochemically reduced[4] by heating to a high temperature (2100 - 2400K) under a high pressure (4-7 atm) of metal (Mg or Ca as is the case) vapor, in a tantalum bomb. F centers are formed in these samples, when two electrons are trapped at oxygen vacancy sites. Hydrogen impurities present in the sample can go to some of these oxygen vacancy sites to form H^- ions.

A substantial amount of work has been reported[29-36] concerning the vibrational properties of substitutional H^- ions in alkali halides, which are also known as U centers; and some detailed work has also been

reported[37] on H^- ion and D^- ion vibrations in the alkaline-earth fluorides and in rare-earth trifluorides. However, little has been done on this H^- ions in alkaline earth oxides until recently. Gourley and Vance[2] and Vance and Mallard[3] reported sharp infrared-absorption lines near 900 cm^{-1}, in arc melted CaO. More recently Gonzalez et al.[4] observed substitional H^- ion vibrations in thermochemically reduced MgO, CO and SrO. Gonzalez et al.[4] reported that after heating in the tantalum bomb the cloudiness of the crystal decreased and in the infrared region of the absorption sharp lines due to the H^- ion local mode oscillation, appeared. For MgO, lines were observed at 1024, 1032 and 1053 cm^{-1} at room temperature and for CaO at 880 and 911 cm^{-1}, as shown in Figures 9 and 10. They also found that intensity of these lines depends strongly on the initial hydrogen impurities in the sample which was indicated by the cloudiness of the crystal and also by the presence of OH^- bands. Gonzalez et al.[4] also reported the appearance of the first harmonic oscillation for H^- ions at 2098 cm^{-1} in initially very cloudy crystals of MgO. They, however, did not observe any evidence of the first harmonic in CaO. They also observed at low temperature at 80K two sets of three lines particularly in the case of MgO.

Gonzalez et al.[4] argued that in each of the three oxides, the fundamental H^- ion vibrations cause two or more sharp lines to appear in the infrared region, because the H^- ions are surrounded by an environment of different local charge compensators, which lower the O_h symmetry around the defect site. The same reasoning was also given by Gourley and Vance[2], when they noticed two lines of different intensities around 900 cm^{-1} in arc melted CaO. The lowering of symmetry is also indicated

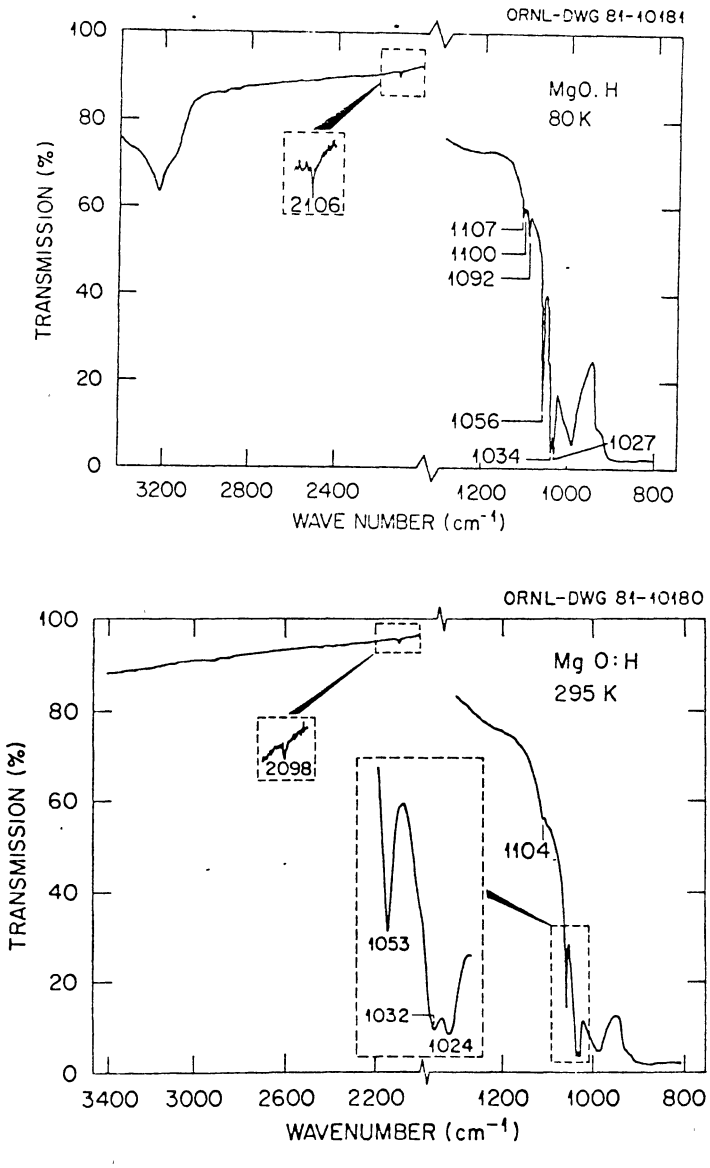

Figure 9. Infrared Absorption Lines Due to H^- Ion Local Mode Oscillation in MgO

Source: Gonzalez et al.[4]

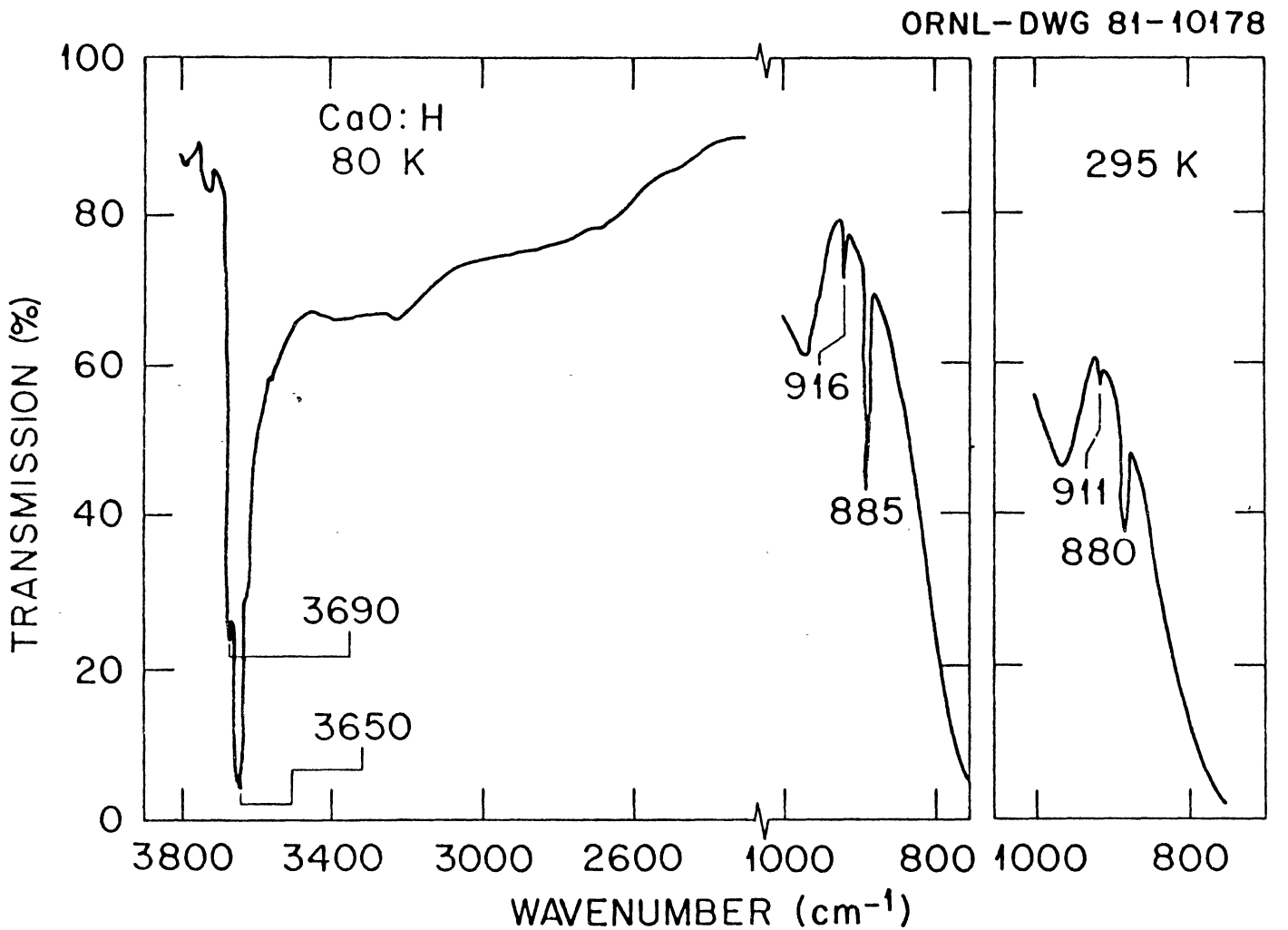

Figure 10. Infrared Absorption Lines Due to H^- Ion Local Mode Oscillation in CaO

Source: Gonzelez et al[4]

by the observation of first harmonic in MgO. O_h symmetry having inversion symmetry, the dipole transition from $\nu = 0$ to $\nu = 1$ to create first harmonic of vibration is forbidden. So the explanation for the appearance of the first harmonic is that the symmetry in the defect site is lowered from O_h to a less symmetric configuration not having inversion symmetry. Also, because there are two sets of three lines which appear at 80K, particularly in MgO, Gonzalez et al. they also indulged the thought that H^- ions may be present in local environments of slightly different symmetries. For similar reasons the satellite lines appear the H^- ion spectra in alkaline halides[29,30] and alkaline earth fluorides.[36]

The crystals which we have studied therefore contain H^- ions, that were introduced into the materials during the growth and coloration as discussed in this chapter. The local mode oscillations produce sharp infrared lines which are an experimental observation of the fact that the intensity of the infrared lines depends on the initial concentration of hydrogen present. The results of further investigation on the role of these H^- ions on luminescence of alkaline earth oxides, will be discussed in the next chapter. In the remainder of this chapter, the experimental apparatus and procedures will be discussed.

C. Absorption Measurements

Visible and ultraviolet absorption measurements were made with a Perkin-Elmer 320 spectrophotometer. The optical density is given by $O.D. = \log_{10} \frac{I_o}{I}$ where I and I_o are the intensity of the light transmitted through the sample and the intensity of the reference beam, respectively. The intensity of the light transmitted through the sample

is given by $I = I_o e^{-\alpha d}$ where I_o is the intensity of the incident beam (reference beam), α is the absorption coefficient, and d, the thickness of the sample. The optical density, O.D., is related to the absorption coefficient by $\alpha = 2.303 \frac{O.D.}{d} cm^{-1}$.

Infrared absorption measurements were made with a Perkin-Elmer Model 580 spectrophotometer. The concentration of H^- ions can be determined from these infrared lines and using the equation given in Chen et al.[37]

$n(H^{-1}) = 5.5 \times 10^{16} \Sigma \alpha(H^-)$ for MgO and

$n(H^-) = 1.2 \times 10^{16} \Sigma \alpha(H^-)$ for CaO.

where $\Sigma \alpha(H^-)$ is the sum of the absorption coefficients for all the peaks in the spectrum, and the concentration of F centers can be determined by the formula given in Reference 17 and Reference 51.

$\eta_F = 5.0 \times 10^{15} \alpha_F$ for MgO

$\eta_F = 3 \times 10^{15} \alpha_F$

where, α_F is the absorption coefficient.

D. Photoconductivity Measurement

A schematic diagram of the photoconductivity experimental arrangement is shown in Figure 11. The incident light falls on the crystal, of thickness d, between plane parallel electrodes. The crystal is located in a cryostat and an electric field, E = v/d, is established across the crystal in a direction parallel to that of the incident

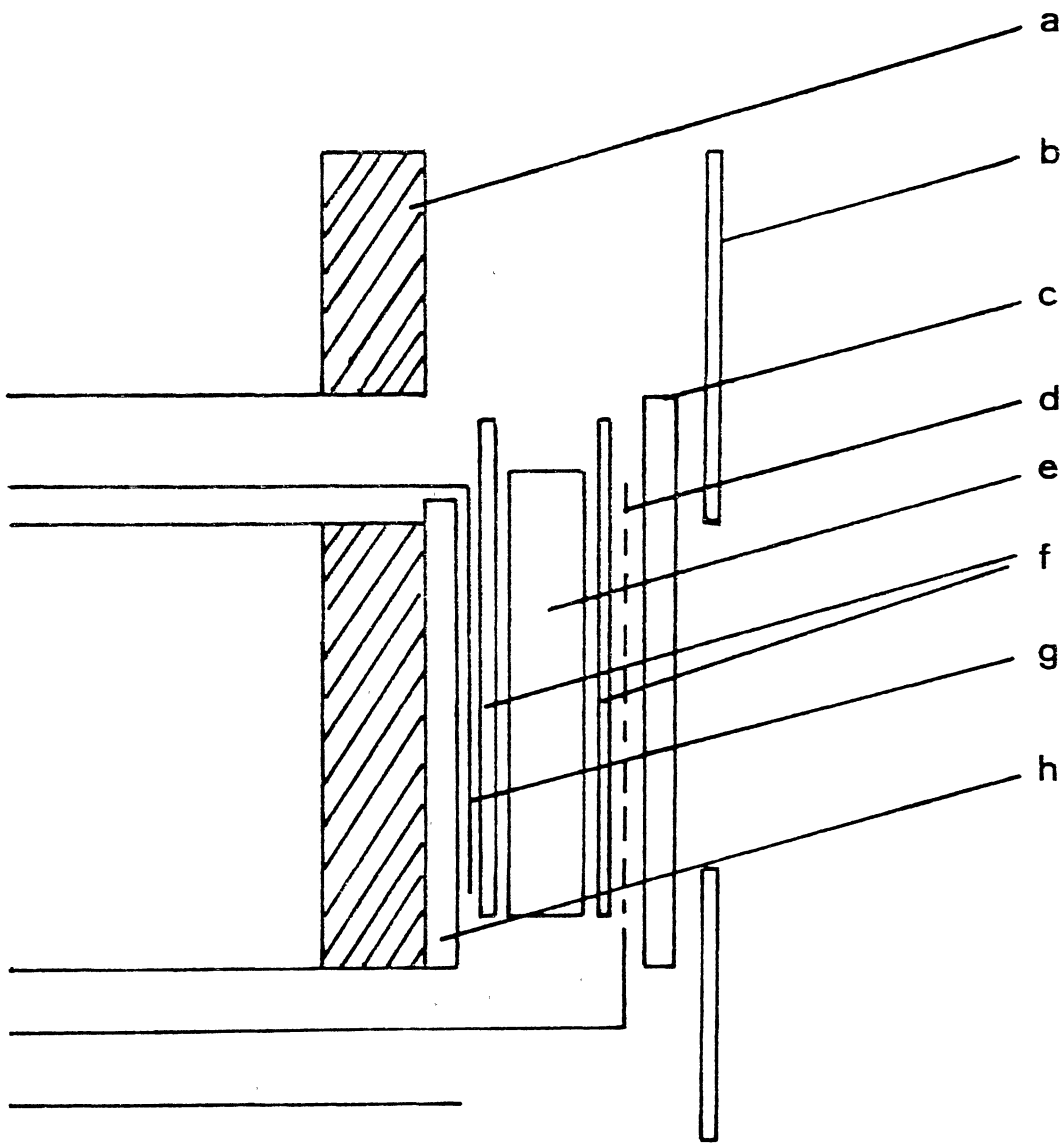

Figure 11. Schematic Diagram of the Experimental Arrangement for Photoconductivity

Sample Holder: a. cryostat tail, b. mask, c. quartz, d. phosphor-bronze screen, e. sample, f. sapphire plates, g. copper electrode, h. sapphire plate

light. This field is set up by a battery in the external circuit in series with the electrometer.

Light from the source was dispersed by McPherson 218 monochromator which had a linear dispersion of 2.6 nm/mm. With both slits set 2mm wide, the band width was a constant 5.3 nm and the reflection grating was blazed at 3000 A and had 1200 grooves/mm.

The light source was calibrated in a separate experiment by placing a Molectron 100 pyroelectric radiometer at the sample position. The radiometer was used to determine the power, in μ watts, of the incident light falling on the front surface of the sample holder as a function of wavelength. For a given wavelength, x, of the incident light, the number of photons/sec, $n_{\lambda o}$, striking the front surface of the sample assembly is given by $n_{\lambda o} = p\lambda/hc$ where p is power in μ watts, h is Planck's constant, and c is the speed of light.

The photoconductivity measurements were made with the sample holder shown in Figure 11. The sensitive electrode g, made up of copper foil 0.05 mm thick, 3 mm wide and 8 mm long, was connected to the electrometer. This electrode was electrically insulated from the copper tail of cryostat, a, by a sapphire plate, h, 0.25 mm thick. The incident light passes into the crystal, e, through the front electrode, d, a phosphor-bronze screen of 0.55 mm diameter wire and 100 mesh. The screen was held against the crystal by a sapphire plate, c, which was supported by phosphor-bronze springs. Sapphire plates, f, 0.25 mm thick could be placed on either side of the crystal between the crystal and the corresponding electrode to prevent charge from entering or leaving the sample. The screen electrode assembly transmitted about 35% of the incident light.

A shielded lead connected the phosphor-bronze screen electrode to a battery in the external circuit which produced an electric field, typically about 500 v/cm, in a direction parallel to that of incident light. The direction of the applied electric field could be reversed after individual measurements to prevent polarization effects in the sample.

The sensitive electrode was connected, by a shielded lead, to the input of a Cary 401 vibrating reed electrometer which could be used in either the "rate of charge" or current mode. The output of the electrometer was fed to an Omnigraphic Y-t potentiometric recorder.

E. Electrical Conductivity

In the electrical conductivity or dark current measurements almost the same set up as described above was used except in this case no light source was necessary and as such no monochromator. Whenever it was necessary to excite F band light for CaO and MgO, a suitable interference filter in conjunction with the source was used. Details of this are given in the experimental results in Chapter IV.

F. Thermoluminescence

Thermoluminescence occurs when electrons (holes) are thermally released from a trap and radiatively recombine with holes (electrons) trapped at another site. In TL, what is measured is the light given off when electron-hole recombination occurs at some site. The transition energy will be determined by the nature of the recombination center whereas the light intensity is proportional to the number of recombination sites which have captured carriers. The key equation

describing the thermoluminescence is

$$I = -\lambda \frac{dn}{dt} = nNva\lambda \rightarrow \quad (5)$$

where, I = light intensity

λ = constant of proportionality

N = # of trapping sites/cc

n = # of carriers/cc

v = carrier velocity

a = capture cross section

This equation shows that the light intensity, which is directly proportional to the rate of radiative recombination, reflects the concentration of thermally released carriers. The constant of proportionality, λ varies more slowly with temperature than the other variables.

In actual experiments the samples were cooled down to low temperature, then illuminated with ultraviolet light for few minutes and then warmed up at a rate of 5°K per minute. The Oxford Instruments cryostat heater heats the sample up to room temperature. Temperature above 300K were achieved by a constantum heating coil wound around the cold finger of a cryostat. Standard potentiometric techniques were employed for monitoring temperatures. The cryostats were equipped with copper vs. constantum thermocouples attached to the tail piece near the sample.

G. Decay Kinetics

Decay kinetics in MgO and CaO were studied at different temperatures with emphasis given on the kinetics of decay near the thermoluminescence peaks, one near room temperature, the other at low temperature.

Luminescence was excited in the samples by two different sources for two different materials. For MgO, a 60 W deuterium lamp in conjunction with a 230 nm interference filter was used. For CaO a 150 W xenon lamp in conjunction with a CS 5-58 was used to select the F-band light. The emitted light was detected with photomultiplier tube (EMI 9313B for MgO and thermoelectrically-cooled C31034 for CaO) and was recorded on a Y-t recorder. Sharp cut-filter Corning CS-3-71 in the case of MgO and CS 3-67 for CaO were used to cut off stray light. In each case the sample was illuminated until the emission reached a maximum intensity and then the excitation was removed. Decay which lasted for several minutes for samples with high concentration of H^-, were studied extensively and the natures of these decays are reported in the next chapter.

H. Infrared-Stimulated Emission

In the experimental arrangement luminescence was excited in the sample by exciting the main $^1A_{1g} - {}^1T_{1u}$ absorption transition of the F center using radiation from a 150 W xenon lamp which was dispersed by a 0.25m Spex monochromator used in conjunction with suitable glass filters. Emission was detected by a thermoelectrically-cooled C31034 photomultiplier tube after passing through sharp cut filters to cut off stray light. The luminescence from this excitation was allowed to reach

maximum intensity and the excitation was removed by closing the shutter. This long-lived luminescence near room temperature was then suddenly quenched by forcing liquid nitrogen into the dewar. The sample temperature then dropped to 78K in few seconds. The luminescence was then reactivated at this low temperature by giving a short pulse of low energy light (much lower than F center light) to the sample. This is done by replacing the filter quickly by another filter which allows much lower energy light, during the time when the luminescence was decaying at room temperature. A schematic diagram of the experiment is shown in Figure 12.

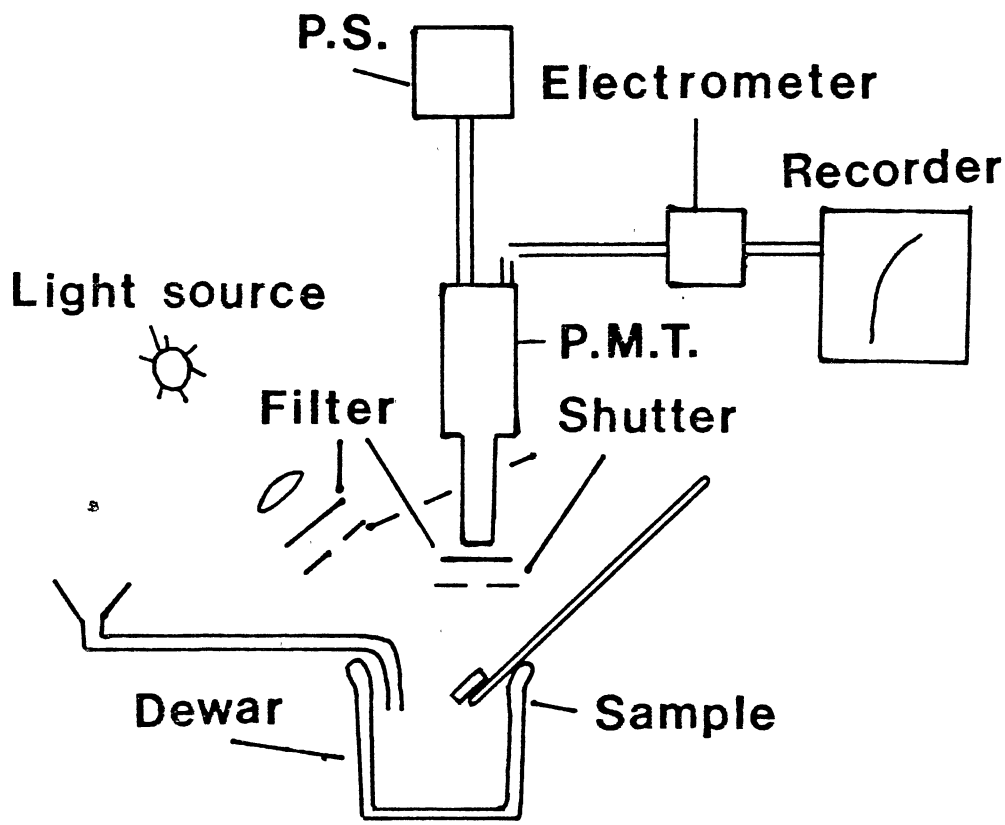

Figure 12. Schematic Diagram of the Experimental Arrangement for Infrared Stimulated Emission Experiment

CHAPTER IV

EXPERIMENTAL RESULTS AND DISCUSSIONS

A. Introduction

In the previous chapters experimental and theoretical studies made on F center luminescence in MgO and CaO have been surveyed. Studies made on the recently detected H^- ions in these samples have also been discussed and infra-red absorption lines from the local mode oscillation of these H^- ions have been described. In this chapter we will show the results of further studies made on MgO and CaO which were thermochemically reduced and also discuss the role of hydrogen on these results.

The characteristics of the different samples of MgO and CaO, used in this study are given in table III and table IV respectively, where the concentrations of F and F^+ centers were calculated from the intensity at the absorption peak and the formulae given in Chapter III. The concentration of H^- ions were obtained from the intensity of the infrared absorption peak and the formulae shown in Chapter III. Although it is possible to minimize the concentration of hydrogen introduced into MgO crystals during the growth, because of the hygroscopic nature of CaO, it is almost impossible to grow CaO without hydrogen. However the concentration of H^- ions in CaO can be lowered by electron irradiation. After the irradiation the infrared absorption at 911 cm^{-1} vanished and that at 880 cm^{-1} decreased[51]. The different

TABLE III

CHARACTERISTICS OF THERMOCHEMICALLY REDUCED MGO SAMPLES

Sample	$n_F(cm^{-3})^a$	$n_H(cm^{-3})^b$
MgO I	1.6×10^{18}	3.0×10^{18}
MgO II	4.1×10^{18}	1.3×10^{17}
MgO III	5.5×10^{17}	5.4×10^{16}
MgO IV	3.7×10^{18}	1.6×10^{17}
MgO V	2×10^{17}	6.3×10^{16}

a. Calculated using the formula given in Ref. 17 and Chapter III.

b. Calculated using the formula given in Ref. 37 and Chapter III.

TABLE IV

CHARACTERISTICS OF THERMOCHEMICALLY REDUCED CaO SAMPLES

Sample	$n_F(cm^{-3})^c$	$n_H(cm^{-3})^d$
CaO I	$< 1 \times 10^{15}$	7×10^{16}
CaO II	6×10^{16}	2×10^{16}
CaO III	$> 5 \times 10^{17}$	2.7×10^{16}
CaO IV	$> 5 \times 10^{17}$	1.2×10^{17}
CaO VI	$> 5 \times 10^{17}$	9.4×10^{16}

c. Calculated using the formula given in Ref. 51 and Chapter III.

d. Calculated using the formula given in Ref. 51 and Chapter III.

samples of MgO and CaO with different concentration of F center and H^- ions were used to investigate how these concentrations influence the optical and electrical properties of the crystals.

Previous results[17] have shown that the lifetime of the 2.3 eV luminescence at room temperature in MgO depends on the concentrations of both F centers and H^- ions. The results of an in-depth study on the nature of this 2.3 eV luminescence in MgO and 2.0 eV luminescence in CaO near room temperature and also at low temperatures will be reported and how the concentration of H^- ions and F centers in the sample affect the decay kinetics of F center luminescence will be discussed. A theoretical model will be given to explain these results.

The activation energy for thermal release of electron from $H^=$ ions will be calculated from the thermoluminescence and decay experiments using the "cross cut" method. The results show that electrons can escape to the conduction band from $H^=$ ions at room temperature in both MgO and CaO. The motion of these electrons through the conduction band gives rise to a dark current at room temperature. Although Roberts and Crawford[38] reported this dark current in thermochemically reduced MgO, they could not account for its origin. The experimental results reported[39] recently, indicate that H^- ions in the sample are the cause of this dark current. How this dark current changes with the concentration of H^- ions in the samples and also with temperature will be discussed.

B. Thermoluminescence

Thermoluminescence experiments were carried out in both hydrogen rich and hydrogen free samples of MgO and CaO. The measurements were

made in each case over two different temperature ranges 20-300 K and 77-500 K and the two sets of data were normalized at 220 K. In each case the sample was cooled to the starting temperature, illuminated with F band light for few minutes and then heated at a rate of ~ 0.1 K s^{-1} .

Figure 13 shows the results of TL experiment on MgO I which is hydrogen rich and MgO III which is almost hydrogen free. The result shows that the intensity of the TL peak at 260 K depends clearly on the concentration of H^- ions in the sample, therefore, this peak is attributed to the release of electron from unstable $H^=$ ions. Similar results were found in CaO, shown in Figure 14 in which CaO IV is hydrogen rich and CaO III is almost hydrogen free. In this material also the intensity of near room temperature 320 K TL peak was found to decrease dramatically when the concentration of H^- ions in the sample was lowered.

Although the near room temperature peak in both MgO and CaO has been identified and attributed to the release of electrons from unstable $H^=$ ions, there is also another peak at low temperature in both these samples, the exact origin of which is not known. There is no direct correlation with the concentrations of H^- ions in the sample and the TL intensity at low temperature. For MgO, this peak lies at 40 K and for CaO at 80 K. Therefore the TL experiments show that in both thermo-chemically reduced samples of MgO, and of CaO there exists shallow electron traps which become unstable at lower temperatures, and therefore have much smaller trap depth or activation energy compared to the $H^=$ ion traps. The activation energies estimated from the temperatures of the TL peaks are ~ .086 eV and ~ .12 eV for MgO and CaO respectively compared to 0.56 eV and 0.74 eV of $H^=$ ions in MgO and CaO,

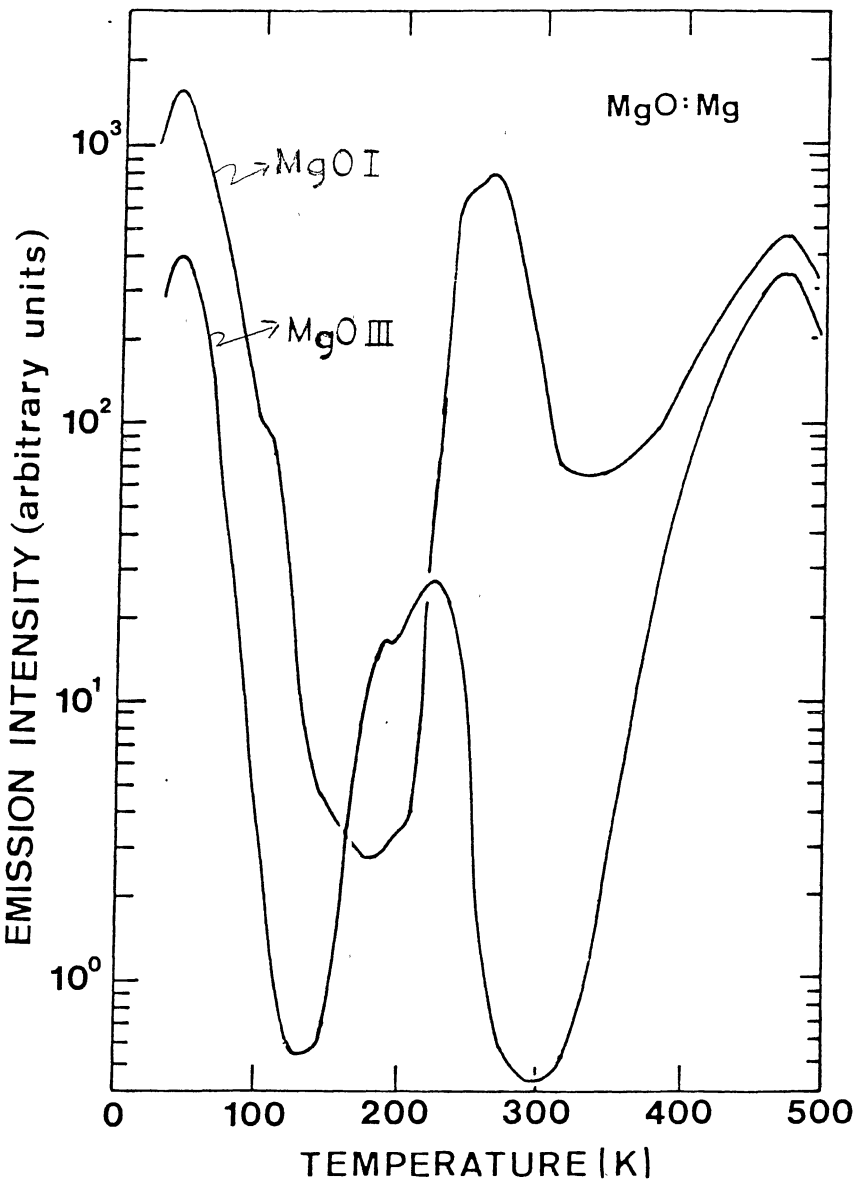

Figure 13. Thermoluminescence in MgO

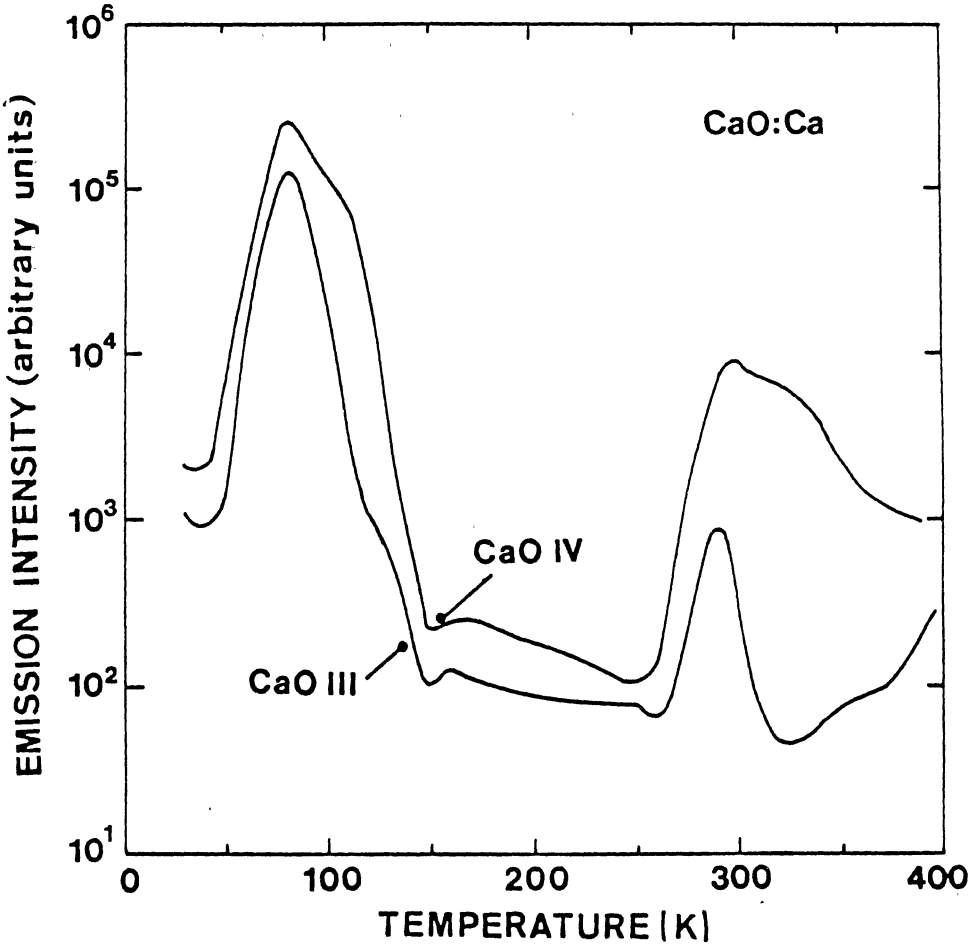

Figure 14. Thermoluminescence in CaO

calculated by separate measurements[44] which will be described in the next section.

As discussed in the previous chapter Gonzalez et al.[4] suggested that the presence of more than one line in the infrared absorption spectra of MgO and CaO, is possibly due to local mode vibrations of H^- ions located at different sites which are distinguished by different local charge compensators, for example. Release of electrons from these $H^=$ ions, which would be in an environment of different charge compensators, may be the cause of the low temperature TL peaks as has been suggested by Summers et al.[16] and Summers and Chakrabarti[40].

Another possible explanation of the low temperature TL peak has been suggested by Wilson[41]. His calculations show that the excited state orbitals of the F center and $H^=$ ions are quite diffuse. Because of the extended nature of the excited states of $H^=$ ions and F centers, they may overlap, especially in samples containing large concentrations of $H^=$/F center pairs. Electrons could therefore be trasnferred from an $H^=$ ion to the excited state of an F center by a tunneling mechanism.

Although the nature of the shallow trap is not certain, it does play an important role at low temperature. The activation energy of this shallow trap is about one seventh the activation energy of the deeper trap (H^- ion) in CaO and about one sixth of the energy of the deeper trap in MgO. At room temperature, therefore, the shallow traps are mostly empty and are expected to play little role in the decay kinetics of F center luminescence at room temperature. Therefore the nature of the F center luminescence at room temperature is essentially guided by the concentration of H^- ions. However, at low temperature, near the TL peak, the decay kinetics of F center luminescence is more

complex, because at low temperature not just the shallow traps play a dominant role, but also the deep traps are important. This will be discussed in detail in the next sections with experimental result and a theoretical model, which explains the decay kinetics near the two TL peaks.

Results of the thermoluminescence experiments bring out some valuable information about the traps, charge motion and trapping mechanism in these crystals. Also the intensity of TL peak enabled us to compare the concentration of shallow traps in various samples of MgO and CaO studied. Although the number of H^- ions can be calculated directly from the equation in Chapter III and the intensity of the infrared absorption, the exact concentration of shallow traps cannot be calculated directly. The knowledge of these shallow traps and their thermal activation energy obtained from the TL experiments are very important in understanding the decay kinetics of luminescences in these crystals. Furthermore, from the results of the TL a model has been proposed whichs explain phenomenlogically the infrared stimulated emission from oxygen ion vacancies in MgO and CaO. Also, it is the knowledge of the deep traps and their thermal activation temperature obtained from the TL experiments, that helped us to explain the dark current in these samples and to interpret the electrical conductivity experiments monitored the charge motion at RT. All these experimental results will be discussed in this Chapter.

In case of MgO there is a third TL peak at ~ 470 K, as is seen in Figure 13. This peak has been reported before[42] and attributed to the thermal release of electrons from iron impurity in the sample and can act as an electron trap to become Fe^+ centers. TL occurs after the

electrons are released from Fe^+ centers and get captured by F^+ centers. This model has been confirmed by the paramagnetic signal obtained from Fe^+ ions and F^+ centers after bleaching the sample with 5 eV F band light at 4.2 K and also from the TL spectrum which resembles with 2.3 eV photoluminescence band. This TL peak is, however, not of direct interest in this study.

C. Decay Kinetics

When F centers in both MgO and CaO are optically excited at room temperature there is a very high probability that electrons are released to the conduction band. These electrons then move through the conduction band and are continually trapped and released by H^- ions before being ultimately captured by a F^+ center, producing F center luminescence. The lifetime of this luminescence changes with the concentration of H^- ions in the sample. As was shown by Jeffries et al.[15], MgO I which has a high concentration of both F centers and H^- ions has a life time of ~ 330 s, whereas MgO III which has a much lower concentration of H^- ions has a life time of ~ 3s. In this section we will describe investigations made on the decay kinetics of F center luminescence as a function of H^- ion concentration and the temperature.

The study of the decay kinetics in various samples of MgO and CaO indicate that at room temperature the samples with long lifetime, i.e., with high concentration of H^- ions, exhibit second order decay after a relatively brief transient process is over. For a second order process it is found that $I^{-1/2}$ is directly proportional to t, where I is the luminescence intensity at time t. The reason for this relationship is as follows. If x, is the number of unactivated luminescent centers then

$I = - dx/dt$. For a second order process

$$I = - \frac{dx}{dt} \alpha x^2$$

$$\frac{dx}{dt} = - k_2 x^2 \rightarrow \quad (1)$$

k_2 is a second order rate constant, therefore on integrating

$$\int_o^t dt = - \frac{1}{k_2} \int_{xo}^{x} \frac{dx}{x^2} \rightarrow \quad (2)$$

$$k_2 t = - \left[- \frac{1}{x}\right]_{xo}^{x} = \frac{1}{x} - \frac{1}{x_o} \rightarrow \quad (3)$$

$$\text{or } mt = \frac{1}{I^{1/2}} - \frac{1}{I_o^{1/2}} \rightarrow \quad (4)$$

where m is a constant

$$\text{or } \frac{1}{I^{1/2}} = mt + \frac{1}{I_o^{1/2}} \rightarrow \quad (5)$$

therefore, the plot of $1/I^{1/2}$ vs t for a second-order decay process produces a straight line.

For hydrogen rich MgO I, Figure 15 shows that the linear region of a plot of $1/I^{1/2}$ vs t after a transient period of only ~ 100s. In contrast a plot of $1/I^{1/2}$ vs t for MgO III, a relatively hydrogen free sample, results in a nonlinear curve up to a time of 700 s.

Similar behavior is noticed in CaO. Figure 16 shows the decay of F center luminescence with time in various CaO samples. With the same concentration of F centers in CaO IV and CaO II, the higher

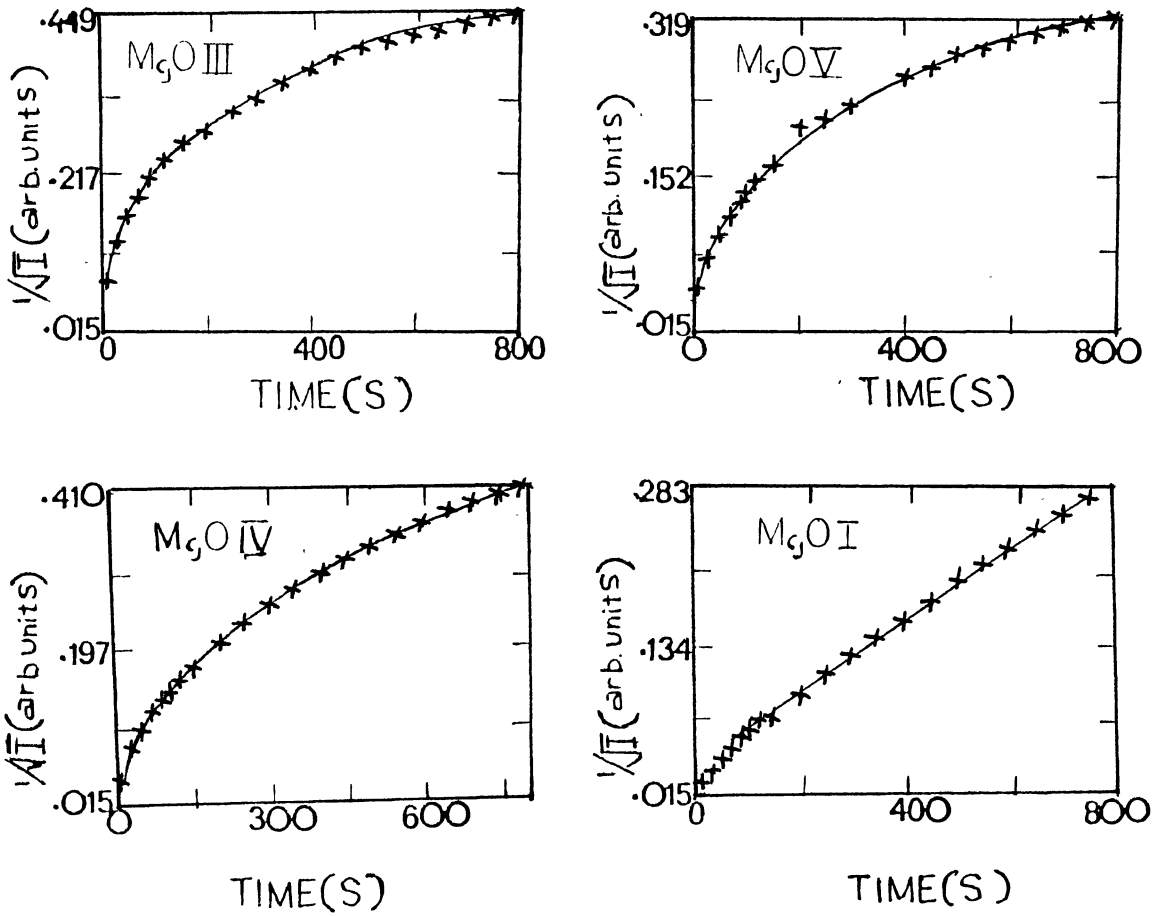

Figure 15. Inverse of Square Root of Intensity of F Center Luminescence Decay vs. Time in MgO at RT

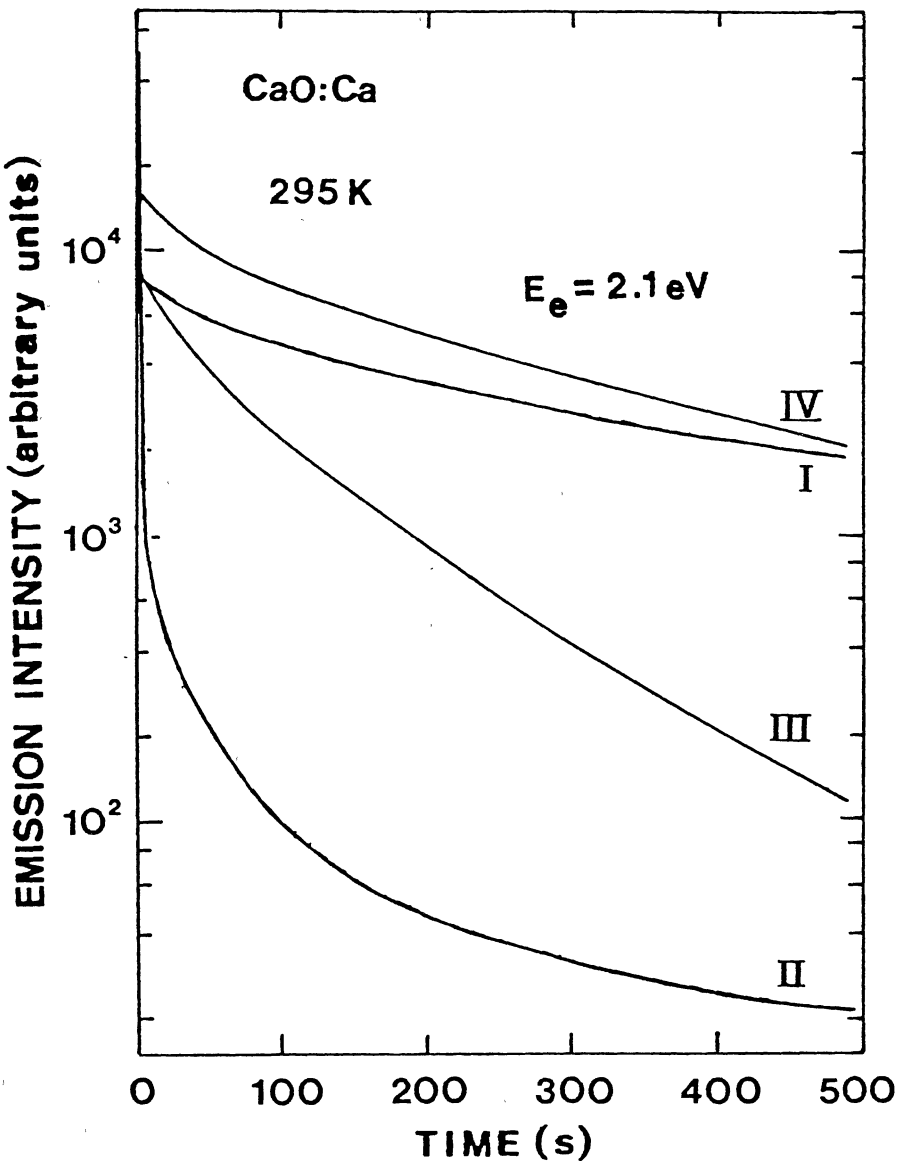

Figure 16. Lifetime of F Center Luminescence of Various Samples of CaO

concentrations of H^- ions in CaO IV causes longer lifetime of 640 s compared to lifetime of luminescence of 35 s in CaO II, having lower concentration of H^- ions. Similarly the onset of the second order decay is found to depend on the concentration of H^- ions. Figure 17 shows a plot of $1/I^{1/2}$ vs t for CaO IV and CaO II.CaO IV is a relatively hydrogen rich sample whereas CaO II has a relatively low concentration of H^- ions. CaO IV can be seen to exhibit a second order luminescence decay which is demonstrated by a long linear region in a $1/I^{1/2}$ vs t plot after a transient period of only 25 s. On the other hand CaO II $1/I^{1/2}$ was plotted with time up to 800 s, indicating that the decay kinetics at room temperature in CaO II, is not of the second order type.

We see that H^- ions, acting as electron traps, influence the decay kinetics of F center luminescence in both MgO and CaO in several ways. The presence of high concentrations of H^- ions cause these samples to have the following characteristics;

a. a strong TL peak near room temperature,

b. a relatively long life time for the F center luminescence,

c. a luminescence decay of a second order type after a only relatively short transient period.

Since the luminescence decay kinetics at room temperature in these samples are complex and cannot be fitted to a single simple function, it is difficult to evaluate the activation energy of H^- ions electron traps by a straight forward "isothermal decay" method. Instead the activation energy was calculated using the methods called "cross-cut" method[43,44]. This method is useful, because it is applicable to complex decay kinetics. In this method the number of unactivated luminescent ion at any instant of time and temperature is involved rather than the

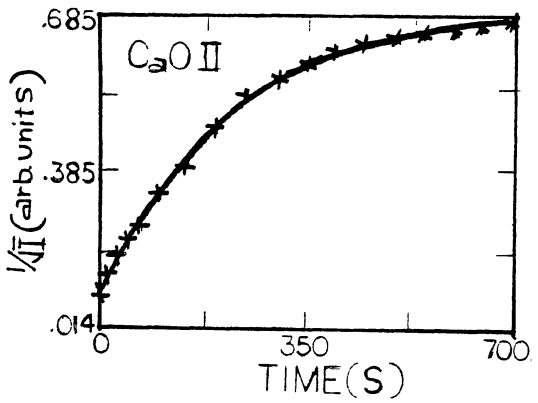

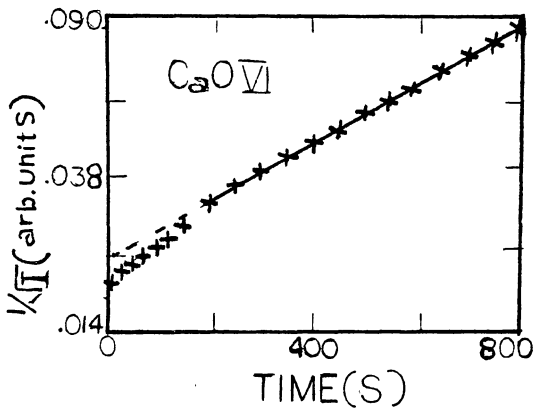

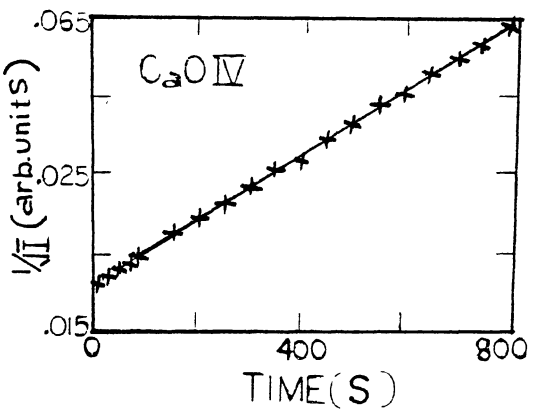

Figure 17. Inverse of Square Root of Intensity of F Center Luminescence Decay vs. Time in CaO at RT

intensity of the luminescence. We do this by calculating the light sum S(t) at time t, where

$$s(t) = \int_t^\infty I(t')dt' \tag{6}$$

It can be seen that the light sum represents the number of luminescent centers that remain unactivated at time t. We calculated s(t) at several temperatures such as 240 K, 250 K, 260 K and 270 K for MgO and at 300 K, 310 K, 320 K, and 330 K for CaO. The plots of the normalized light sum, which are s(t)/s(o) as a function of time are shown in Figure 18 and Figure 19. The calculation of the values of s(t) presented some computational difficulties. Each value was calculated in two steps. The second order part of the decay was extrapolated back to zero time using the equation

$$\frac{1}{I^{1/2}} = k_1 t + k_2 \rightarrow \tag{7}$$

$$I = \frac{1}{(k_1 t + k_2)^2} \rightarrow \tag{8}$$

This enables the integral S'(t) to be calculated as,

$$s'(t) = \int_t^\infty \frac{1}{(k_1 t + k_2)^2} = -\frac{1}{(k_1(k_1 t + k_2)} \Big|_t^\infty \tag{9}$$

Therefore, knowing the slope k_1 and intercept k_2 from the $1/I^{1/2}$ vs t plots, s'(t) can be calculated.

But in both MgO I and CaO IV, the non second order transient decay process is observed in the earlier part of the decay. This non second

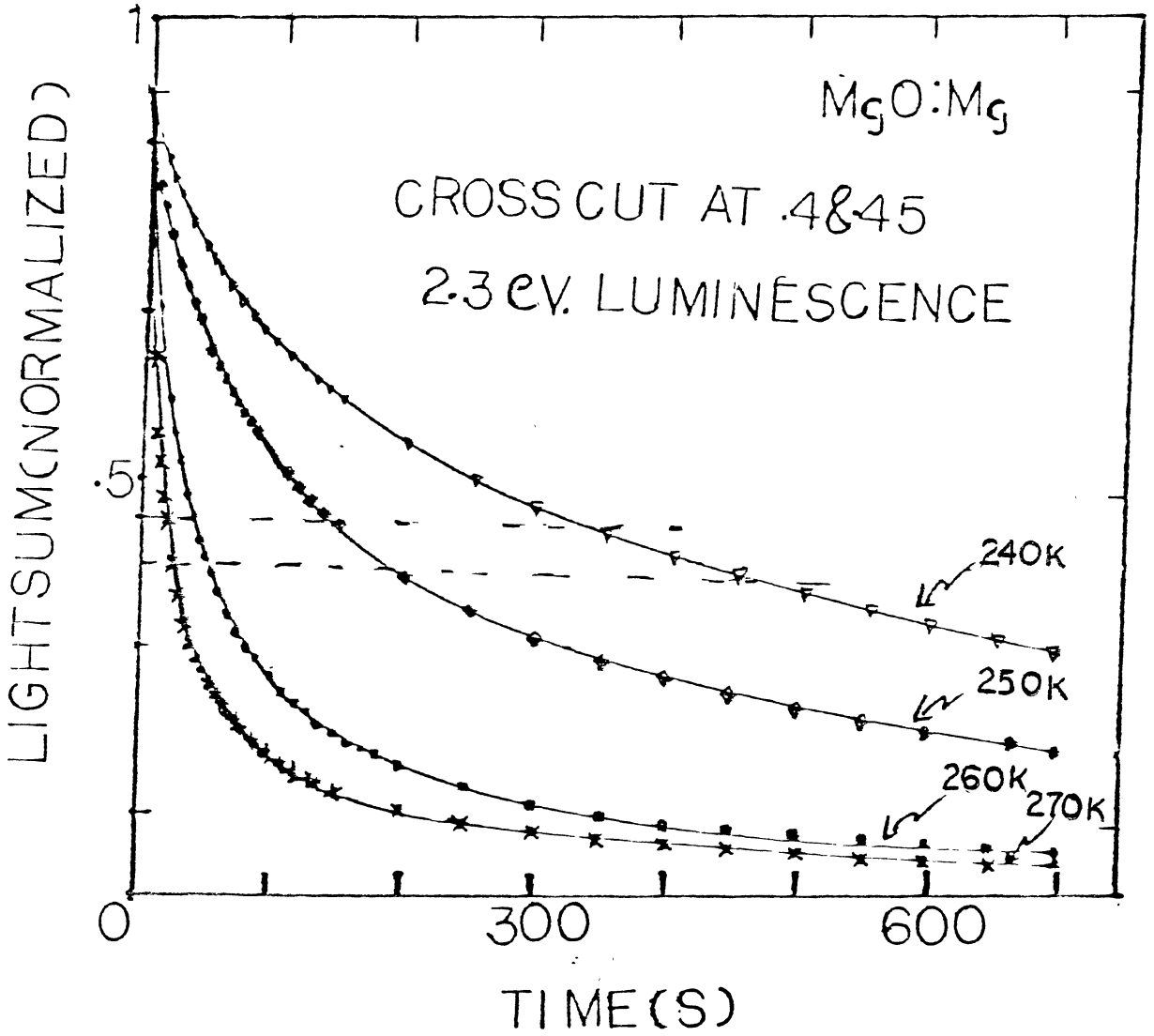

Figure 18. Plot of Normalized Light Sum vs. Time at Various Temperature Near Upper Temperature TL Peak in MgO

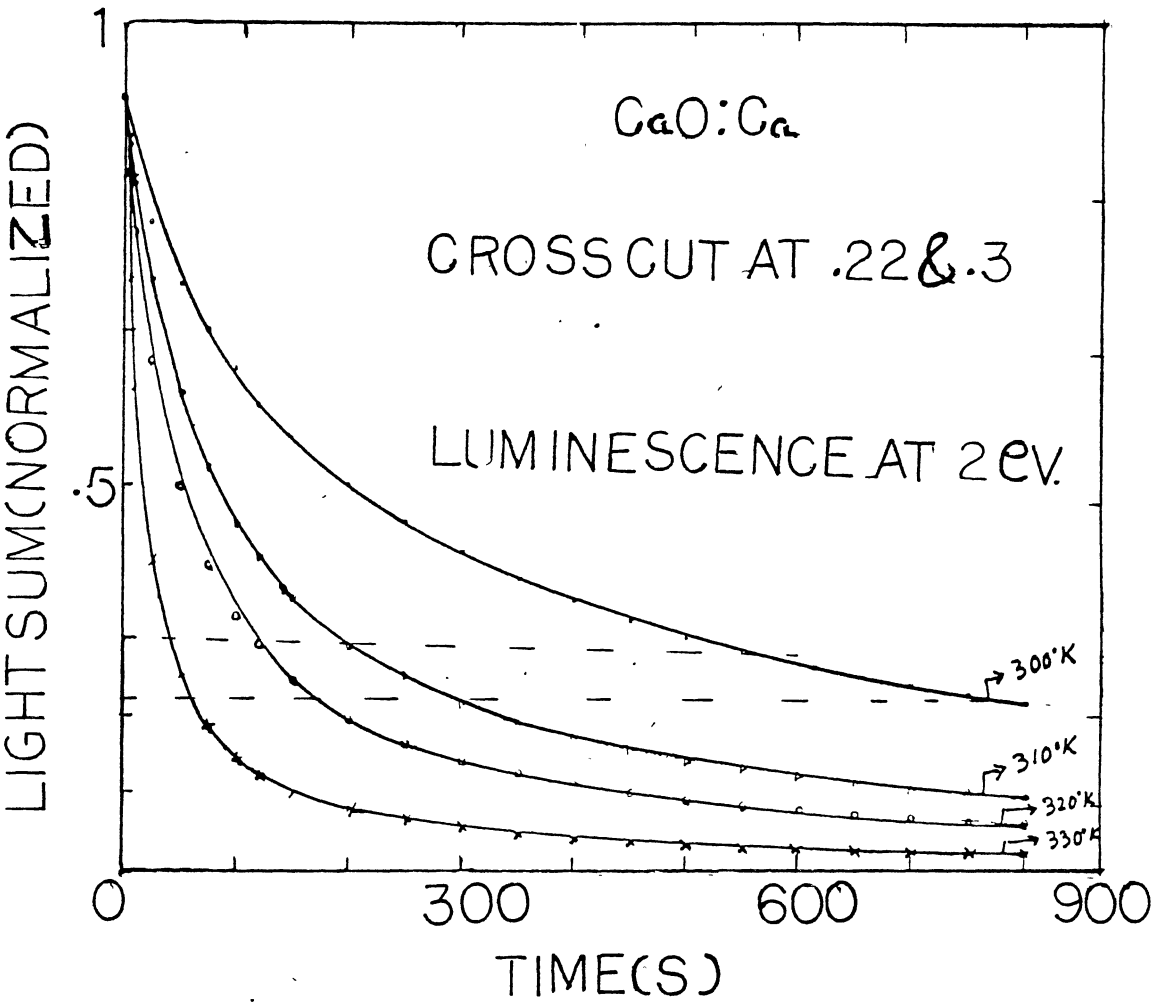

Figure 19. Plot of Normalized Light Sum vs. time at Various Temperature Near Upper Temperature TL Peak in CaO

order type decay is represented by the non linear part in $1/I^{1/2}$ vs plot as is seen in Figure 20 and Figure 21, whereas the major second order decay is reflected through the linear region of the plot $1/I^{1/2}$ vs t.

However, in this calculation, part of the luminescence decay curve is left out. This is the part during the initial-transient non-second order process. This was taken care of by evaluating this area graphically and by a weighing method. This contribution was then added to s'(t) at each temperature, obtained by (9) to obtain the total light sums s(t). The light sums were then normalized $\frac{s(t)}{s(o)}$ at each point, and were plotted against time to obtain Figs. (18) and (19).

The following is briefly a description of the cross cut method for calculating the activation energy from the plots of s(t). Suppose the rate of decrease of a certain defect can be written as

$$\frac{d\nu}{dt} = - K_o e^{-E/kT} P(\nu) \rightarrow \qquad (10)$$

where, ν is the fractional concentration of the defect remaining, $P(\nu)$ is a continuous function of ν; , and k_o is constant. Equation (10) can be integrated to give

$$- \int_{\nu(o)}^{\nu(t)} \frac{d\nu}{P(\nu)} = K_o t \, e^{-E/kT} \rightarrow \qquad (11)$$

Now, if two isothermal experiments are performed at two different temperatures T_1 and T_2 and during each experiment ν is measured as a function of t, then comparing the times t_1 and t_2 when the concentrations are the same, i.e., when $\nu(t_1,T_1) = \nu(t_2,T_2)$, it can be set

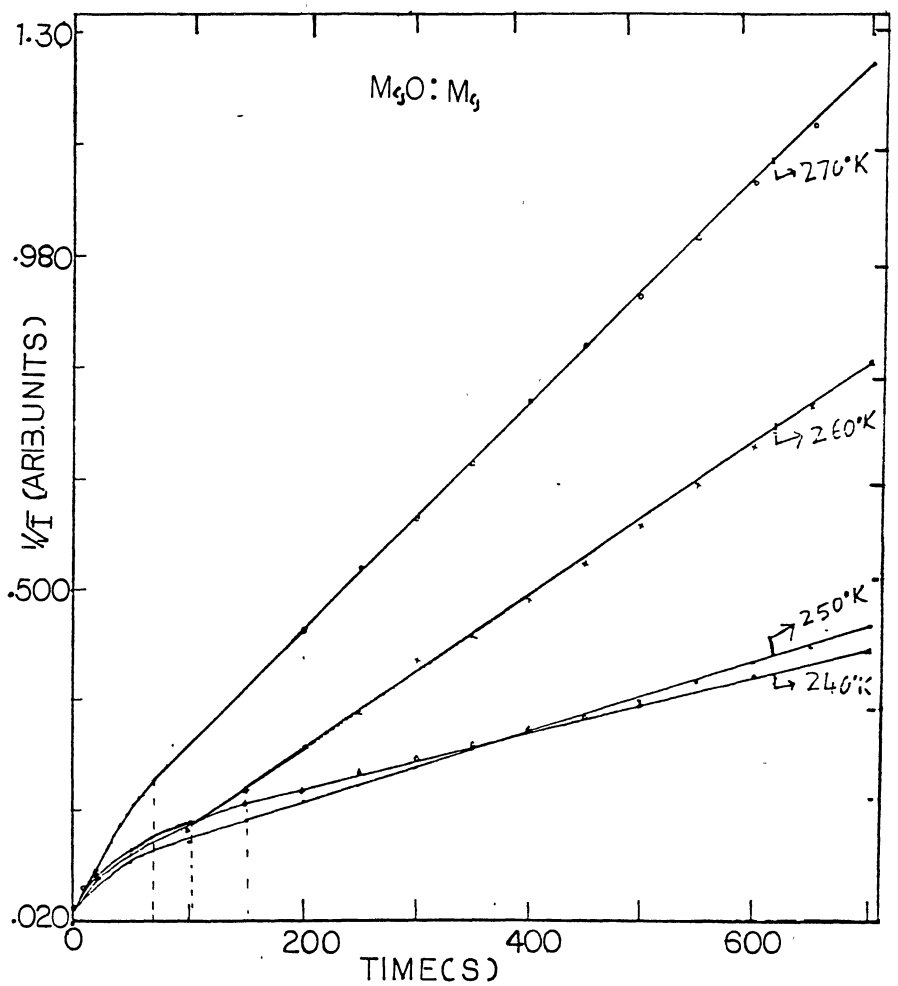

Figure 20. Plot of $1/I^{1/2}$ vs. t at Various Temperatures Near Upper Temperature TL Peak in MgO

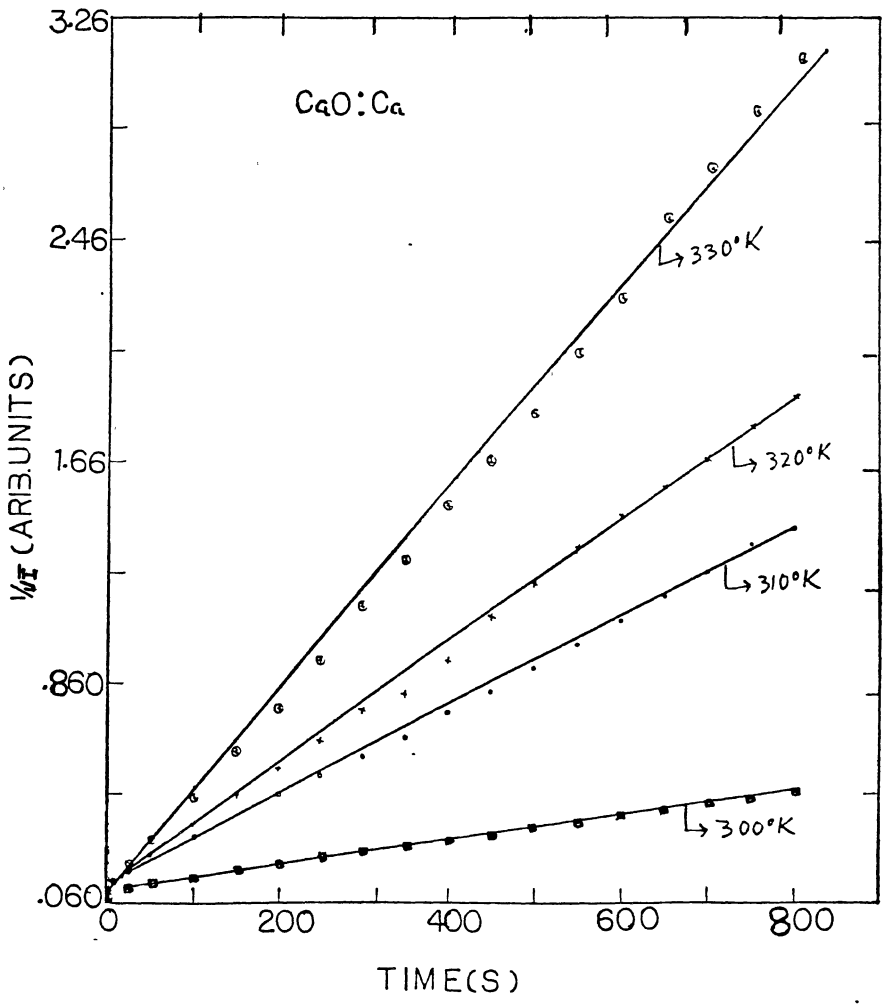

Figure 21. Plot of $1/I^{1/2}$ vs. t at Various Temperatures Near Upper Temperature TL Peak in CaO

$$\int_{\nu(o)}^{\nu(t_1,T_1)} \frac{d\nu}{P(\nu)} = -\int_{\nu(o)}^{\nu(t_2,T_2)} \frac{d\nu}{P(\nu)} \rightarrow \quad (12)$$

i.e.

$$t_1 e^{-E/kT_1} = t_2 e^{-E/kT_2} \rightarrow \quad (13)$$

$$\text{or, } \ell_n(t_1/t_2) = (E/k)(1/T_1 - 1/T_2) \rightarrow \quad (14)$$

If more than two experiments are performed, then for a given $\nu(t_i,T_i)$ the times and temperatures are related by

$$\ell_n(t_i) = (E/k)(1/T_i) + \text{constant} \rightarrow \quad (15)$$

The subscript i stands for ith experiment.

In Figure 18 and 19, the horizontal dashed lines are typical cross cuts. These are taken at 0.40 and 0.45 for MgO and 0.22 and 0.30 for CaO. Figures 22 and 23 are the plot of $\ln(t_i)$ vs $1/T_i$ for MgO from the respective cross-cuts. Similarly, for CaO, these are represented in Figures 24 and 25.

The experimental points were computer-fitted to a straight-line. The starts show the calculated points. Computer-fit of these lines are also indicated with different symbols. From the slope of these lines, the activation energy for thermal release of electrons from $H^=$ ions are, calculated to be equal to 0.56 ± .02 eV for MgO and 0.74 ± .04 eV for CaO.

The experimental results indicate that the major component of the upper temperature TL peak is due to electrons released from $H^=$ ions, and

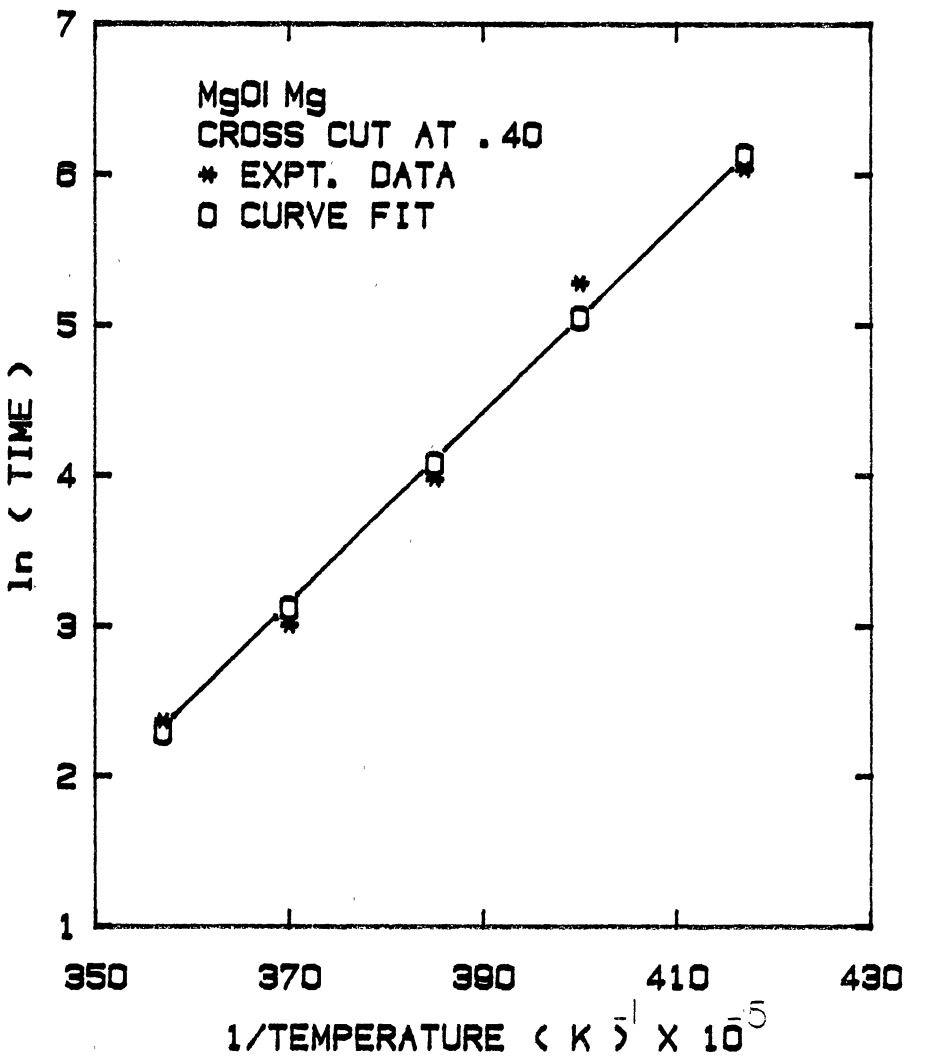

Figure 22. Log of Time vs I/Temperature Plot in MgO From the Cross-Cut at .40

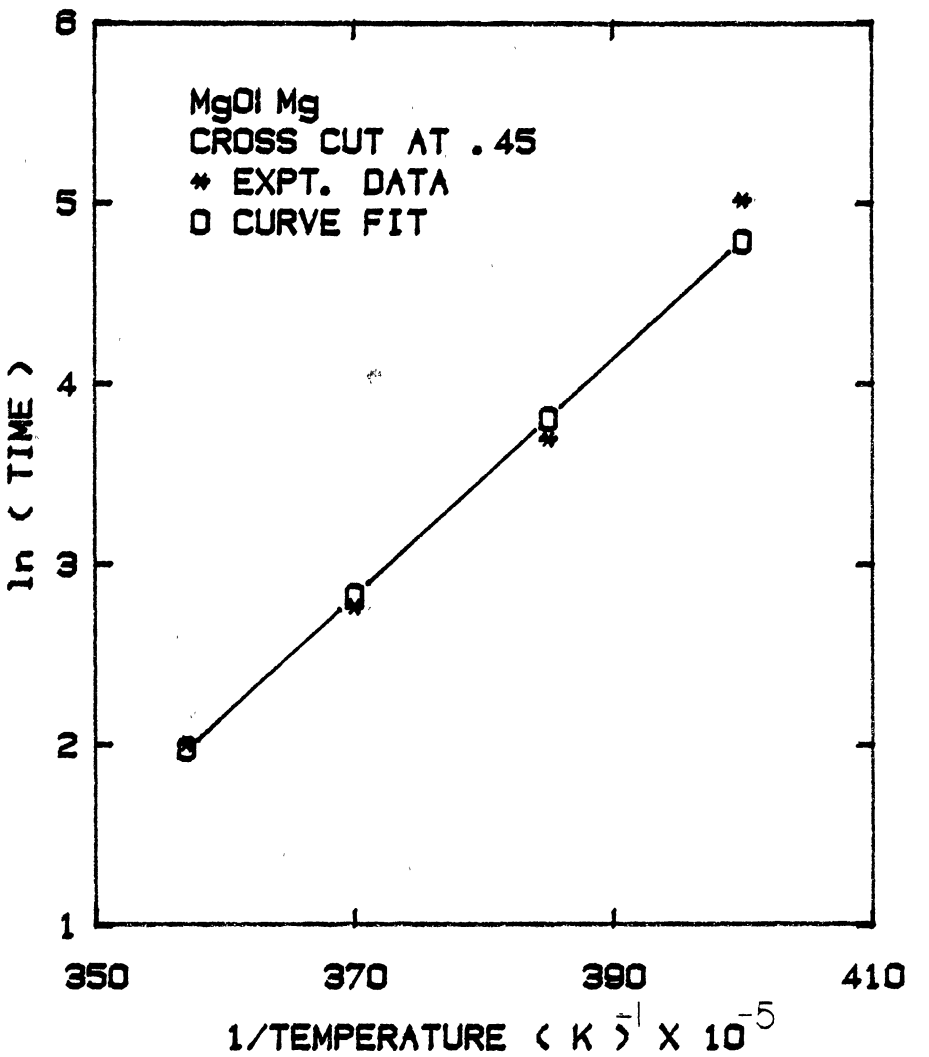

Figure 23. Log of Time vs. 1/Temperature Plot in MgO from the Cross-Cut at .45

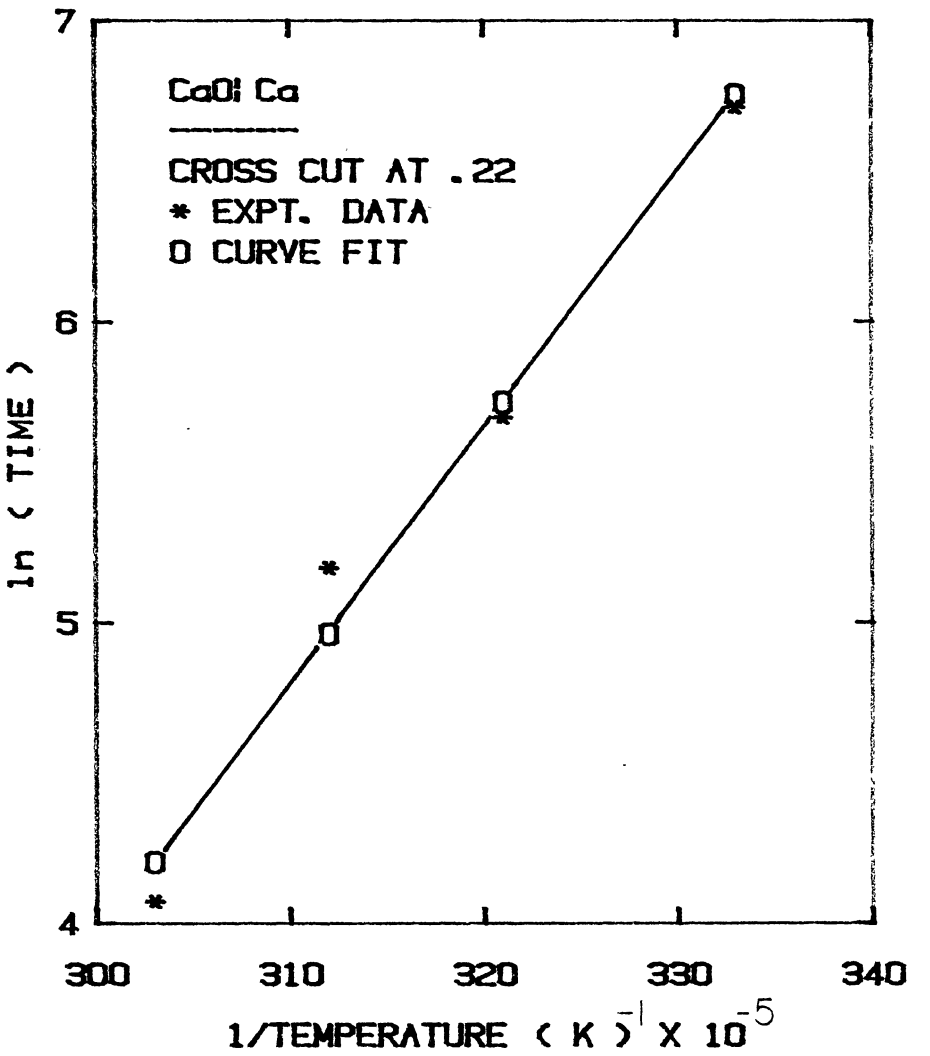

Figure 24. Log of Time vs. 1/Temperature Plot in CaO from the Cross-Cut at .22

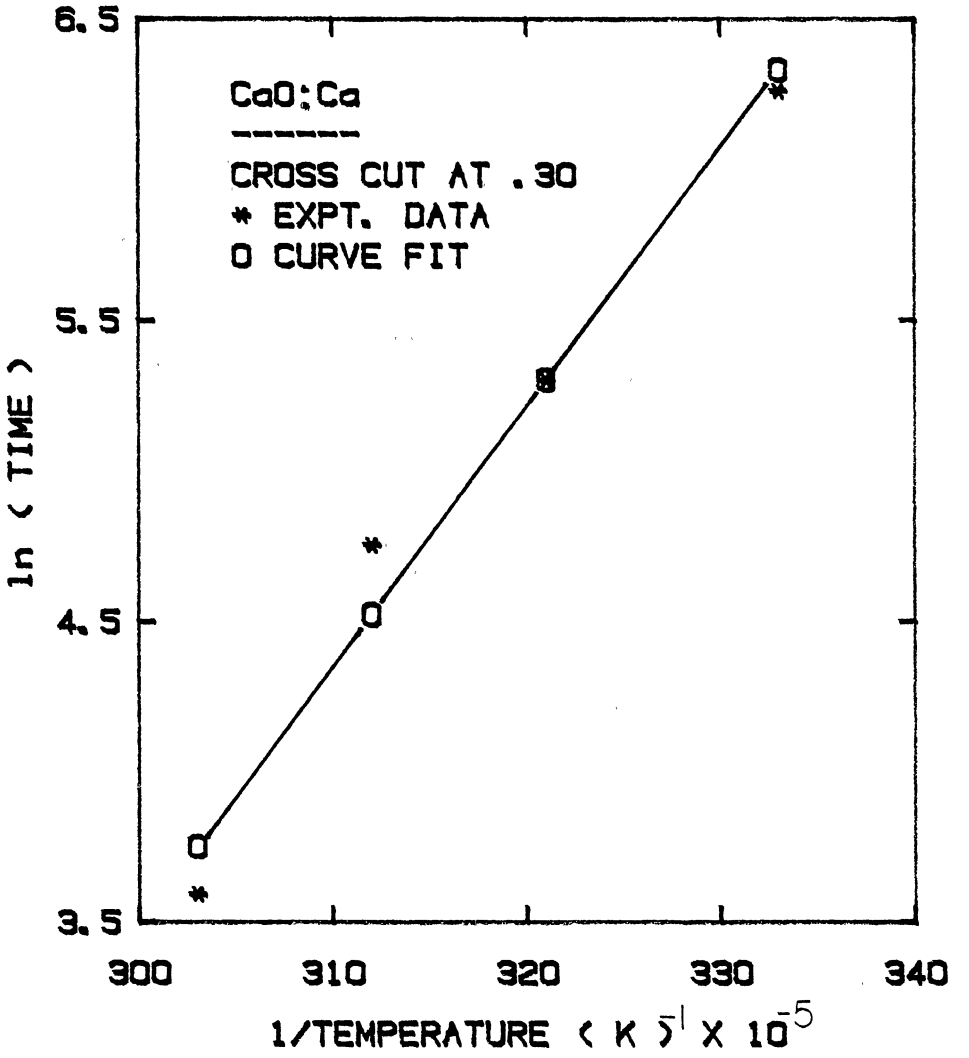

Figure 25. Log of time vs. 1/Temperature Plot in CaO from the Cross-Cut at .30

the variance of concentration of H^- ions in the sample significantly changes the intensity of this upper temperature TL peak. However, the intensity of the low temperature TL in either CaO or MgO does not change appreciably from sample to sample even when there is considerable differences in H^- ion concentration. The exact origin of this TL is currently not known. However, we have estimated the activation energy of the trap responsible for the low temperature TL peaks using $E(eV) = 25\ k\ T_m(k)$ where E(eV) is the activation energy, k the Boltzmann Constant and T_m is the temperature where the TL peak lies[53]. The activation energies were found to be equal to 0.086 eV for MgO and 0.12 eV for CaO.

It can be seen from the activation energies that the trap depth of the deep traps is about six times the trap depth of the shallow traps in both MgO and CaO. So at room temperature where the thermal release of electrons from deep traps take place, the shallow traps are essentially empty and play no significant role in F center luminescence at room temperature. Lifetime of F center luminescence and kinetics of the decay of luminescence at room temperature is therefore dictated by H^- ions, the deep traps, which is seen in results of Jeffries for MgO in Figure 4 and Figure 16 for CaO.

We next investigated the decay of F center luminescence near the low temperature TL peak, i.e. at ~ 40 K for MgO and ~ 80 K for CaO. Plots of $1/I^{1/2}$ vs t for several samples of MgO and CaO are shown in Figure 26 and Figure 27. In MgO III, the decay is second order after only a short transient decay, whereas in MgO I, the decay is not second order type as $1/I^{1/2}$ vs t produces a nonlinear curve. In both MgO I and MgO III, concentration of shallower traps appear to be comparable as is

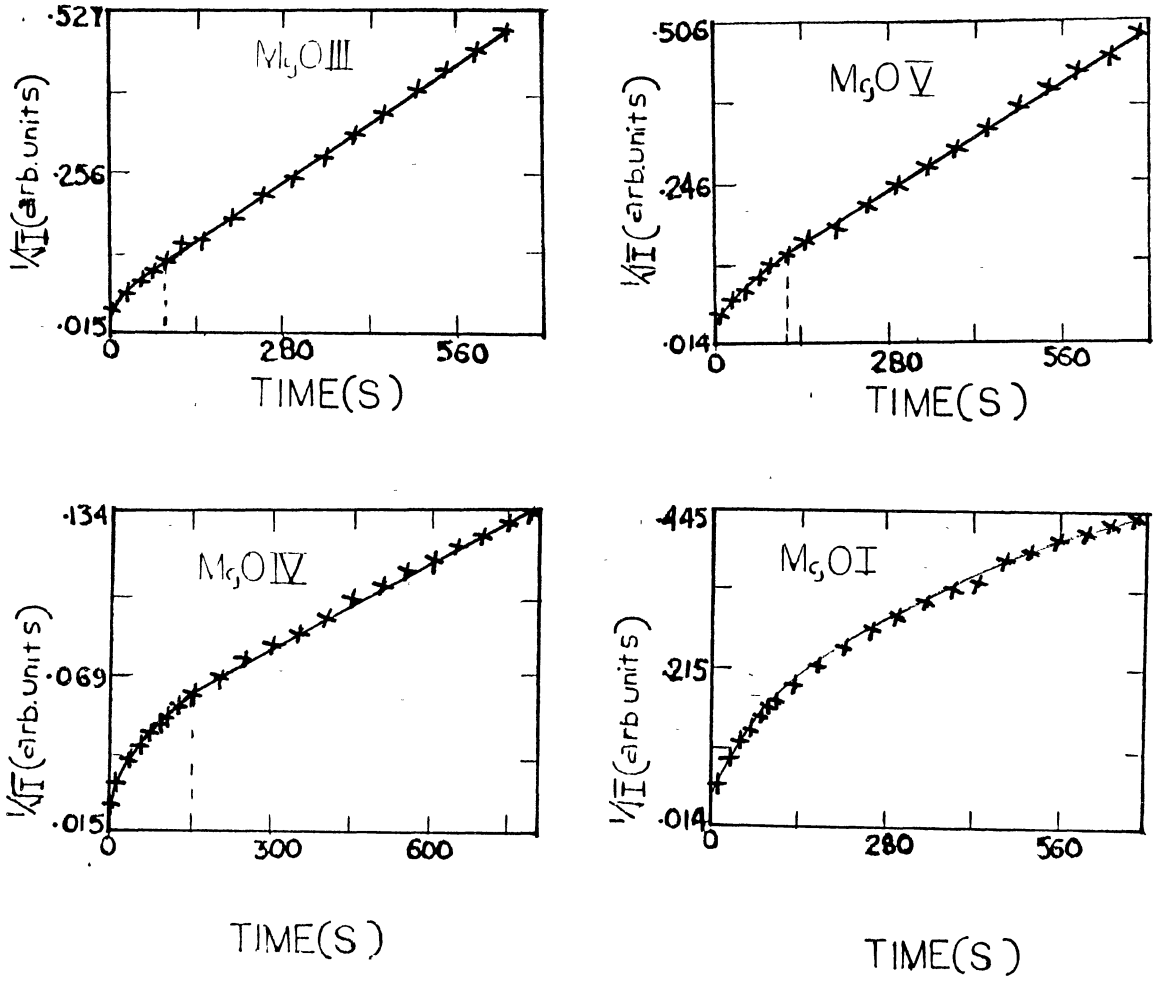

Figure 26. Inverse of Square Root of Intensity of F Center Luminescence Décay vs. Time in MgO at 40 K

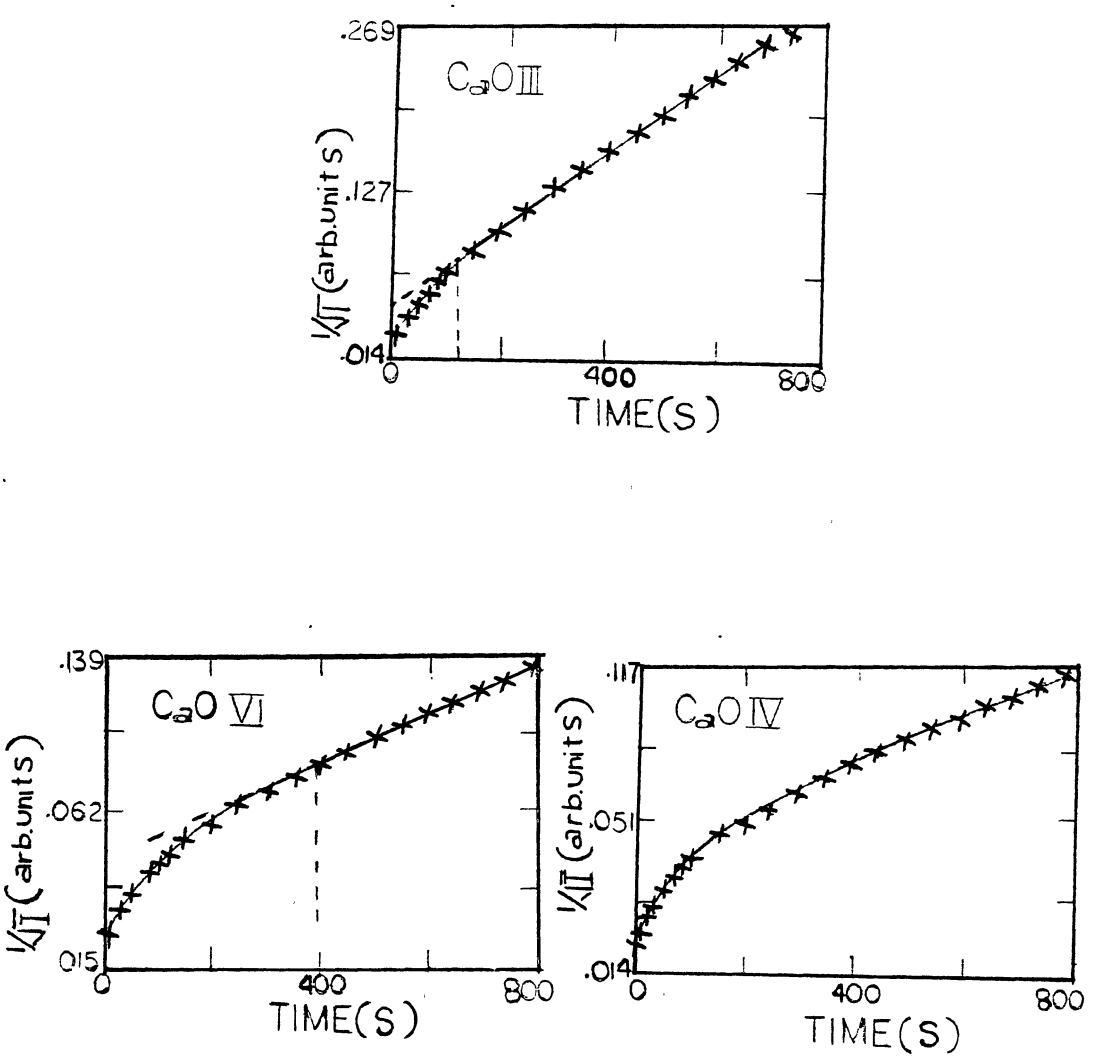

Figure 27. Inverse of Square Root of Intensity of F Center Luminescence Decay vs. Time in CaO at 80 K

seen by the comparable intensity of the low temperature TL peak. It is apparent that the concentrations of deeper traps are also influencing the kinetics of decay at low temperatures. In MgO I which has a relatively high concentration of H^- ions, the decay kinetics is of non second-order type, whereas in MgO III with a relatively low concentration of H^- ions, the second order decay starts after only 105 sec. We estimate the start of the second order process as the time where the linearity begins in a $1/I^{1/2}$ vs t plot. In MgO V which has a slightly higher concentration of H^- ions than to MgO III, the second order decay starts later at 130 sec. The point at which the start of the second order process occurred, are tabulated for different samples in table V. We conclude from Table V that, in contrast to the effect near room temperature the higher the concentrations of H^- ions, the longer the period before a second order process is apparent.

Similar pattern is noticed in the decay kinetics of CaO. In CaO III with a low concentration of H^- ions, the second order decay process at low temperature starts much earlier than in hydrogen rich CaO IV, whereas at room temperature the second order decay process in CaO IV, starts within few seconds after the ceasation of exciting source. Therefore, in the case of CaO also, it is the concentration of H^- ions that determine the start of the dominant second order process in the sample. At room temperature the higher concentration of H^- ions favors the second order process, at low temperature on the other hand, the high concentration of H^- ions delays the start of the second order process in the luminescence decay. We will next present a theoretical model, that will explain more quantitatively, the results of decay kinetics both at room temperature and at low temperature. This model is based on the

TABLE V

SET POINT FOR THE START OF SECOND ORDER DECAY PROCESS OF F CENTER LUMINESCENCE IN VARIOUS MgO SAMPLES AT LOW TEMPERATURE

Sample	$n_F(cm^{-3})$	$n_H(cm^{-3})$	Set point for the start of second order process in seconds
MgO III	5.5×10^{17}	5.4×10^{16}	105
MgO V	2×10^{17}	6.3×10^{16}	130
MgO IV	3.7×10^{18}	1.6×10^{17}	150
MgO I	1.6×10^{18}		> 600

work of previous authors[45-50] in which only one trap was considered. Below we extend this model to the case of two effective traps.

1. Theoretical Model and Interpretation of Results

Figure 28 shows the model with energy level scheme that includes ith traps, and one type of luminescence centers or the recombination centers, where X is the number of empty luminescent centers and y_i and z_i are the number of empty traps and number of filled traps respectively α_i and γ_i are the probabilities of filling empty traps and emptying filled traps, β is the probability of filling empty luminescent centers.

The following rate equations describe the process

$$\frac{dz_i}{dt} = -\frac{dy_i}{dt} = -\gamma_i z_i + \alpha_i n y_i \rightarrow \quad (16)$$

$$\frac{dx}{dt} = -\beta n x \rightarrow \quad (17)$$

$$\frac{dn}{dt} = \sum_i \gamma_i z_i - \sum \alpha_i n y_i - \beta n x \rightarrow \quad (18)$$

$$N_i = y_i + z_i \rightarrow \quad (19)$$

Where, n is the number of electrons in the conduction band and N_i is the total number of traps.

As long as $x \gg n$, one can also write

$$\frac{dn}{dt} \approx 0 \rightarrow \quad (20)$$

and from (16), (17) and (18), $\frac{dn}{dt} = \frac{dx}{dt} - \sum \frac{dz_i}{dt} = 0 \rightarrow$ (21)

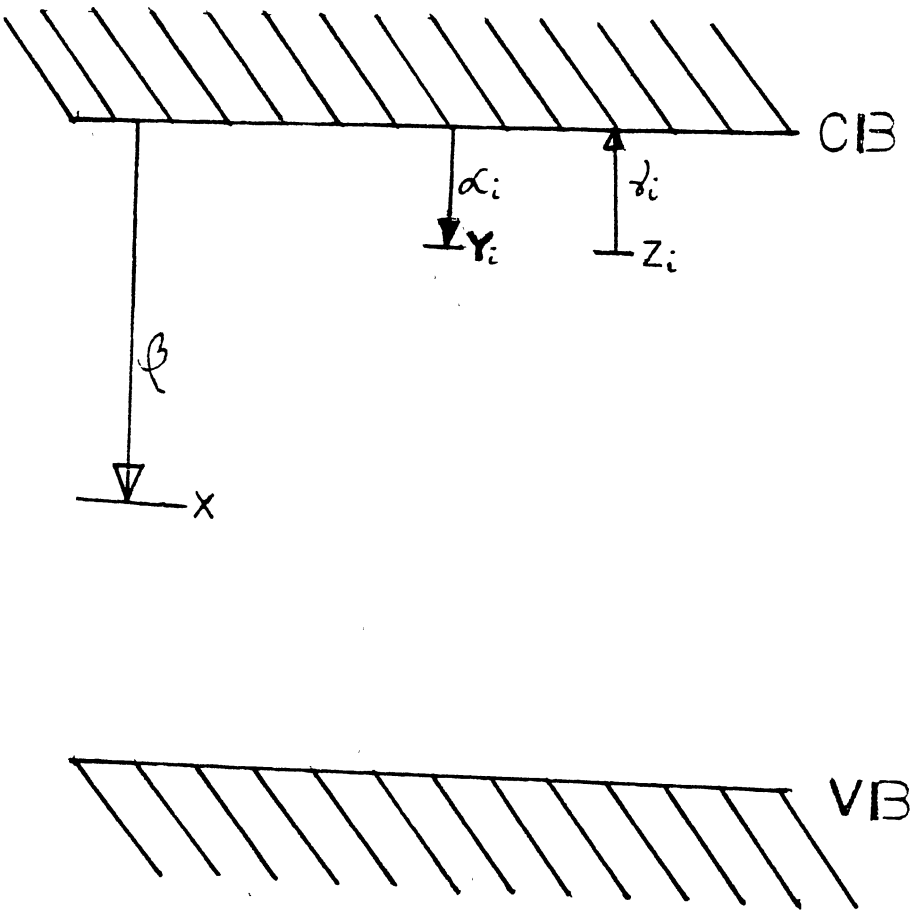

Figure 28. Energy Level Scheme for Charge Motion and F Center Luminescence with i^{th} Kinds of Traps and One Luminescence Center

therefore,

$$\sum_i \gamma_i z_i = \sum \alpha_i n y_i + \beta n x = \sum \alpha_i n(N_i - z_i) + \beta n x \rightarrow \quad (22)$$

$$\text{so, } n = \frac{\Sigma_i \gamma_i z_i}{\Sigma_i \alpha_i (N_i - z_i) + \beta x} = \frac{\Sigma_i \gamma_i z_i}{\Sigma_i \xi_i (N_i - z_i) + x} \frac{1}{\beta} \rightarrow \quad (23)$$

Where, $\xi_i = \frac{\alpha_i}{\beta}$ is the ratio of the probability of retrapping to the probability of capture by luminescent centers.

Therefore,

$$I = -\frac{dx}{dt} = \beta n x = \frac{x \Sigma_i \gamma_i z_i}{\Sigma \xi_i (N_i - z_i) + x} \rightarrow \quad (24)$$

This is the general equation for decay with ith traps. In case of one trap, which essentially is the case near room temperature where the shallow traps are virtually non existant, we write i = 1, so that,

$$I = -\frac{dx}{dt} = \frac{x \gamma z}{\xi(N-z) + x} \quad (25)$$

If the rate of emptying traps is equal to the rate of filling luminescent centers, then $x \approx z$. Therefore,

$$I = -\frac{dx}{dt} = \frac{\gamma x^2}{\xi N + x(1-\xi)} \rightarrow \quad (26)$$

If N, the number of deep traps are large then in the early part of the decay the term involving x, the unfilled luminescence center becomes negligible in the denominator. Therefore the Equation (26) boils down to

$$I = -\frac{dx}{dt} = \frac{\gamma x^2}{\xi N} \rightarrow \tag{27}$$

which is a representation of a second order decay process. And indeed in case of MgO I, with high concentration of H^- ions at room temperature, we notice a second order decay after a certain time has elapsed, when $x \ll N$.

Integrating (27), one can write,

$$\frac{1}{x} - \frac{1}{x_o} = \frac{\gamma}{\xi N}(t - t_o)$$

$t = t_o$, is the time when just the exciting source is cut off and the decay starts,

$$\frac{1}{x} = \frac{\gamma}{\xi N}(t - t_o) + \frac{1}{z_o} = \frac{\gamma}{\xi N}\left[(t - t_o) + \frac{\xi N_o}{\gamma z_o}\right]$$

$$\text{so, } x = \frac{\xi N}{\gamma}\left[\frac{1}{\xi N/\gamma\, z_o + (t - t_o)}\right] \rightarrow \tag{28}$$

Plugging this in (27) results.

$$I = -\frac{dx}{dt} = \frac{\xi N}{\gamma}\left[\frac{1}{\xi N/\gamma\, z_o + (t - t_o)}\right]^2$$

$$I = \frac{\gamma}{\xi N} z_o^2 \left[\frac{b}{b + (t - t_o)}\right]^2 \rightarrow \tag{29}$$

where, $b = \xi N/\gamma\, z_o$, is inversely proportional to the fractional number of traps filled at $t = t_o$. Equation (29) represents, in fact, well known Bequirel's formula[52,53]

$$I = I_o\left(\frac{b}{b+t}\right)^m \rightarrow \qquad (30)$$

Decay curves of the form of Equation (30) in general are attributed to a second order mechanism. b is a function of activation time, and for a time $t >> b$, and $m = 2$, $I = I_o t^{-2}$ results from (30). In fact we fitted our experimental datas of MgO I and CaO IV at room temperature to achieve m close to 2. A departure from the $I = I_o t^{-2}$ type form occurs in very early part of the decay, which shows non linear region in $1/I^{1/2}$ vs t plot in these samples.

Equation (29) is the result of simplification of our model, which includes only one trap. This is justified at room temperature where the shallow traps do not come into play. However, at low temperature, the reverse is not true and the deep traps cannot be ignored as there is always a probability that the electrons released from the shallow traps at low temperature can be retrapped at the unfilled deep traps.

We'll therefore, use a more general approach that involves both type of traps and then separately consider the two cases 1) room temperature case, ii) low temperature case.

For two traps i = 1,2, Equation (23) can be written as

$$n = \frac{\gamma_1 z_1 + \gamma_2 z_2}{\xi_1(N_1 - z_i) + \xi_2(N_2 - z_2) + x}\,\frac{1}{\beta}$$

therefore,

$$I(x) = -\frac{dx}{dt} = \beta n x = \frac{x(\gamma_1 z_1 + \gamma_2 z_2)}{\xi_1(N_1 - z_1) + \xi_2(N_2 - z_2) + x} \rightarrow \qquad (31)$$

Writing, $x = z_1 + z_2$, i.e., the rate of emptying trap is equal to the

rate of filling luminescent centers. Equation (31) can be rewritten with z_1 substituted in terms of z_2 and vice versa

$$I(x) = \frac{x(\gamma_1 x + (\gamma_2 - \gamma_1)\, z_2)}{\xi_1 N_1 + \xi_2 N_2 + x(1 - \xi_1) + (\xi_1 - \xi_2) z_2} \rightarrow \tag{32}$$

and

$$I(x) = \frac{x(\gamma_2 x + (\gamma_1 - \gamma_2)\, z_1)}{\xi_1 N_1 + \xi_2 N_2 + x(1-\xi_2) + (\xi_2 - \xi_1) z_1} \rightarrow \tag{33}$$

From the solution of Equation (16) written as

$$\frac{dz_i}{dt} = -\gamma_i z_1 + \alpha_i n(N_i - z_i) = \alpha_i N_i n - (\gamma_i + \alpha_i n) z_i$$

one can get a better look at z_i as

$$z_i = \frac{N_i}{1 + \frac{\gamma_i}{\alpha_i n}} + \left(z_{io} - \frac{N_i}{1 + \frac{\gamma_i}{\alpha_i n}}\right) e^{-(\gamma_i + \alpha_i n)t} \rightarrow \tag{34}$$

a. Case I - At Room Temperature

At room temperature $kT \gg E_1$, where E_1 is the activation energy of the shallow traps. Therefore at room temperature, the shallow traps are essentially empty, where γ_1 is very high. Now the equation shows that at large value of γ_1, z_1 is very small.

For very small z_1 therefore Equation (33) reduces to

$$I(x) = \frac{\gamma_2 x^2}{\xi_1 N_1 + \xi_2 N_2 + x(1-\xi_2)} \rightarrow \tag{35}$$

For large number of deep traps, i.e., for high N_2, the term involving x in the denominator quickly becomes insignificant compared to N_2, and therefore we observe the second order decay process in the major part of the decay in hydrogen rich MgO I and CaO IV.

On the other hand, in MgO III and CaO II, where the number of deep H^- ion traps i.e., N_2, is small, the term containing x, the number of unfilled luminescent centers, can not be ignored compared to a small value of N_2 and therefore the decay process is non second order type. This is indicated by the nonlinear smooth curve in $1/I^{1/2}$ vs t plot for MgO III and CaO II.

It is evident from this model that at room temperature the decay kinetics of F center luminescence in these samples, is determined by the number of deep traps and the number of unfilled luminescence centers present. How quickly the second order process will start depends on how quickly the terms containing x becomes insignificant compared to $N_2\xi_2$. If the number of deep traps N_2 is not high in a sample then, throughout the decay process in the sample x remains significant and as such the second order process is not observed.

The model also suggests that for a given sample, if the intensity of excitation is varied so that a different number of unfilled luminescence centers, x, are created, a change in time for the start of second order decay kinetics will be noticed. This is indeed experimentally observed, when the intensity of excitation was changed. MgO II was chosen as a test sample which contains a fairly large concentration (1.3×10^{17} cm^{-3}) of H^- ions, but the concentration of H^- ions in it is not, as high as in MgO I, where the second order process starts too early to observe any noticeable change with variances of x.

Neutral density filters with O.D. 0.5, 1, and 1.5 were used in conjunction with 230 nm interference filter, which passes the F band light. A 60W deuterium lamp was used as a source. Exciting light from the source through the 230 nm interference filter was reduced by factors of 3.2, 10 and 31.6 respectively with the use of the neutral density filters.

If we define the case A is the case when no neutral density filter was used and case B, C, and D are the cases respectively where the exciting light was cut off by the factor of 3.2, 10, and 31.6 with the use of neutral density filters, then in case D, the minimum number of F centers were excited thereby creating minimum number of unfilled luminescence centers x, conversely in case A, with the exciting light of maximum intensity, the maximum number of unfilled centers, x, were generated. The second order process, exactly as indicated by the model, started earliest in case D with fewest x as shown in $1/I^{1/2}$ vs t plots in Figure 29. The times for the onset of the second order process where calculated from the $1/I^{1/2}$ vs t plots. The characteristic times are 475 s, 385 s, 265 s and 240 s for cases A, B, C and D respectively.

b. Case II - At Low Temperature Near the First TL Peak of the Sample

At room temperature, the shallow traps are virtually empty and as such were not considered in the decay equations. However, at low temperature both the traps come into play, because we cannot ignore the possibility that electrons being released from the shallow traps can be retrapped in the unfilled deep traps. In fact the experimental results indicate that change of concentration of deep traps in the sample

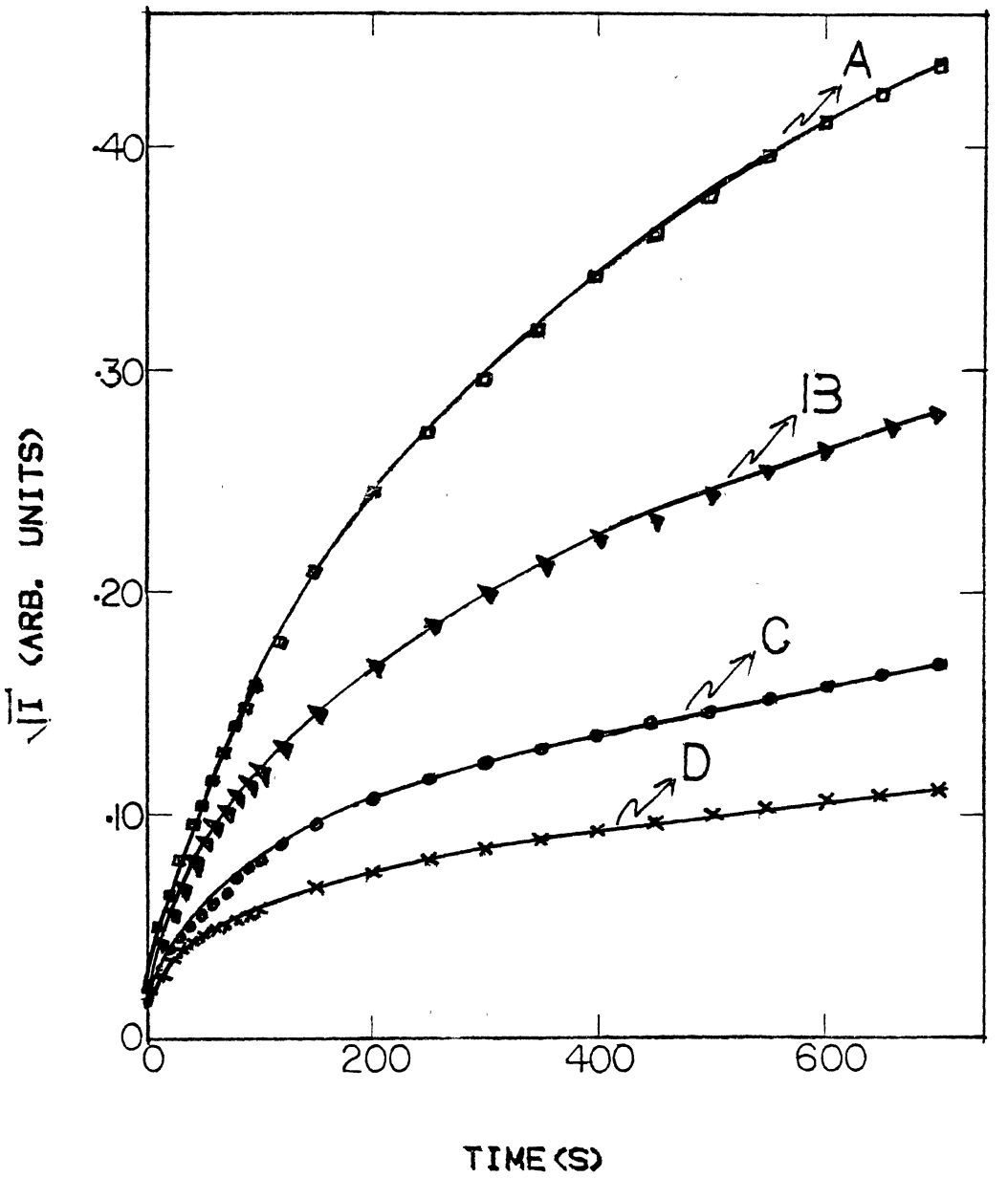

Figure 29. $1/I^{1/2}$ vs. Time in MgO at RT with Different Exciting Energies

shows that higher the concentration of deep traps, longer it takes for the second order process to start. We will now explain this decay kinetics at low temperature from the proposed model. At low temperature γ_2, the probability of emptying the filled deep traps, can be considered to be zero. With this the Equation (24) can be written as

$$I(x) = \frac{x\,\gamma_1 z_1}{\xi_1(N_1 - z_1) + \xi_2(N_2 - z_2) + x} \rightarrow \tag{36}$$

$$= \frac{x\,\gamma_1\,(x - z_2)}{[\xi_1 N_1 + \xi_2 N_2) + (1-\xi_1)x + (\xi_1 - \xi_2)z_2]}$$

$$\text{or, } I(x) = \frac{\gamma_1 x^2}{(\xi_1 N_1 + \xi_2 N_2)} \frac{(1 - \frac{z_2}{x})}{[1 + \frac{1 - \xi_1}{(\xi_1 N_1 + \xi_2 N_2)} x + \frac{(\xi_1 - \xi_2)z_2}{\xi_1 N_1 + \xi_2 N_2}]}$$

Deviation from the second order process can be seen by expanding the denominator as,

$$I(x) \simeq \frac{\gamma_1 x^2}{\xi_1 N_1 + \xi_2 N_2} [1 - \frac{z_2}{x} - \frac{(1 - \xi_1)}{\xi_1 N_1 + \xi_2 N_2} x + \ldots .]$$

The terms $- \frac{z_2}{x} - \frac{(1 - \xi_1)}{\xi_1 N_1 + \xi_2 N_2} x = q(x)$ say, and the second order process starts when $q(x) \leq r$, when $r \ll 1$

This can be represented graphically as shown

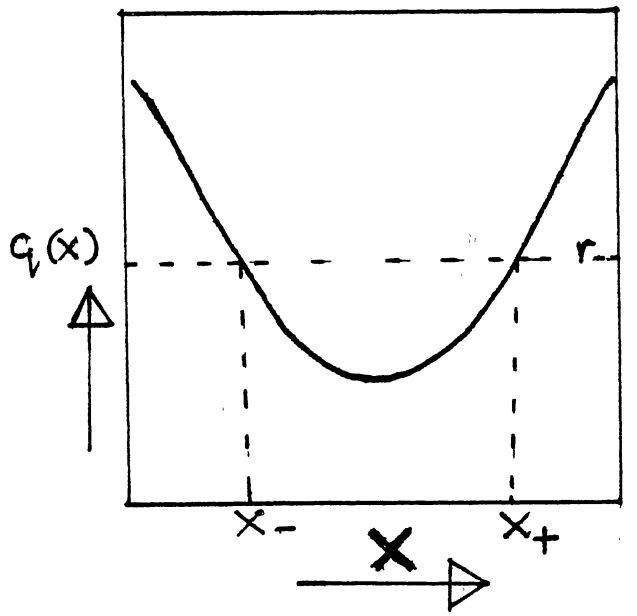

$x\pm$ are the roots of

$$A\,x^2 - rx + B = 0$$

where $A = \dfrac{1 - \xi_1}{\xi_1 N_1 + \xi_2 N_2}$, $B = z_2 = f(N_2)$, where f is a constant $\leqslant 1$.

and $x\pm = \dfrac{r \pm (r^2 - 4AB)^{1/2}}{2A}$

The decay process is therefore second order, when

$$|q(x)| \leqslant r \quad \text{i.e.,} \quad x_- < x \leqslant x_+$$

Again from $x\pm = \dfrac{r \pm (r^2 - 4AB)^{1/2}}{2A}$, it demands that for the second order process $r^2 > 4AB$

i.e., $r^2 > f\,(1 - \xi_1)\,\dfrac{N_2}{\xi_1 N_1 + \xi_2 N_2}$

i.e., $N_2 \ll N_1$.

In otherwords for a second order luminescence decay at low temperature the number of deep traps must be much smaller than the number of shallow traps. This can be seen in MgO III and in CaO III, where the intensity of the room temperature TL peak is much smaller than that of the TL peak at low temperature. In both MgO III and CaO III the second order decay process starts early in the decay.

For $r^2 \gg 4AB$.

$$x_+ \simeq \frac{r + r(1 - \frac{2AB}{r^2})}{2A} \approx \frac{r}{A} - \frac{B}{r}$$

$$\text{i.e., } x_+ \approx \frac{r}{1 - \xi_1} \xi_1 N_1 (1 + \frac{\xi_2 N_2}{\xi_1 N_1}) - \frac{f\ N_2}{r}$$

From the expression of x_+, the following can be concluded:

1. The second order decay process starts when $N_2 \ll N_1$.
2. In this range the second order process starts earlier as N_1 increases (with constant N_2).
3. The second order process starts later in time as N_2 increases (for constant N_1).

The various samples of MgO and CaO, studied experimentally appear to have a comparable number of shallow traps (as seen from the height of the low temperature of TL peak) and F centers. The concentration of deep traps (i.e. N_2) in these samples were varied and we recorded the delay in the start of second order process. For high N_2 as in MgO I, the second order process is not observed. For other samples such as MgO

III, MgO V and MgO IV, the start of the second order process began at 105 s, 130 s and 150 s respectively. Therefore with the increase in concentration of H^- ions i.e., N_2, the delay in the start of the second order process was noticed.

For CaO also, the set point for the start of the second order decay process of low temperature luminescence shifted to a later time as the concentration of deep traps, i.e., N_2 is increased. This is seen in Figure 27.

We, therefore, see that the observed complex behavior of the low temperature luminescence decay curves is explained by this model and theoretical calculations. At high temperature limit also this model works well. It is difficult to vary the concentrations of shallow traps in these samples but we predict from this model, that for a fixed number of N_2, the deep traps, the second order process will be favored or be delayed as the concentration of shallow traps (N_1) are increased or decreased respectively.

D. Infrared Stimulated Emission

In the previous sections we have discussed the presence of two types of traps in MgO and CaO and their influence on F center luminescences. In this section we will discuss other experiments that describe an effect caused by the presence of these traps. This effect is noticed when the long lived phosphorescence near room temperature is suddenly interupted by quickly reducing the temperature of the sample. The luminescence is then reactivated at the lower temperature by illuminating the sample with a short pulse of infrared light which has an energy much lower than F band light used initially to excite the

luminescence near room temperature. This process which can be called infrared stimulated emission has been observed in both MgO and CaO.

Figure 30 shows the results of an experiment using sample CaO VI. The sample was illuminated at room temperature with F center light. When the luminescence reached a maximum the excitation was cut off in a time of ~ 1 ms. The luminescence intensity dropped rapidly by about an order of magnitude before continuing to decay more slowly by a non-first order process (Figure 30). After a few seconds, liquid nitrogen was forced into the dewar and the luminescence was quenched in a matter of seconds. This behavior is indicative of phosphorescence due to charge trapping. After a further five minutes the sample was excited with a 40 ms pulse of 1.7 eV(730 nm) radiation with band width of ~ 10 nm. A sharp cut filter excluded light < 680 nm. The intensity of the luminescence grew to a peak intensity with a time constant of a few milliseconds. When the excitation was removed the luminescence intensity decayed with a lifetime of 3 ms before a component with a longer time constant became apparent (Figure 30). The luminescence would be reactivated in this way many times with only a small drop in peak luminescence intensity.

Figure 31 shows the excitation spectrum for the emission with different exciting energy. This survey of the excitation efficiency of the effect was made by repeating the experiment using a series of sharp-cut filters. The results indicate that the excitation spectrum for the emission extends beyond 900 nm (1.38 eV) and rises monotonically with increasing excitation energy to ~ 550 nm, where the excitation can be absorbed directly into the F band.

The thermoluminescence results of the sample suggest a

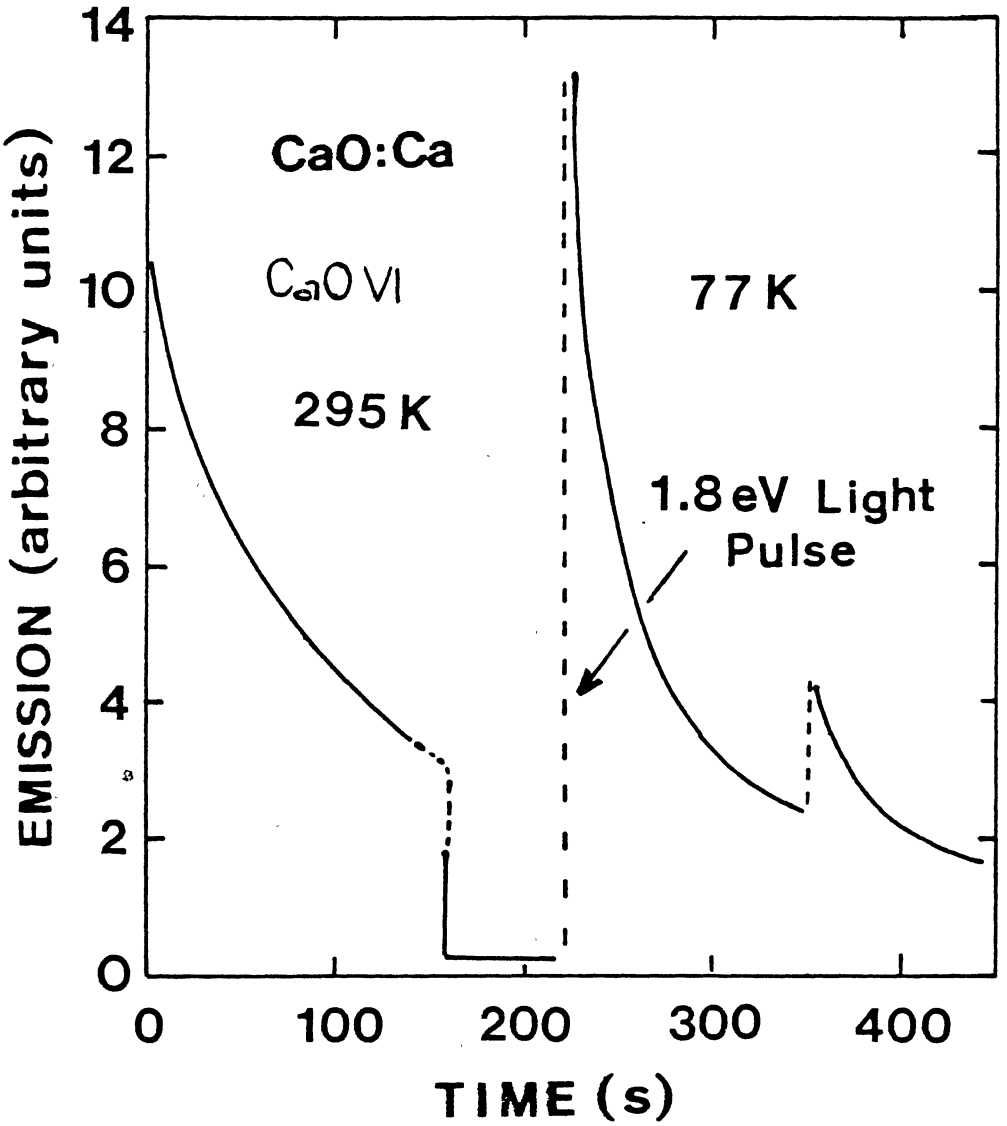

Figure 30. Infrared Stimulated Emission in CaO

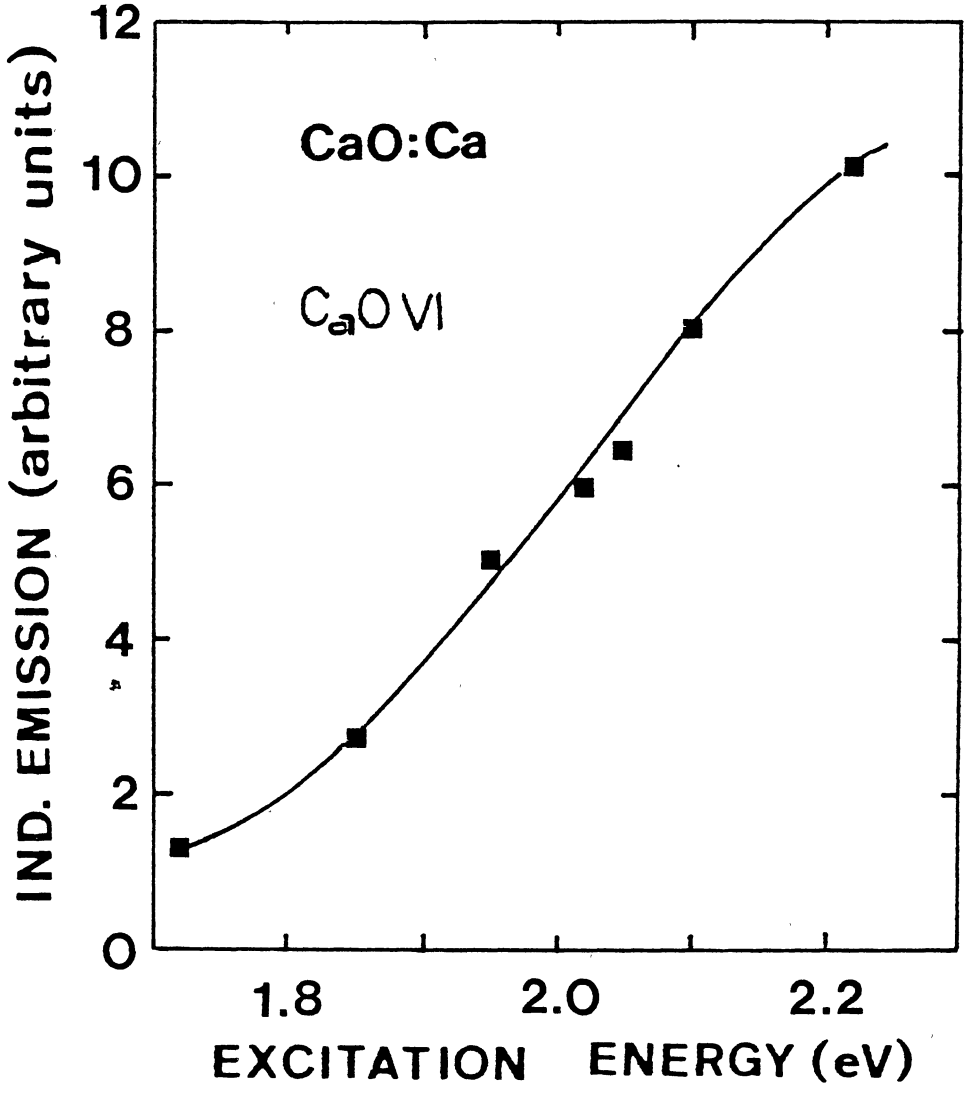

Figure 31. Excitation Spectrum of Infrared Stimulated Emission in CaO

phenomenological explanation of this infrared stimulated emission. This explanation takes note of two main types of electron traps described earlier which lead to the two TL peaks. For CaO the deeper of these traps is thermally emptied near room temperature (320 K) and the shallower is emptied near liquid nitrogen temperature. As explained before, the F center phosphorescence occurs near room temperature when optically-excited electrons are captured metastably before they return to F^+ centers. When the sample is rapidly cooled to 77 K, itinerant electrons are frozen into the deeper traps and the phosphorescence is quenched. Low energy radiation (e.g. with E = 1.7 eV) can excite electrons from these traps into the conduction band, from which some are captured directly into the excited state of the F centers. Other electrons are captured at shallower traps, from which they leak slowly back to F^+ centers. The latter process is similar to that which occurs when F centers are optically excited at 77 K. In this model, therefore, the excitation spectrum of the infrared-stimulated emission corresponds to the excitation of an electron from an $H^=$ ion into the conduction band. Because of the location of the F center absorption, the peak of this excitation spectrum could not be located experimentally. However, using the formula $E_o/E_t = \varepsilon/e_o$ to obtain a rough estimate of the optical excitation energy, E_o, from the thermal activation energy E_t(= 0.74 eV) the high frequency (3.4) and low frequency (11.8) dielectric constants, ε_o and ε respectively, E_o is calculated out to be ~ 2.5 eV (490 nm). This value is consistent with the experimental data so far obtained.

Similar experiment was performed on MgO. In this case, the sample was illuminated with F center light (5.0 eV) at 260 K. The starting

temperature was chosen to be 260 K in order to ensure a long lived luminescence. TL peak of MgO lies around 260 K. The 2.3 eV luminescence was then quenched by pumping liquid nitrogen in the dewar. The luminescence was quenched in few seconds. A short pulse of 2.5 eV light reactivated the luminescence at this low temperature. The effect is shown in Figure 32. A survey of the excitation efficiency of the effect was made. Similarly to CaO, the efficiency increases with increasing efficiency, and the excitation was observed with exciting energy light as low as 1.8 eV, Figure 33.

A series of this experiment were then carried out with different samples of CaO and MgO. For CaO, the efficiency of the excitation was comparable for each of the samples studied. However for MgO the efficiency of the excitation changed noticeably from MgO II to MgO IV. The efficiencies of the reactivated luminescence were found to be equal to 1, 2 and 5 in arbitrary units for MgO II, MgO III and MgO IV respectively.

It is seen from these experiments each of which were repeated several times, that the efficiency of the reactivated luminescence at low temperature is consistent with the results of low temperature TL of the sample. MgO IV has a higher TL intensity at low temperature, than MgO II, and the efficiency is higher in MgO IV than in MgO II. Where as in case of CaO, the low temperature TL are of comparable intensity and efficiencies of reactivated luminescence at this low temperature are comparable.

The electrons which are being excited from the traps at low temperature by the short pulse of low energy light and are captured by the shallow traps produce long lived luminescence when they finally leak

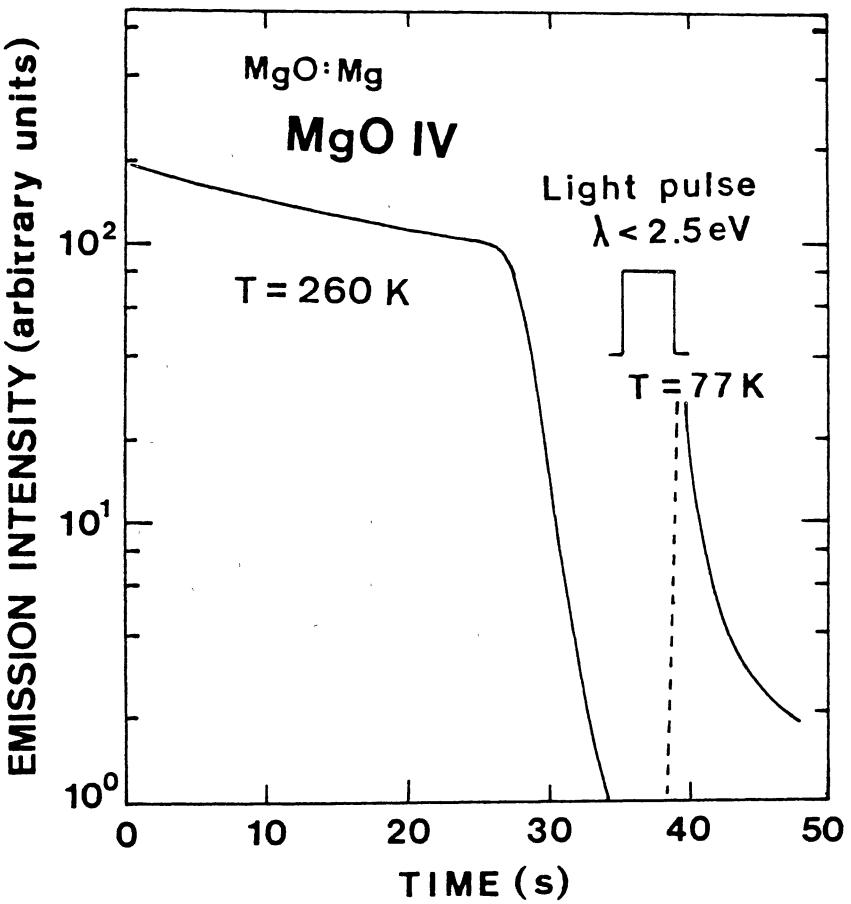

Figure 32. Infrared Stimulated Emission in MgO

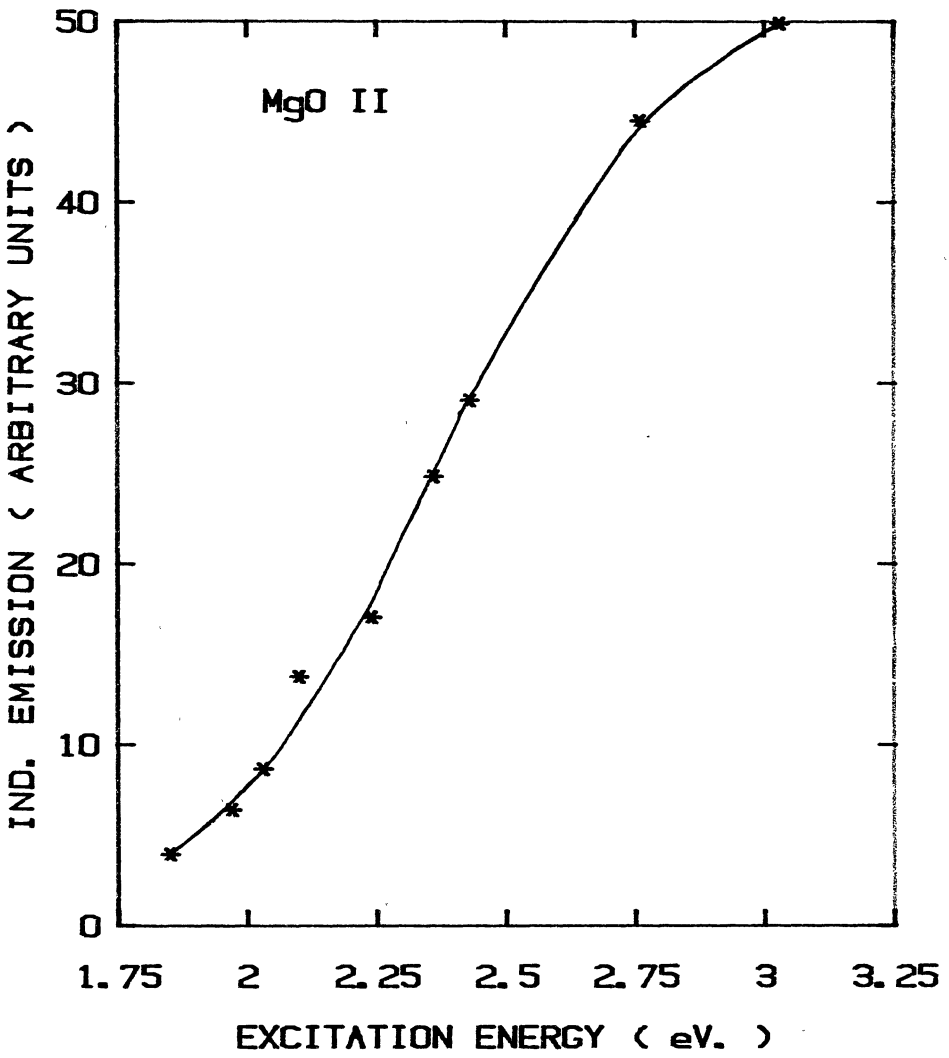

Figure 33. Excitation Spectrum of Infrared Stimulated Emission in MgO

back to F^+ centers. If the number of shallow traps is very small or if the temperature is lowered to a point where the shallow traps are stable thermally, the long lived luminescence at low temperature is not observed. In one of the experiments, with CaO VI, the luminescence at room temperature was quenched by lowering the temperature to 60 K, below the low temperature TL peak, where the shallow traps are stable and as such no long-lived infrared stimulated emission was observed. The electrons which went directly from $H^=$ ions to F^+ center produced luminescence whose lifetime was too short to be recorded in the experimental arrangement described. We, therefore, see that the presence of shallow traps and their number play a key role in the long lived luminescence reactivated at the low temperature. The luminescence decay at the low temperature is indeed different from the kinetics decay at room temperature. This is being seen from the plots in Figures 34 and 35.

E. Photoconductivity

In this dissertation, all the results of transient d.c. photocurrents, which will be discussed either in this section or the results of YAG which will be discussed later are secondary photocurrent [52]. An insulator placed between metal electrodes usually has no conductivity in the dark (unless there is dark current, associated with some electron traps, which will be discussed in the next section) because the electrons do not have sufficient energy to pass into the conduction levels. If such a crystal is illuminated with light of suitable wavelength, electrons in the crystal are raised to the conduction level, and drawn toward the anode giving rise to primary

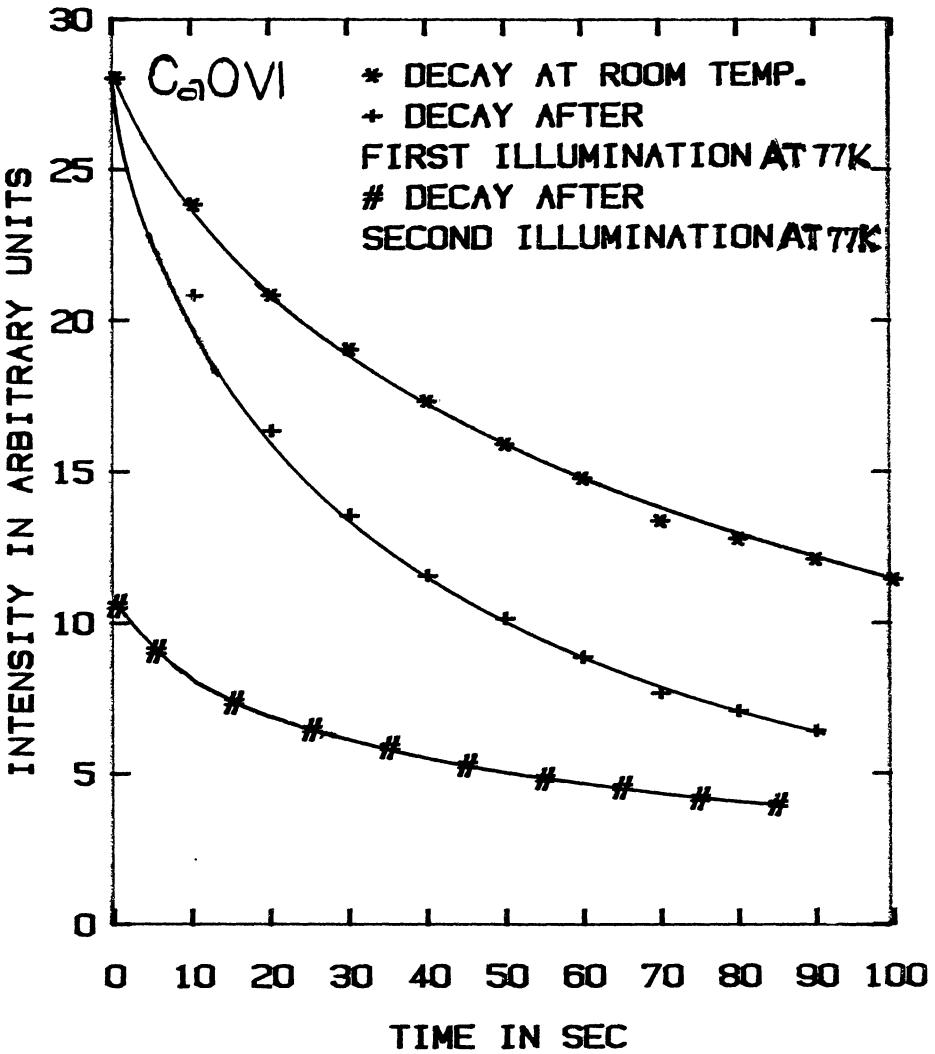

Figure 34. Decay Kinetics Before and After Infrared Stimulation in CaO

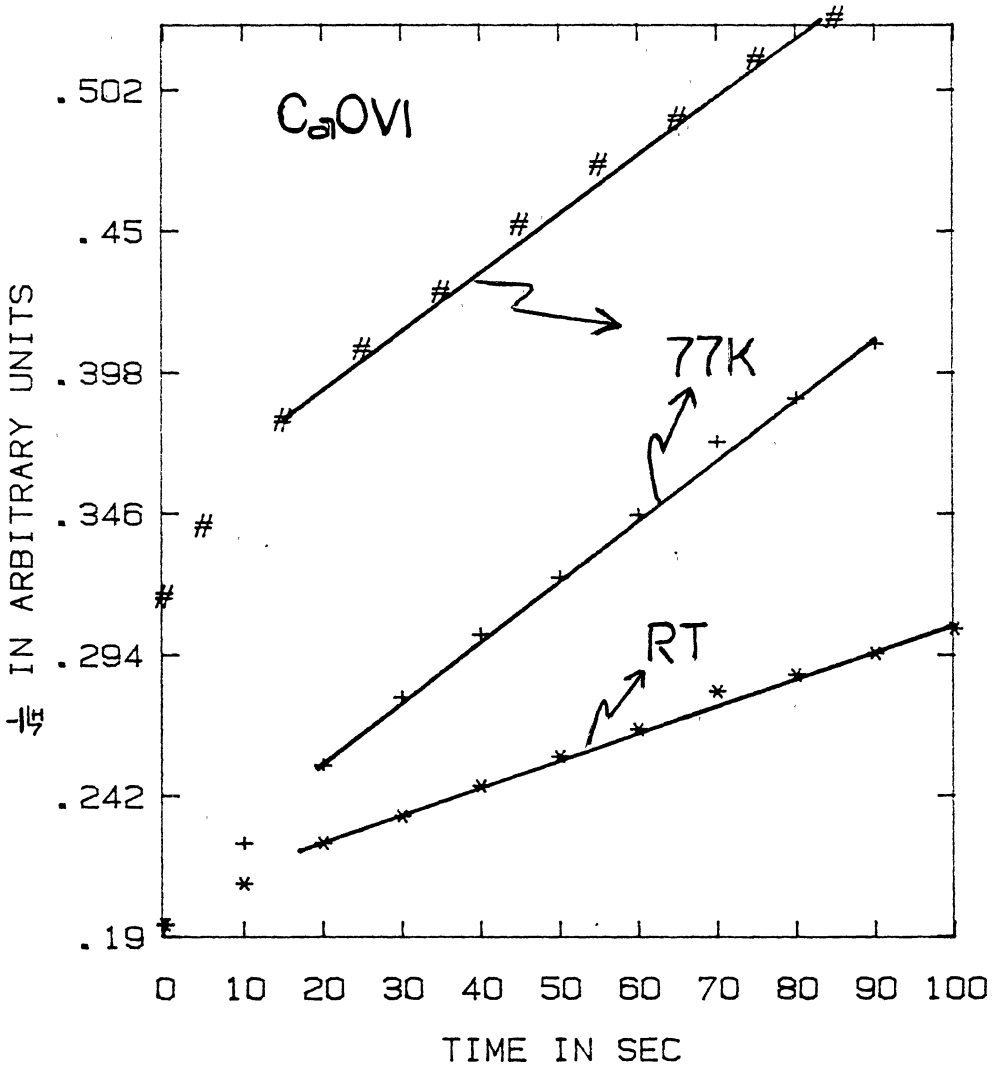

Figure 35. $1/I^{1/2}$ vs. t Plot Showing the Nature of Decay Kinetics Before and After Infrared Stimulated Emission in CaO

photocurrent. In some crystals, the continued passage of the primary photocurrent appears to break down the resistance of the crystal so that electrons can enter the crystal from the cathode and pass through it. The current that results from this is what is called a secondary photocurrent.

When a 'slice' of the crystal, mounted between the parallel electrodes, is illuminated with light which is capable of exciting electron from the electron state, the electrons are released into the conduction band and are drawn by the field into the unilluminated portion where they are trapped after drifting a certain distance. If no electric field is present the electron executes a Brownian type of motion before it gets trapped. Though the point where the electron is trapped may lie, for example, about 10^{-3} cm from the point where it was released, the total length of Brownian path covered by the electron may be more than a centimeter[52]. In the absence of an electric field, summing over all the random displacements would produce no net displacement of charge in any one direction. With an applied electric field the number of electrons which are trapped at points lying towards the anode from the point where they were released is greater than the number of electrons which are trapped at points lying toward the cathode from where they were released. An effect of this is observed consequently as current, detected by the electrometer and is the same as it would be if all the photoelectrons had drifted down the field a certain small distance w, the same for all. This distance w is known as the mean range of the photoelectrons in the field.[52]

If the released electron travels all the way across the crystal, the charge measured by the electrometer would be the electronic charge,

e. If the electron travels only a distance x, the charge measured will be

$$q = e \frac{x}{d} \rightarrow \quad (37)$$

where, d is the distance between the electrodes.

Assuming that the electron remains in the free state for a time τ before it is captured, and that τ is independent of the field E, the range w is given by,

$$w = \mu E \tau \rightarrow \quad (38)$$

where, μ is the mobility (velocity of drift/unit electric field). If an electron is in the free state, the probability that it is captured in time dt is dt/τ . If at a given instant of time, no electrons are freed, the number remaining free at time t is given by

$$n = n_o e^{-t/\tau} \rightarrow \quad (39)$$

As an analysis given by Mott and Gurney, (52) consider first the situation in which the n_o electrons are released at a distance x_o from the anode. After travelling a distance x in the direction of the field, the number left n is given by,

$$n = n_o e^{-x/\mu E \tau} \quad \text{i.e.,} \quad n = n_o e^{-x/\omega} \rightarrow \quad (40)$$

The number which end their path in the range dx is,

$$-\frac{dn}{dx}\,dx = \frac{n_o}{\omega}\,e^{-x/\omega}\,dx \quad \rightarrow \tag{41}$$

The total distance drifted by the n_o particles is the sum of two terms, the first term giving the distance drifted by the particles which do not reach the anode and the second giving the distance drifted by the particles which do reach the anode. The total distances drifted by the particles which are traped before reaching the anode is given by

$$-\int_o^{x_o} x\,\frac{dn}{dx}\,dx = \int_o^{x_o} x\,\frac{n_o}{\omega}\,e^{-x/\omega}\,dx = \frac{n_o}{\omega}\left[\frac{e^{-x/\omega}}{(-\frac{1}{\omega})^2}\,(-\frac{x}{\omega} - 1)\right]\Bigg|_o^{x_o}$$

which can be simplified to

$$n_o\,\{\omega(1-e^{-x_o/\omega}) - x_o e^{-x_o/\omega}\} \quad \rightarrow \tag{42}$$

The total distance drifted by the $n_o e^{-x/\omega}$ particles which reach the anode is

$$x_o n_o e^{-x_o/\omega} \quad \rightarrow \tag{43}$$

Summing Equation (42) and Equation (43) and dividing by n_o particles, the mean distance drifted by an electron is given by,

$$\bar{x} = \omega(1 - e^{-x_o/\omega}) \rightarrow \tag{44}$$

If d is the length of the crystal, the ratio ψ of the charge passing through the electrometer, $n_o e\,\frac{\bar{x}}{d}$, to the charge released, $n_o e$, is given by

$$\Psi = \frac{\omega}{d}\left(1 - e^{-x_o/\omega}\right) \rightarrow \qquad (45)$$

this formula is given by the Hecht[54]

All these considerations can be used to derive the net charge flow in the external circuit for the simple case described above. In actual practice, however, the relation between measured charge and the charge released is complicated by the penetration of light into the crystal. The discussion which follows is based on one given by Van Heyingen and Brown[55]. The light intensity at a depth x in terms of the incident intensity is given by

$$I = I_o e^{-\alpha x} = N_o(1 - R)e^{-\alpha x}$$

$N_o(1-R)$ is the actual number that enters the crystal out of N_o the total number of photons that are incident. R is the reflection coefficient and α is the absorption coefficient for a given wavelength. The number of photons actually absorbed within the crystal in the interval of x and x + dx is

$$dN = \alpha N_o(1 - R)e^{-\alpha x}dx$$

But only those absorptions which produce free electrons are of interest to us. The quantum efficiency, η_T, or the number of free electrons, dn, produce per absorbed photon in interval dx is therefore,

$$\eta_T = \frac{dn}{dN}$$

and $dn = \eta_T \alpha N_o (1-R) e^{-\alpha x} dx \rightarrow$ (46)

Integrating from 0 to d over the thickness of the crystal, results

$$n = \eta_T N_o (1-R)(1-e^{-\alpha d}) \rightarrow \quad (47)$$

Where n is the total number of electrons released within the crystal. The electrometer records a charge $q = ex/d$, for each electron that is drawn to a distance x in the crystal, and the charge which flows in the external circuit is given by,

$$Q = nq = e\, \eta_T N_o (1-R)(1-e^{-\alpha d})\psi \rightarrow \quad (48)$$

where, ψ is a saturation factor defined as $\frac{\bar{x}}{d}$, and ψ takes into account the mean range of the electron and finite depth of optical absorption. ψ is derived in a similar manner as described for a simpler case by Equation (40) to Equation (45). This is described by Feldott[56], in great detail.

The expression obtained for ψ is given by,

$\psi = \frac{\omega}{d}\left[\frac{1 - \frac{\omega}{d}(1-e^{-d/\omega})}{1 - \alpha\omega}\right]$, which again in the limit $\alpha \rightarrow o$ which is of particular interest in our experimental studies reduces to

$$\psi = \frac{\omega}{d}\left[1 - \frac{\omega}{d}(1 - e^{-d/\omega})\right] \rightarrow \quad (49)$$

Again for small electric field, since $\omega << d$ the saturation factor is

approximated by, $\psi \sim \frac{\omega}{d}$

therefore $\psi = \frac{\bar{x}}{d} \sim \frac{\omega}{d} \rightarrow$ (50)

The photocurrent is given by,

$$I = e\eta_T N_o (1-R)(1-e^{-\alpha d}) \frac{\omega}{d} \rightarrow \quad (51)$$

which, on further rearrangement yields,

$$\eta\omega_o = \frac{I}{N_o} \frac{d^2}{eV} \rightarrow \quad (52)$$

where, $\omega_o = \omega\, d/v$ and $\eta = \eta_T(1-R)(1-e^{-\alpha d})$

In actual experimental results, which will be discussed in this section and later for γ-irradiated YAG, the photocurrent given by Equation (51) or photoresponse given by Equation (52) have been used.

Photoconductivity studies were made in CaO IV in the region, of excitation energy where the infrared stimulated luminescences at 77 K were observed in the same sample. Figure 36 shows the plot of photocurrent against the excitation energy. Measured photocurrents were corrected for the spectral dependence of the lamp output which was measured using a Molectron 100 pyroelectric radiometer. The photocurrent observed were of the order 10^{-14} amp and such a small current was measured in "rate of charge" mode. Under this condition, the photocurrent corresponding to incident light of a given wavelength is given by the expression

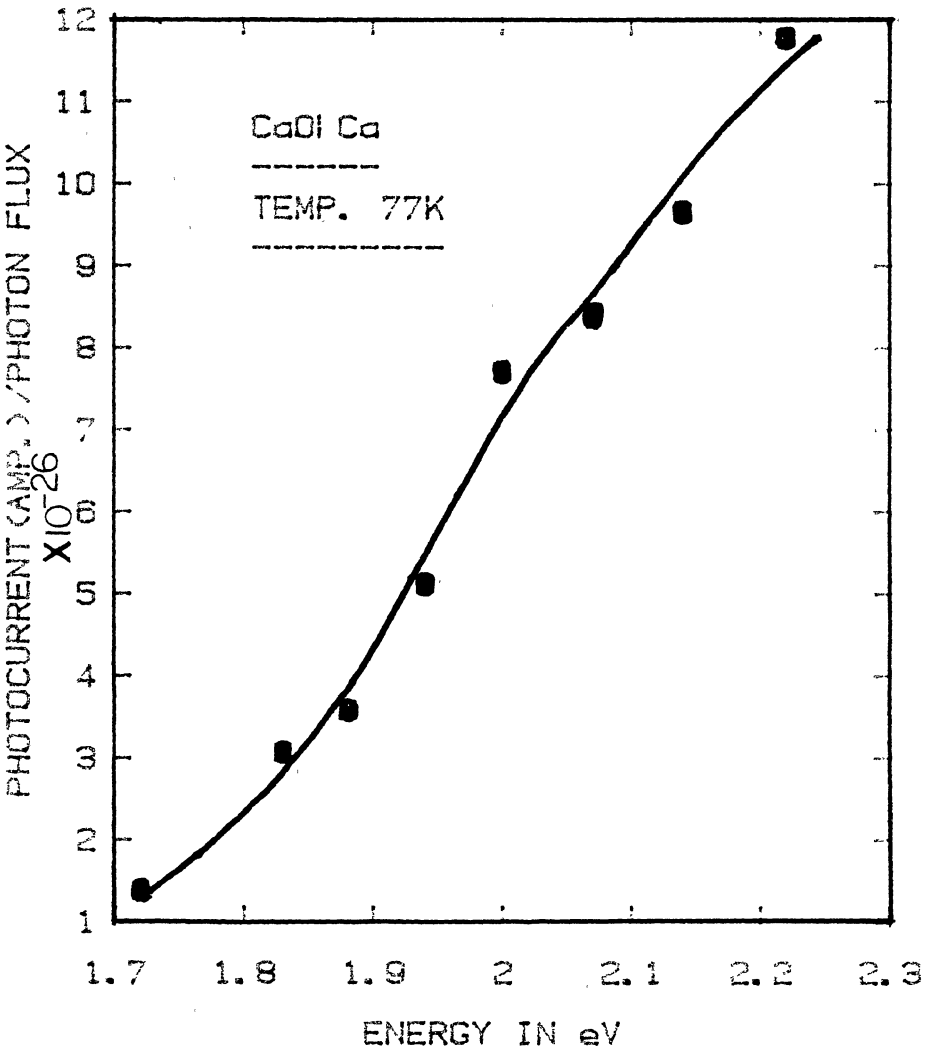

Figure 36. Infrared Simulated Photocurrent in CaO at 77 K

$$I_\lambda = \frac{dQ}{dt} = C_c \frac{\Delta E_r}{\Delta t}$$

Where Q is the charge in Coulombs, C_c is the charge collecting capacitance (2×10^{-11} farad) of the electrometer, ΔE_r is the change in the recorder reading as a fraction of the full scale times the electrometer range in volts in a small interval of time Δt.

These results of photocurrent at 77 K are in good agreement with the spectral dependence of efficiency of infrared stimulated emission shown in Figure 30. At low temperature, a short pulse of low energy light releases electron from the frozen $H^=$ ion, this then moves through the conduction band, and gives photocurrent. This electron after being captured by F^+ centers gives off luminescence. These infrared stimulated photocurrents have the same type of energy dependence as the infrared stimulated emissions and as such these results of infrared stimulated photocurrents together with the infrared stimulation luminescence help us to see the structure of defects better and to understand the charge motions more clearly. Figure 37 shows the temperature dependence of normalized photocurrent I/N_o. We note that the photoresponse $\eta\omega_o$ is proportional to I/N_o, as is given by Equation (40). The temperature dependence of photoresponse was taken with incident light energy of 2.2 eV, which was selected with an interference filter

It is evident from the Figure 37 that there are two regions where the photocurrent increases sharply with increasing temperature. The first sharp increase begins immediately above 77 K, and the photocurrent remains almost steady around 135-155 K. After that, it begins to increase again and observed data indicates that the final saturation

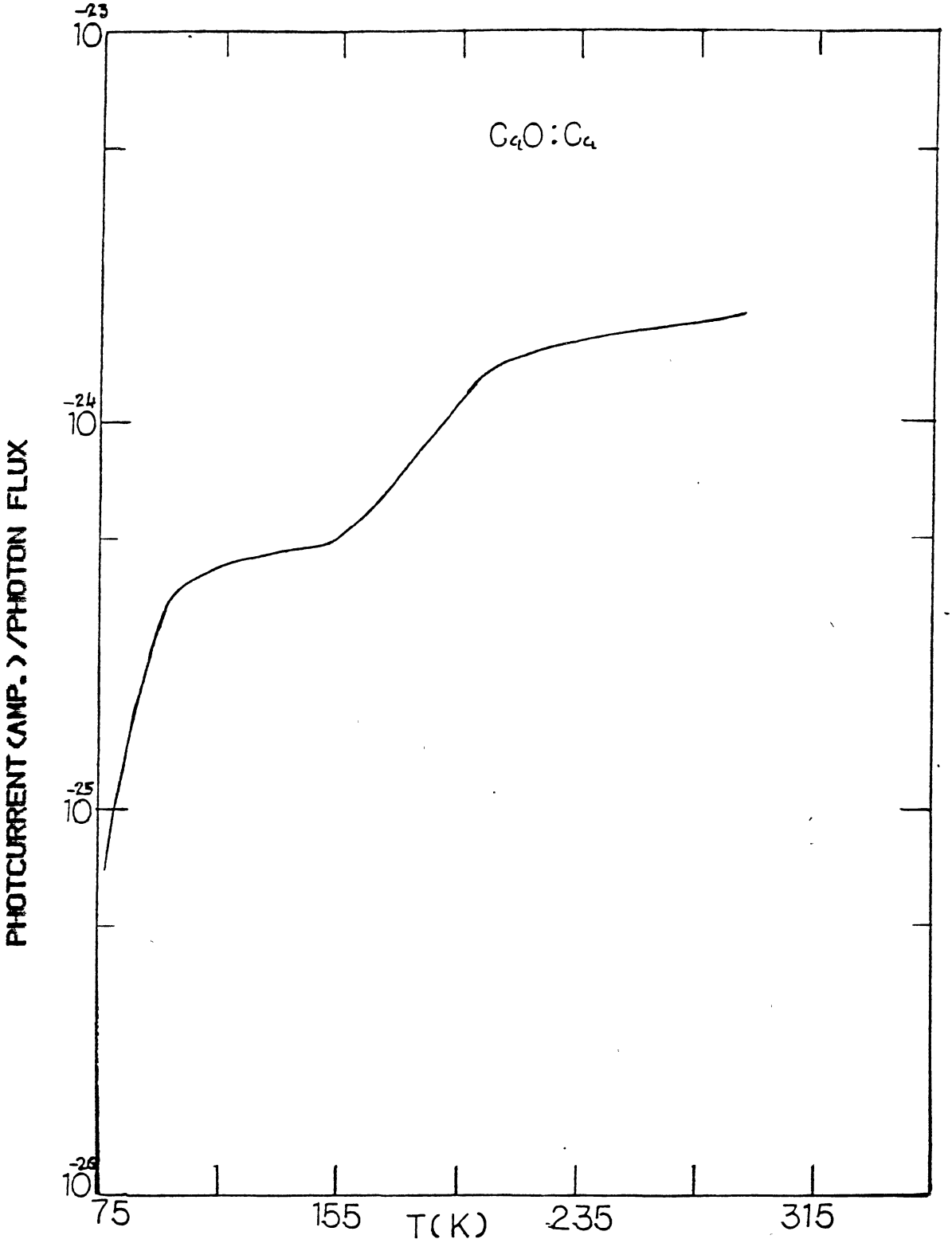

Figure 37. Temperature Dependence of Normalized Photocurrent in CaO with Exciting Energy of 2.2 eV

point is somewhere above the room temperature.

The two temperature regions where the photocurrent was observed to increase are the same regions where TL peaks were observed (Figure 14.) The temperature dependence of the photocurrent therefore indicates that the photocurrent is due to electrons released from the two types of traps, after these traps were excited by low energy (2.2 eV) light and the range ω_o has a sharp increase in the temperature range where these traps are thermally unstable. As is known from the TL of the sample, and as discussed earlier that the upper temperature TL is due to the release of electrons from deep H^- ion traps, the peak of which lies around 320 K. Therefore, as expected the photocurrent does not saturate at room temperature but still has a rising trend.

Both these effect the infrared stimulated emission and infrared stimulated photoconductivity, therefore, can be explained from the TL of the sample and two main types of traps are responsible for these effects. These two experiments therefore support our model for the structure of defect that includes two effective types of traps in thermochemically reduced MgO and CaO.

In the next and concluding section on the results of MgO and CaO, another related effect due to the presence of H^- ions will be discussed. The experimental arrangement was the same as described above for the photoconductivity experiments, except in these cases the current is measured at room temperature without light being allowed to fall on the samples. Continued thermal release of electrons from unstable $H^=$ ions at room temperature and the continued passage of the primary current (when the crystal is placed between the electrodes) therefore, increases the conductivity of the crystal. Electrons can enter the

crystal from the cathode and can pass through the crystal and give a secondary current, which is measured as dark current through the electrometer.

F. Electrical Conductivity

Long-lived photoluminescence from F centers in MgO and CaO is accompanied by photoconductivity. Typically a sample which has been exposed to UV light and then stored in the dark exhibits dark current. We have found that electrons released from $H^=$ ions are the cause of this dark current and that the dark current lasts for a surprisingly long time as shown in Figure 38.

A series of experiments were carried out with different samples of MgO containing various H^- ions concentrations. In each case, the sample was exposed to F band light and was then mounted between the electrodes. A thin film of Ag-Au alloy was deposited on the crystal surfaces in order to have a good contact with the metal electrodes. For a given exposure the magnitude of the dark current was found to increase with the increase of concentration of H^- ions in the sample, this is shown in table VI. From these observations it is suggested that the electrical conductivity at room temperature in MgO and CaO, is associated with electrons that are continually trapped and released by H^- ions.

When MgO:H samples are heated above 325 K or CaO:H samples heated above 375 K and maintained in the dark, the electrical conductivity becomes very small. Figure 13 shows that annealing to 325 K heats the sample above the upper TL peak in MgO and similary annealing to 375 K heats the sample above the upper TL peak in CaO Figure 14. The annealing, therefore, empties $H^=$ ions of trapped electrons. The dark

TABLE VI

CHANGE OF ELECTRICAL CONDUCTIVITY WITH VARIANCE OF H^- IONS IN THE SAMPLE

Sample	$n_H(cm^{-3})$	Conductivity $k(ohm\text{-}cm)^{-1}$
MgO II	1.3×10^{17}	121×10^{-14}
MgO V	6.3×10^{16}	6×10^{-14}
MgO III	5.4×10^{16}	2×10^{-14}

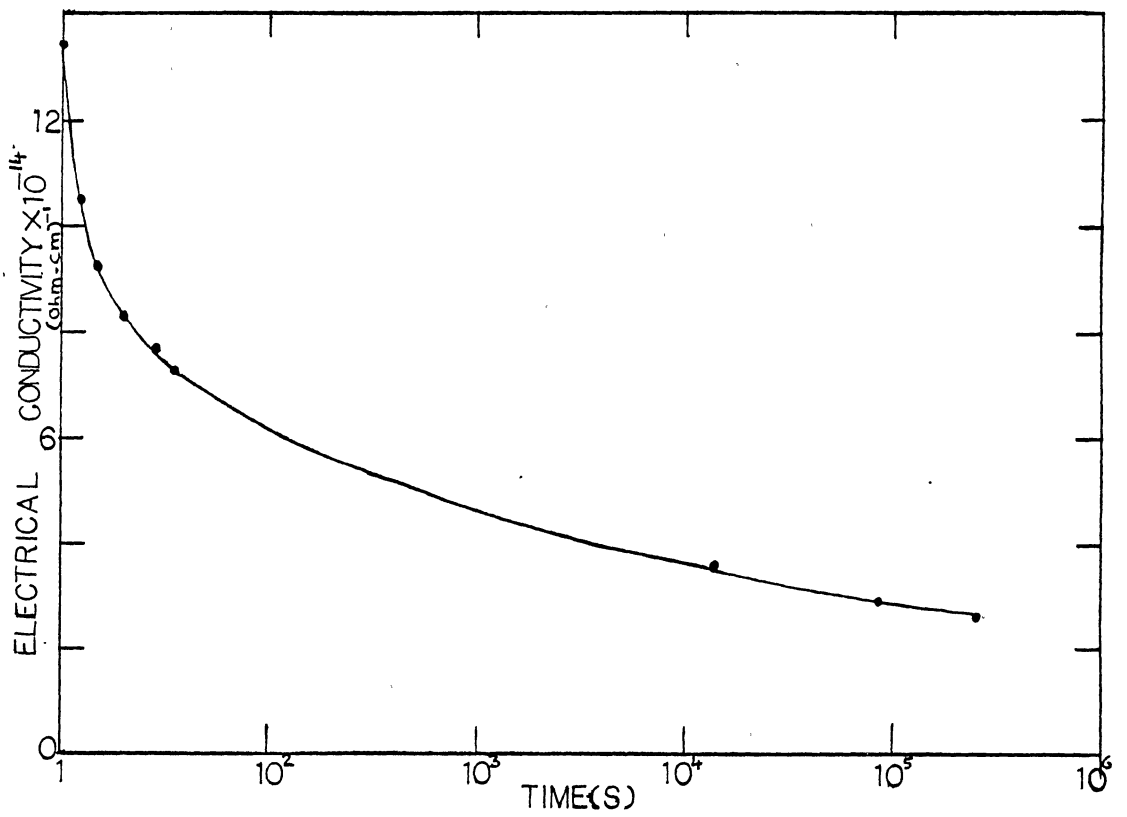

Figure 38. Electrical Conductivity vs. Time in MgO

current, however, is restored by exposing the sample to UV radiation.

The lifetime of the conductivity is quite long. The decay of the electrical conductivity was observed in dark over a period of 72 hours, as shown in Figure 38. Even after 72 hours a conductivity was observed which is 2.6×10^{-14} (ohm cm)$^{-1}$ and is greater than the observed value of conductivity of 1.04×10^{-16} (ohm cm)$^{-1}$, recorded after the sample is annealed above the upper TL.

A series of experiments were also carried out in case of MgO to see how this dark current saturates with time. Each time the sample was heated in the dark to 325 K and was then mounted between the electrodes and was shinned by the F band light. The light was shinned at different duration, starting from one minute to the time when the dark current became saturated. It was seen that in three minutes, the dark current became saturated with number of photons, striking on the face of the sample, at this time for saturation was $497 \times 10^{11}/cm^2/sec$.

As expected the dark current was found to be temperature dependent. The temperature dependence of the dark current was measured in MgO II. The dark current was measured from room temperature down to 245 K, below TL glow curve of the sample. The dark current was found to be vanishingly small at this temperature. This is because at this temperature the electrons are unable to be released thermally from $H^=$, and move in the conduction band to produce dark current. As a first approximation it is assumed that changes in the conductivity with temperature are due entirely to changes in the number of free carriers. Under this assumption the conductivity would be $\alpha \exp(-E_a/kT)$, where E_a is the activation energy for thermal release of an electron from an $H^=$ ion, k is Boltzman's constant, and T is the

temperature. Figure 39 shows a plot of the conductivity against inverse temperature for MgO II. From the slope of the straight line, obtained through the plot, activation energy E_a is calculated to be 0.60 eV. This value compares well with a value of 0.56 eV for thermal release of electron from $H^=$ ions near room temperature, obtained by the "cross cut" method from the decay of F center luminescence in the sample.

The results of the electrical conductivity consolidated our understanding about the electron motion near room temperature, which we already gathered from the previous results of luminescence and photo-conductivity. Moreover, this experiment enabled us to calculate activation energy for thermal release of an electron from an $H^=$ ion, and the value showed an excellent agreement with that obtained from luminescence decay.

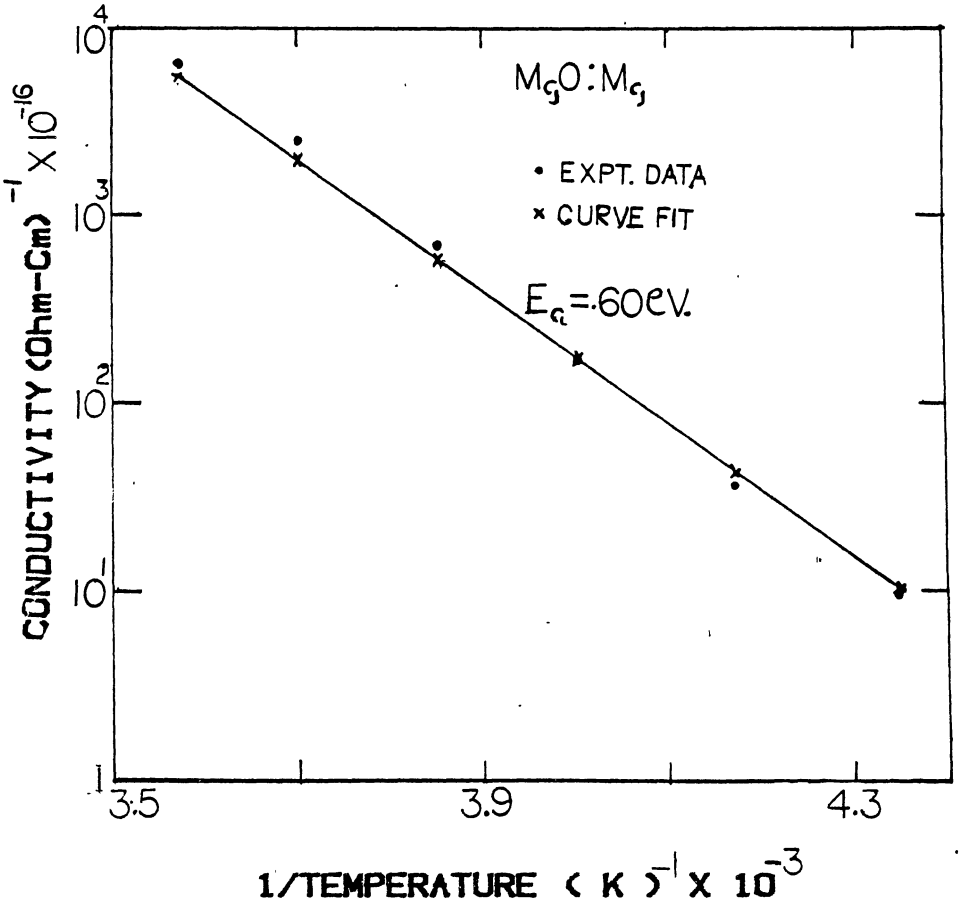

Figure 39. Plot of Electrical Conductivity vs. 1/Temperature in MgO

CHAPTER V

SUMMARY AND SCOPE OF FURTHER WORK

A. Summary

Investigations reported in this dissertation can be summarized as

i) Nature of F center luminescence in thermochemically reduced MgO and CaO is controlled by metastable electron traps present in these samples.

ii) There are two main types of electron traps present in these materials. Thermal release of electrons from the deep traps produce thermoluminescence near room temperature with TL peak at 320 K and 260 K respectively for CaO and MgO. The shallow traps generate TL at low temperature with peak at 80 K and 60 K for CaO and MgO respectively. Respective thermal activation energy for deep and shallow traps in MgO are 0.56 eV and 0.086 eV and in CaO 0.74 eV and .12 eV. Deep traps in these samples are identified as H^- ions and the concentration of H^- ions significantly change the intensity of upper temperature TL in both MgO and CaO. Exact origin of the shallow traps are not known.

iii) Lifetime and the decay kinetics of F center luminescence at RT is controlled by the concentration of H^- ions present in the sample. High concentration of H^- ions in the crystal result in long lifetime of F center luminescence and decay of luminescence is second order type in major part of the decay. On

lowering the concentration of H^- ions, lifetime of F center luminescence decreases dramatically and the decay kinetics become non secondorder type in major part of the decay process.

iv) Concentration of H^- ions also influence the decay kinetics at low temperature. High concentration of deep traps which favors or quickens the start of the second order process at room temperature, delays the second order process at low temperature.

v) Infrared stimulated emission and infrared stimulated photo-current are observed because of the charge trapping in these two main effective traps.

vi) Electrical conductivity or dark current is noticed in these samples at RT. This is assigned to H^- ions present in these materials. The dark current is found to increase or decrease with the increase or decrease in the concentration of H^- ions in the sample.

B. Scope of Further Research

i) In our experimental arrangement for the study of electrical conductivity or dark conductivity, we could not study at a temperature over the RT, and as such we could not monitor the temperature dependence of dark current in CaO. Since the upper temperature TL peak in CaO lies at 320 K; around that temperature the dark current would be maximum. Further improvement of the apparatus is therefore necessary which would enable one to see the temperature dependence of

electrical conductivity and from that to calculate the activation energy of H^- ions as was done in case of MgO.

ii) In infrared stimulated photoconductivity when we studied the temperature dependence of photoresponse we saw a rising trend of photoresponse in CaO at RT. If we could study the photoresponse over RT we would see the saturation point of photoresponse in the region of 320 K, the upper temperature peak. This study should be made after the improvement of the instrument.

iii) Infrared stimulated emission phenomenon can be studied in other oxides like Al_2O_3 and $MgAl_2O_4$ where more than one traps are detected by TL studies[57,58] and the long lived F center fluorescence is observed[57]. A better effect of this reactivated emission at low temperature can be observed in MgO, if the temperature can be controlled near 40K, the lower TL peak. In this dissertation we reported this effect in MgO at a temperature of 77K, because if was difficult to control the temperature at 40K. In both CaO and MgO, the energy transfer mechanism in these four level systems containing F centers, conduction band, deep traps and shallow traps, can be studied by this infrared stimulated emission effect.

iv) Electrical conductivity experiments can also be performed in other materials wher the long lived fluorescence are observed. From this experiment more light can be thrown about the charge motion and trapping mechanism in the sample.

REFERENCES

1. Briggs, A., J. Mater. Sci. 10, 729 (1975).

2. Gourley, J. T. and E. R. Vance, Phys. Status Solidi B77, K85(1976).

3. Vance, E. R. and W. C. Mallard, Phys. Status Solidi B91, K155 (1979).

4. Gonzalez, R., Y. Chen and Mark Mostoller, Phys. Rev. B24, 6862 (1981).

5. Sonder, E. and W. A. Sibley, In Point Defects in Solids, edited by J. H. Crawford and L. M. Slifkin (Plenum, New York, 1972).

6. Henderson, B. and R. D. King, Phil. Mag. 13, 1149 (1966).

7. Chen, Y., W. A. Sibley, F. D. Srygley, R. A. Weeks, E. B. Hensley and R. L. Kroes, J. Phys. Chem. Solids 29, 863 (1968).

8. Wertz, J. E., P. Auzins, R. A. Weeks and R. H. Silsbee, Phys. Rev. 107, 1535 (1957).

9. Ward, W. C. and E. B. Hensley, Phys. Rev. 175, 1230 (1968).

10. Henderson, B., S. E. Stokowski and T. C. Ensiogn, Phys. Rev. 183, 826 (1969).

11. Wood, R. F. and T. M. Wilson, Phys. Rev. B15, 3700 (1977).

12. Bates, J. B. and R. F. Wood, Solid State Commun. 17, 201 (1975).

13. Hughes, A. E. and B. Henderson, In Point Defects in Solids, edited by J. H. Crawford and L. M. Slifkin (Plenum, New York, 1972).

14. Edel, P., B. Henderson, Y. Merle d'Aubigne, R. Romenstain and L. Kappers, J. Phys. C12, 5245 (1979).

15. Chen, Y., J. L. Kolopus and W. A. Sibley, Phys. Rev. 182, 960 (1969).

16. Summers, G. P., T. M. Wilson, B. T. Jeffries, H. T. Tohver, Y. Chen and M. M. Abraham, Phys. Rev. B29, 1283 (1983).

17. Jeffries, B. T., R. Gonzalez, Y. Chen and G. P. Summers, Phys. Rev. B25, 2077 (1982).

18. Tohver, H. T., Private communication. Boston, Mass., Nov. 15, 1983.

19. Wilson, T. M., Private communication, Oklahoma State University, Stillwater, Oklahoma, April 25, 1983.

20. Mostoller, M. and R. F. Wood, Phys. Rev. B7, 3953 (1973).

21. Boswarva, I. M. and A. B. Lidiard, In Atomic Energy Research Establishment Report No. T.P. 232 (revised), Harwell, England (unpublished); and Philos. Mag. 16, 805 (1967).

22. Wilson, T. M. and R. F. Wood, J. Phys. (Paris) Colloq. 37, C7-190 (1976).

23. Toyozawa, T. Prog. Theor. Phys. (Kyoto) 12, 422 (1954).

24. Haken, H. and W. Schottky, Z. Phys. Chem (Frankfort), 16, 218 (1958).

25. Wood, R. F. and U. Opik, Phys. Rev. 162, 736 (1967).

26. Kirklin, P. W., P. Auzins and J. E. Wertz, J. Phys. Chem. Solids 26, 1067 (1965).

27. Glass, A. M. and T. E. Searle, J. Chem. Phys. 46, 458 (1967).

28. Sibley, W. A., C. M. Nelson and Y. Chen, ibid 48, 4582 (1968).

29. Fritz, B., In Proceedings of International Congress of Lattice Dynamics, Copenhagen, 1963, edited by R. F. Wallis (Pergamon, London, 1965) and In Local Excitation in Solids, edited by R. F. Wallis (Plenum, New York, 1968).

30. Timsuk, T. and M. V. Klein, Phys. Rev. 141, 664 (1966).

31. Gethins, T., T. Timusk and E. J. Woll, Jr., Phys. Rev. 157, 744 (1967).

32. Klein, M. V. In Physics of Color Centers, edited by W. B. Fowler (Academic Press, New York, 1968).

33. Dostch, H. and S. S. Mitra, Phys. Rev. 178, 1492 (1969).

34. Wood, R. F. and B. N. Ganguly, Phys. Rev. B7, 1591 (1973).

35. deSouza, M., A. Gongora, M. Aegerter and F. Luty, Phys. Rev. Lett. 25, 1426 (1970).

36. deSouza, M. and F. Luty, Phys. Rev. B8, 5866 (1973).

37. Elliot, R. J., W. Hayes, G. D. Jones, H. F. MacDonald, and C. T. Sennet, Proc. R. Soc. (London) A289, 1 (1965).

38. Chen, Y., R. Gonzalez, O. E. Chow, and G. P. Summers, Phys. Rev. B29, 1283 (1983).

39. Roberts, R. W. and J. H. Crawford, J. Nonmetls 2, 133 (1974).

40. Summers, G. P. and K. Chakrabarti, In Proceedings of Material Research Society, edited by A. W. Kenneth Metzner (Elseiver Science Publishing Co., 1983).

41. Summers, G. P., K. Chakrabarti and Y. Chen, Phys. Rev. B29, 5878 (1984).

42. Wilson, T. M., Bull. Am. Phys. Soc. 27, 413 (1982).

43. Kappers, L. A., R. L. Kroes and E. B. Hensley, Phys. Rev. B1, 4151 (1970).

44. Keller, F. J. and R. B. Murray, Phys. Rev. 150, 670 (1966).

45. Summers, G. P., K. Chakrabarti, R. Gonzalez and Y. Chen, Bull. Am. Phys. Soc. 28, 453 (1983).

46. Halperin, A. L. and A. A. Braner, Phys. Rev. 117, 408 (1960).

47. Medlin, W. L. Phys. Rev. 122, 837 (1961).

48. Lord, M. P., A. L. G. Rees, and M. E. Wise, Proc. Phys. Soc. (London) 59, 473 (1947).

49. Ellickson, R. T. and W. L. Parker, Phys. Rev. 70, 290 (1946).

50. Klasen, H. A. and M. E. Wise, Nature 158, 483 (1946).

51. Summers, G. P., R. Gonzalez, Y. Chen, Phys. Rev. B, to be published.

52. Mott, N. F. and R. W. Gurney, Electronic Processes in Ionic Crystals (Oxford University Press, New York, 1940).

53. Chen, R. and Y. Kirsh, Analysis of Thermally Stimulated Process (Pergamon Press, 1981).

54. Hecht, K., Zeits, f. Physik 77, 235 (1932).

55. Van Heyingen, R. S. and F. C. Brown, Phys. Rev. 121, 1303 (1961).

56. Feldott, J. M., "Electronic Structure of Defects in Some Oxides" (Unpublished. Ph.D. dissertation, Oklahoma State University, 1977).

58. White, G. S., "A Study of Impurity and Radiation Induced Defects in $MgAl_2O_4$ (Spinel)." (Unpublished Ph.D. dissertation, The University of North Carolina at Chapel Hill, 1978).

59. Bass, M. and A. E. Paladino, J. Appl. Phys. 38, 2706 (1967).

60. Batigov, S. Kh., Yu. I. Voronko, B. I. Denker, A. A. Maier, V. V. Osiko, V. S. Radyukhin, M. I. Timoshechkin, Fiz. tverd. Tela 14, 977 (1972).

61. Vakhidov, Sh.A., In Radiation Induced Effects in Monocrystals, FAN, Tashkent 175 (1973).

62. Bernhardt, Hj. Phys. Stat. Sol. (a)31, 365 (1975).

63. Mori, K., Phys. Stat. Sol. (a)42, 375 (1977).

64. Bernhard, Hj, Phys. Stat. Sol. (a) 61, 357 (1980).

65. Roose, N. S. and N. A. Anisimov, Optika i Spektroskopiya 38, 627 (1975).

66. Jeffries, B. J., J. D. Brewer and G. P. Summers, Phys. Rev. B24, 6074 (1981).

67. Wood, R. F., and V. Opik, Phys. Rev. 179, 783 (1969).

APPENDIX

PHOTOCONDUCTIVITY, LUMINESCENCE AND CHARGE TRANSFER IN γ IRRADIATED YAG

A. Introduction

Yttrium Aluminum Garnet (YAG) has been used for quite some time as a laser material, in particular Nd doped YAG. However, not much work has been done on color centers in this material. Bass and Paladino[59] reported the coloration of YGaG and YAG crystals as a result of annealing and UV irradiation. Batygov et al.[60] and Vakhidov[61] traced back the coloration of YAG after γ irradiation at RT and suggested that rare earth ion impurities and transition metal impurities such as Pr, Tb, Ce, Ee, Dy, Mn act as promoting factors for the coloration process. Bernhard[62] suggested the formation of biparticles in undoped YAG and the charge compensation between Mn and Fe.

We will here report the result of our studies on nominally pure undoped YAG after being γ irradiated and compare the results of our studies with previous results known. We will also report the photoconductivity from the charge trapping in γ irradiated YAG which has not been reported until now.

B. Experimental Results

Optical Absorption

The crystals we studied were supplied by Union Carbide, grown by

Czochralski method (Chemical analysis of the crystal is shown in Table (VII). After γ irradiation the crystal turned brown. Optical absorption measurement before and after γ irradiation showed that after γ irradiation a band at 255 nm is slightly decreased and a new band grew up at 310 nm. On increasing the gain of the spectrophotometer in the O.D. range 0 → .1, a broad band was noticed between 350-475 nm. This broad band and 310 nm band was observed before by Mori[63] in UV irradiated sample.

Thermoluminescence

TL studies of the sample before and after γ irradiation show a significant enhancement of intensity (by a factor of ~ 1000) of 140 K TL peak after γ irradiation, with other mentionable peaks at 180 K and 225 K, Figure 40. Bernhard[64] observed TL peaks at 140 K and 178 K in an undoped YAG, not contaminated with Mn impurities. He also calimed that the presence of Mn impurities or YAG deliberately doped with Mn is associated with green RT fluorescence[62,64]. In our crystal we, however, could not observe any green fluorescence. Bernhardt[64] also observed with maximum intensity at 140 K, emission consisting of one or two broad band in the UV region. We noticed a similar UV emission in our crystal. He argued that these luminescence cannot be correlated with impurity traces and Al sites with different oxygen coordination are the precursors of these luminescence and color centers.

More[63] also observed a main glow peak around 170 K which he considered to be due to Fe^{2+} activators. Iron impurities present in YAG as Fe^{3+} trivalent charge state and is associated with 255 nm absorption band. On γ irradiation, the charge state of these iron impurities change from Fe^{3+} to Fe^{2+}, with the introduction of a band near 310 nm.

TABLE VII

MASS SPECTROGRAPHIC ANALYSIS OF YAG (ppmw)

Elements	$Y_3Al_5O_{12}$ 19-688-1
Li	0.6
Be	<0.006
B	<20(b)
F	6
Na	10
Mg	<0.4
Al	high
Si	20
P	0.02
S	4
Cl	2
K	1.5
Ca	4
Sc	0.02
Ti	0.4
V	<0.2
Cr	0.4
Mn	0.06
Fe	1
Co	<0.04
Ni	< 0.1
Cu	< 0.1
Zn	<0.15
Ga	<0.04
Ge	<0.15
As	<0.04
Se	1
Br	<0.1
Rb	<0.06
Sr	<0.06
Y	~ 40%
Zr	<0.4
Nb	<0.2
Mo	<0.2
Ru	<0.2
Rh	<0.4
Pd	<0.2
Ag	<0.15
Cd	<0.06
In	<0.06

TABLE VII (Continued)

MASS SPECTROGRAPHIC ANALYSIS OF YAG

Sn	<0.2
Sb	<0.15
Te	<0.2
I	<0.06
Cs	<0.06
Ba	<0.1
La	<0.1
Ce	<0.1
Pr	<0.1
Nd	<0.6
Sm	<0.2
Eu	<0.2
Gd	<0.4
Tb	<0.1
Dy	<0.4
Ho	<0.1
Er	<0.4
Tm	<0.1
Yb	<0.4
Lu	<0.1
Hf	<0.4
Ta	<0.1
W	<0.4
Re	<0.2
Os	<0.2
Ir	<0.2
Pt	<0.4
Au	<0.1
Hg	< 4
Tl	<0.2
Pb	<0.2
Bi	<0.15
Th	<0.15
U	<0.15

Source: Union Carbide Corporation

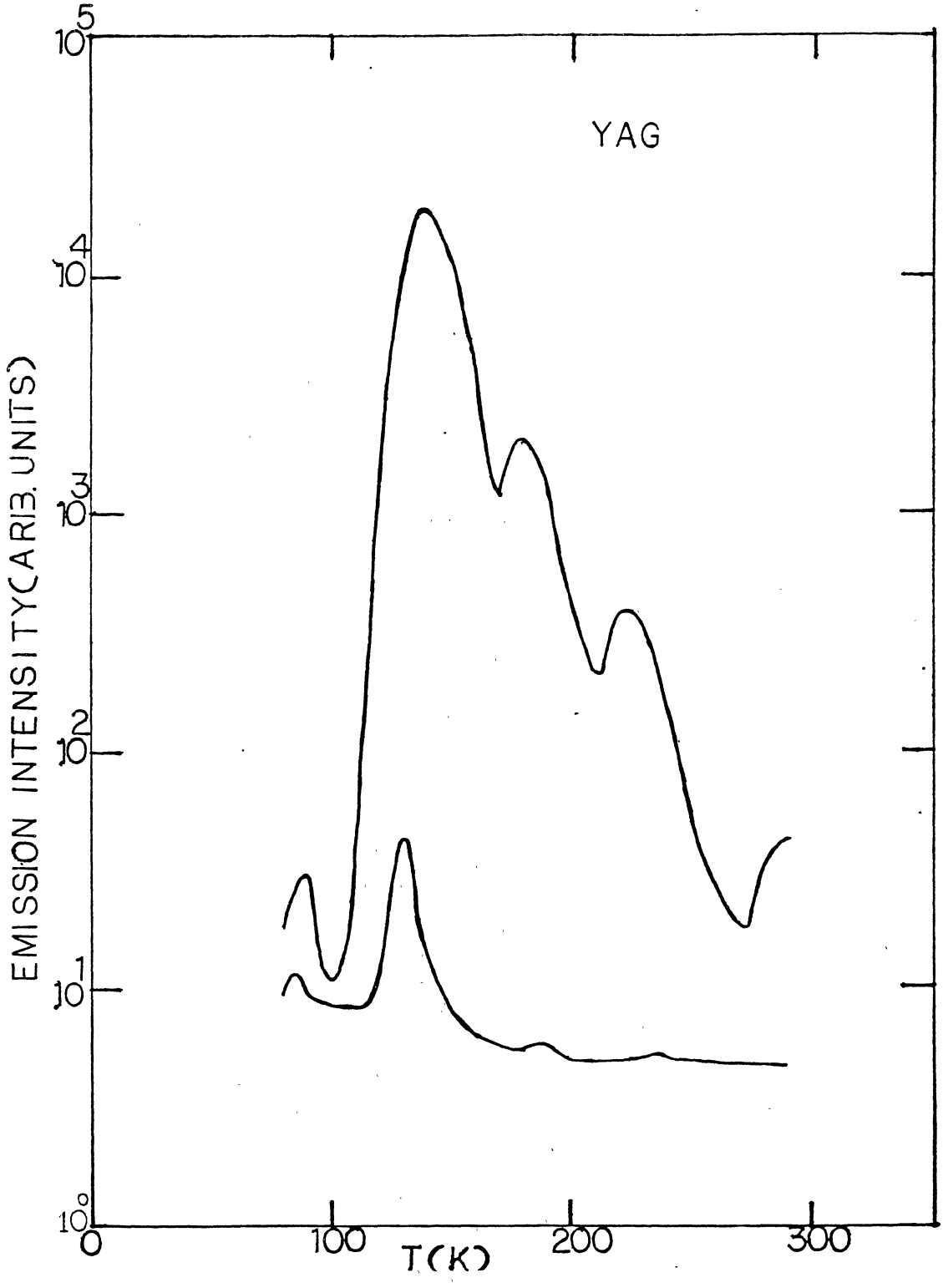

Figure 40. Thermoluminescence Spectra in YAG Before and After γ Irradiation

We observed an absorption peak at 255 nm in unirradiated sample and a peak at 310 nm and also a broad band in the range 350-475 nm after the sample was γ irradiated. We, therefore, support the view of Mori that a possible transition metal impurity present in YAG and a change of charge state from Fe^{3+} to Fe^{2+} takes place after γ irradiation. Although the 140 K TL peak may be intrinsic type and is due to emission of $A\ell_4^{5-}$ and/or $A\ell_6^{9-}$ groups[64,65], the 173 K TL peak is more likely due to Fe^{2+} activators. Also 430 nm emission we detected is possibly due to Fe^{2+} emission. We also observed a sharp emission near 610 nm which we attribute to cromium impurity present in the material. We therefore, suggest a possible charge compensation between Fe^{2+} - Cr^{4+} in the crystal.

C. Photoconductivity

The charge motion in γ irradiated YAG is monitored by photoconductivity experiment, in which a crystal was illuminated by 150 W xenon lamp with a Spex monochromator using 5 mm slit width. Spectral output of the lamp through the Spex is shown in Figure 41. Figure 42 shows the spectral dependence of photoresponse of γ irradiated YAG studied at six different temperatures. At 120 K, three distinct bands with peak at 210 nm, 320 nm and 410 nm were noticed. At 77 K, the band around 320 nm and 410 nm were not observed, and as the temperature was raised from 120 K, the bands peaked at 320 nm and 410 nm more and more overlaped one another and at RT a broad band was noticed which correlates with broad absorption band in an optical absorption spectra.

The third peak lies at 210 nm and was observed at all temperatures studied including at 77 K where the other bands were not noticed. This

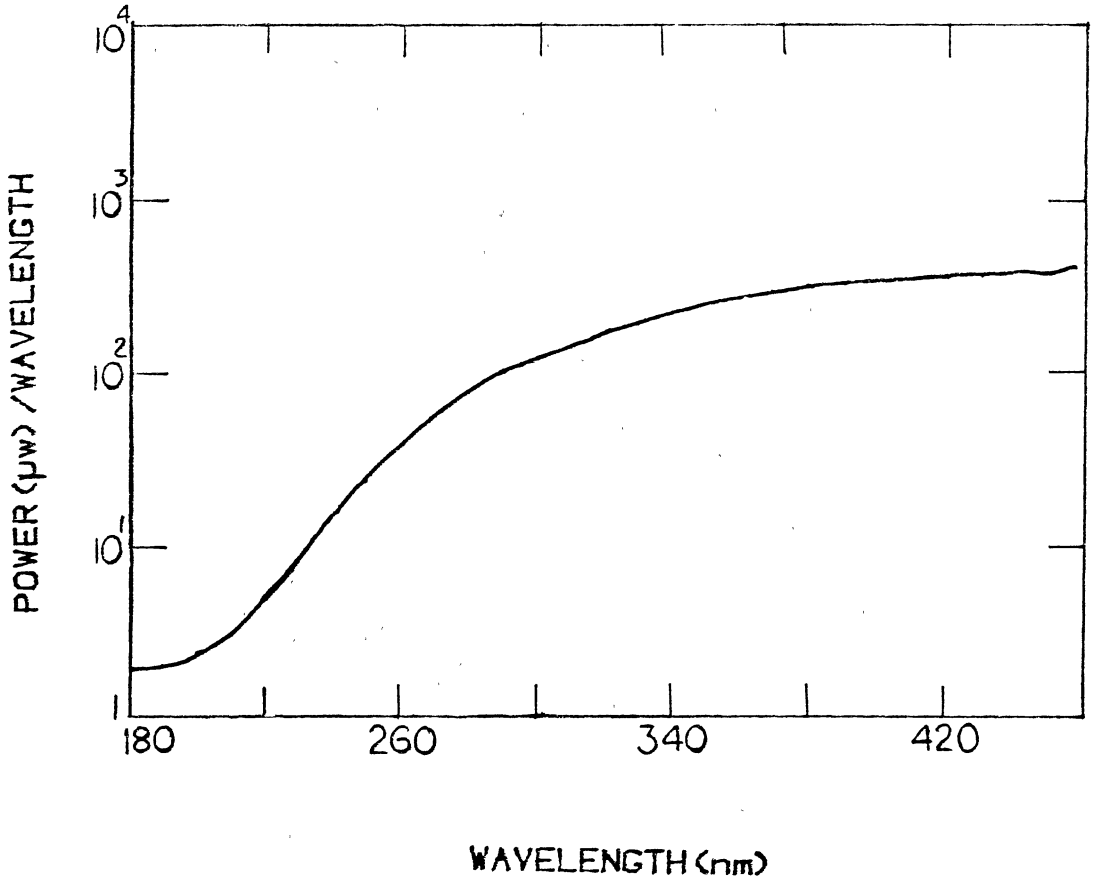

Figure 41. Power Output of 150W Xenon Lamp Through a Spex Monochromator

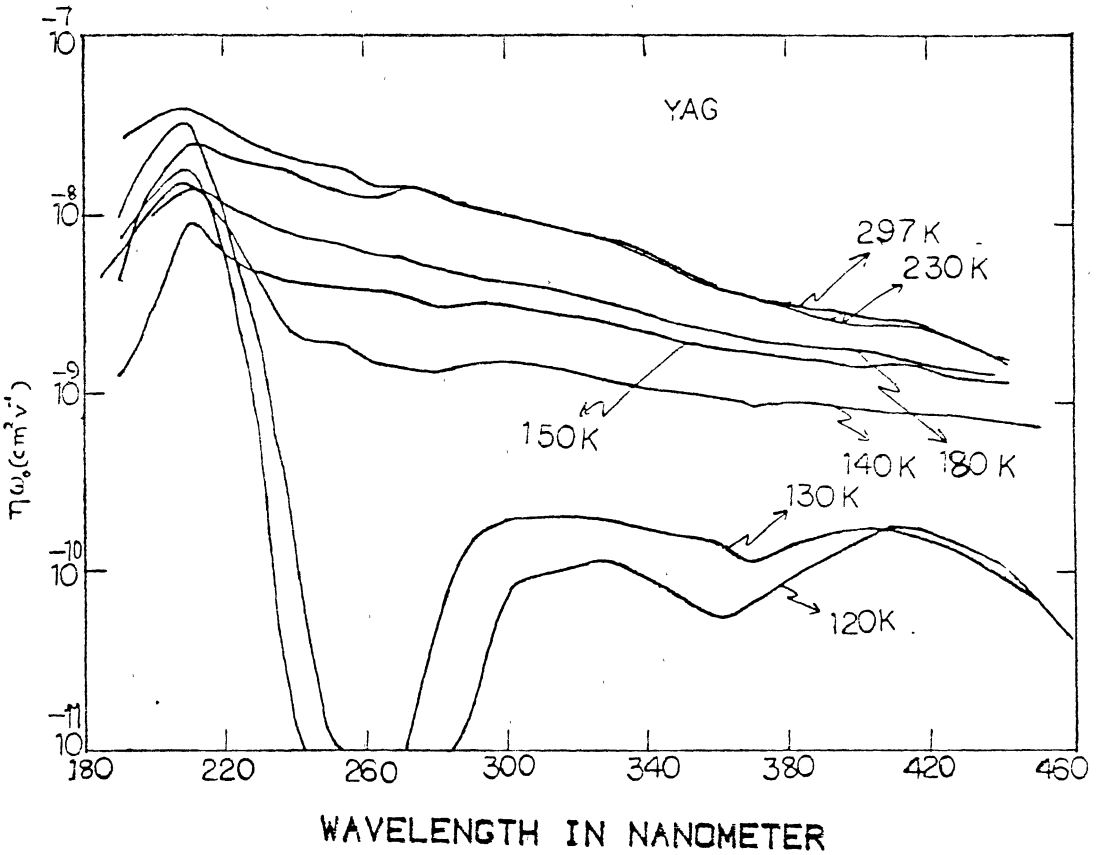

Figure 42. Spectral Dependence of Photoresponse at Various Temperature

peak was found to be close to the position where the photoresponse peak due F center in Al_2O_3 appears.[66] Therefore there is a possibility of creation of F type defect as in Al_2O_3 in the sample.

The photoresponse is not observed in a sample which is not γ irradiated. Photoresponse is observed significantly after one minute of γ irradiation on the sample. On heating the sample over 900 K photocurrent disappears bringing the crystal back to the stage of prior to γ irradiation. Figure 43 shows the photocurrent (arbitrary unit) at 320 nm peak foolowing 10 min annealing at successively higher temperatures.

D. Conclusion

We conclude from this study that in our crystal iron is the main transient metal impurity present in the form of Fe^{3+}. On γ irradition charge state changes and Fe^{3+} becomes Fe^{2+}. The crystal turns brown. This Fe^{2+} acts as an activator resulting 173 K TL peak and 430 nm fluorescence. 140 K TL peak is intrinsic type and is due to $A\ell_4^{5-}$ and/or $A\ell_6^{9-}$ groups. The presence of cromium impurity in the crystal is associated with 610 nm red fluorescence which is independent of γ irradiation. A possible charge compensation between iron and cromium as $Fe^{2+} - Cr^{4+}$ is suggested.

Photoconductivity studies monitor the charge motion in the crystal with a broad band near room temperature which can be correlated to the broad optical absorption band at room temperature. This study also reveals a possible F type defect as in Al_2O_3 with associated photoresponse peak at 210 nm. On annealing the colored YAG over 900 K

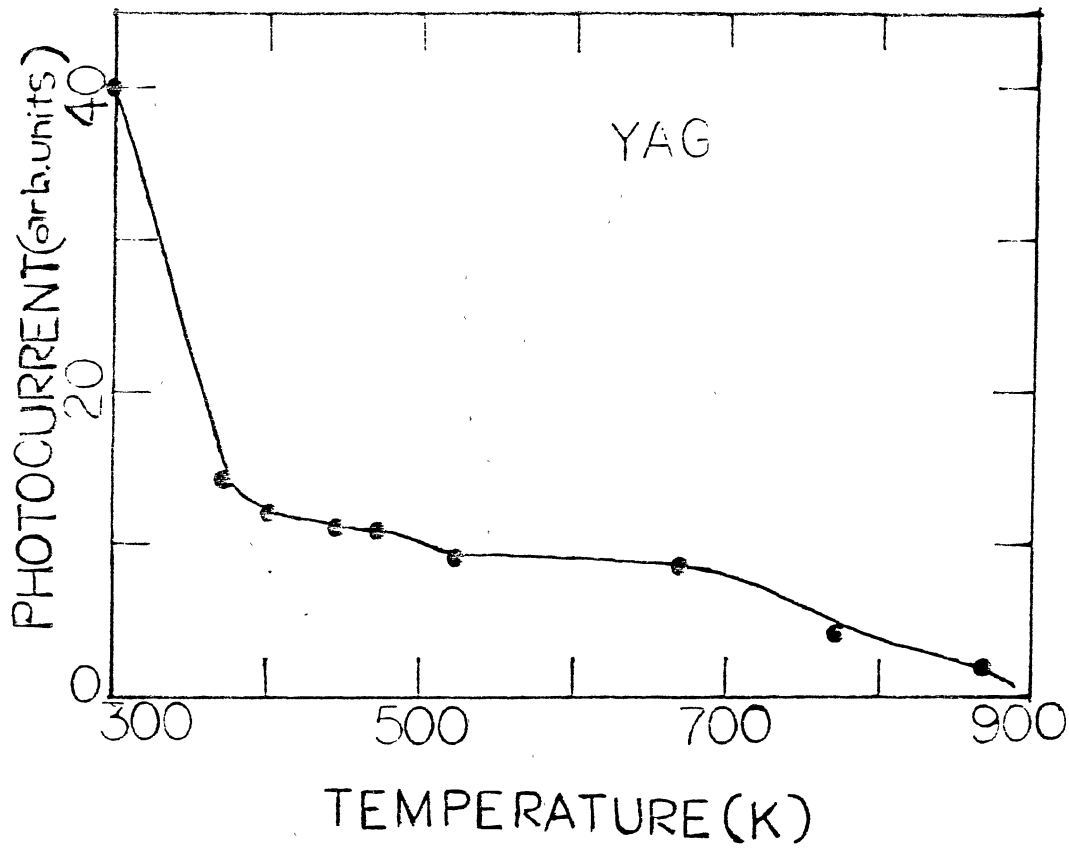

Figure 43. The Effect of Isochronal Annealing (10-Minutes) on 320 nm Photocurrent Peak at Successively Higher Temperatures

for 10 mins. the color centers are removed, no photoconductivity is noticed and the original color of the crystal is restored.

VITA

Kishalaya Chakrabarti

Candidate for the Degree of

Doctor of Philosophy

Thesis: A STUDY OF CHARGE MOTION AND ELECTRONIC STRUCTURE OF DEFECTS IN MgO, CaO AND YAG ($Y_3Al_5O_{12}$)

Major Field: Physics

Biographical:

Personal Data: Born in Berhampore, West Bengal, India, July 21, 1955, the son of Mr. and Mrs. Kedar Chakrabarti.

Education: Graduated from Scottish Church School, Calcutta, India, in August 1971; graduated from University of Calcutta, India, in August 1975 with Bachelor of Science Degree with Honors in Physics; graduated from University of Calcutta, in May 1978 with Master of Science Degree in Physics. Completed requirements for the Doctor of Philosophy degree at Oklahoma State University in July, 1984.

Professional Experience: Teaching Assistant and Research Assistant at Boston College, September 1978 to July 1980. Teaching Assistant at Oklahoma State University from August 1980 to July 1984.

Professional Societies: Member of American Physical Society and Member of Society of Physics Students.

Honor Society: Member of Phi Kappa Phi Honor Society